ANALYSIS OF SONIC BOOM WAVES INCIDENT

ON STRUCTURES

By

BALUSU M. RAO
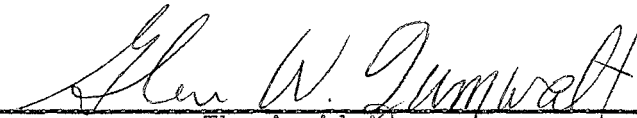
Bachelor of Engineering
Andhra University
Waltair, India
1959

Master of Engineering
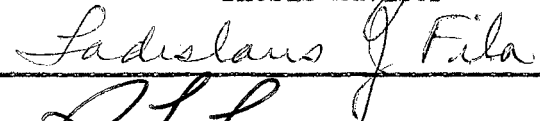Indian Institute of Science
Bangalore, India
1961
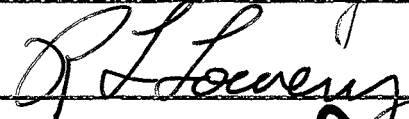
ANALYSIS OF SONIC BOOM WAVES INCIDENT

ON STRUCTURES

Thesis Approved:

_____
Thesis Adviser

_____

_____

_____

_____
Dean of the Graduate College

## ACKNOWLEDGEMENTS

I wish to express my deepest appreciation and gratitude to
Dr. G. W. Zumwalt, who served as my thesis adviser and graduate
committee chairman, for his encouragement, guidance, financial
support, and personal interest throughout my graduate studies at
Oklahoma State University. I am particularly thankful to Prof. L. J.
Fila for his valuable comments in the editing of this thesis. Thanks
are due to Dr. R. L. Lowery, Dr. R. B. Deal, Dr. J. H. Boggs, and
Prof. H. Scholz for serving on my graduate committee.

I would also like to thank the Oklahoma State University, the
Harry Diamond Laboratories, and the National Aeronautics and Space
Administration for their financial assistance during the period of
this study.

I am forever indebted to my wife, Vijaya, without whose
understanding, cooperation, and many sacrifices, this work
would not have been possible.

TABLE OF CONTENTS

LIST OF FIGURES

## NOMENCLATURE

| | |
|---|---|
| a | angle between wall and normal-to-wave (Figure 10) |
| $A(x,y,t)$ | blurring term coefficient for x-direction |
| b | angle between wall and normal-to-wave (Figure 10) |
| $B(x,y,t)$ | blurring term coefficient for y-direction |
| c | speed of sound |
| $C_1, C_2$ ‒ ‒ ‒, $C_n$ | disturbance regions of a reflected wave |
| $D_{gv}, D_{pv}$ | defined on page 10 |
| e | fluid energy per unit volume |
| f | defined on page 55 |
| $f(z)$ | analytic function defined on page 41 |
| $F^x, F^y$ | defined on page 55 |
| h | diagonal of finite mesh |
| $h_1$ | finite mesh spacing in x-direction |
| $h_2$ | finite mesh spacing in y-direction |
| H | height of the wall |
| k | mesh number in x-direction |
| K | time parameters defined on page 59 |
| | constant defined on page 42 |
| $K_1, K_2$ | time parameters defined on page 59 |
| $\ell$ | mesh number in y-direction |
| L | length of the wall |
| m | coefficient of acoustic velocity variation with altitude |

| | |
|---|---|
| $M$ | Mach number |
| $n$ | time plane number |
| | direction normal to a wall |
| $p$ | pressure perturbation defined on page 34 |
| $p_1, p_2, p_3, p_4, p_{2b}$ | defined on page 48 |
| $p_i, p_r, p_{np}, p_{nb}$ | defined on page 75 |
| $P$ | pressure |
| | point on a wall |
| $\Delta P$ | defined on page 75 |
| $\Delta P_o$ | pressure rise across sonic boom shock wave at ground level |
| $q$ | defined on page 57 |
| $r$ | special coordinate defined on page 36 |
| $r(x,y)$ | defined on page 34 |
| $R$ | a reference point |
| | the radial distance of a point from the origin of a disturbance circle |
| $s$ | special coordinate defined on page 36 |
| $S$ | defined on page 10 |
| $S(t), S(t_o)$ | defined on page 35 |
| $t$ | time variable |
| $\Delta t$ | time interval between arrival of bow and tail shock waves of a sonic boom |
| $T, \Delta T_{ir_p}$ | defined on page 11 |
| $T_{iR}$ | defined on page 66 |
| $x, y$ | cartesian coordinates |
| $x_1, y_1$ | cartesian coordinates defined on page 44 (Figure 12) |
| $X, Y, Z$ | cartesian coordinates defined on page 11 (Figure 5) |

$Y_c$              defined on page 11

$z$              a complex variable defined on page 41

$u$              x-component of velocity

$v$              y-component of velocity

$V$              flight velocity

                velocity perpendicular to a shock wave

$w$              a complex variable defined on page 42

$\alpha$              blurring term defined on page 59

$\beta$              blurring term defined on page 59

                Mach angle or incident wave angle measured from the horizontal

$\gamma$              specific heat ratio

$\theta$              angle between the wall axis and the Y-axis (Figure 5)

                variable angle (Figure 9)

$\theta_w$            wave angle (Figure 18)

$\lambda$              defined on page 42

$\xi$              defined in Appendix

$\rho$              density

                defined on page 41

$\rho_1$            defined on page 42

$\tau$              time increment

                time at which pressure disturbance wave was emitted

$\varphi$            general perturbation variable

$\Phi$              angle between the wall and the X,Y plane (Figure 5)

                half-angle of a wall or corner (Figure 9)

$\Phi_w$            wave angle (Figure 19)

$\chi$              finite difference net diagonal angle

| $\psi$ | ray angle (Figure 9) |
|---|---|
| $\psi_1, \psi_2$ | defined in Appendix |
| $\omega$ | defined on page 42 |
| | blurring parameter |

## Superscripts

| $n$ | time plane number |
|---|---|
| $x$ | x-direction |
| $y$ | y-direction |
| $+$ | positive |
| $-$ | negative |

## Subscripts

| o | in undisturbed atmosphere |
|---|---|
| 1 | behind incident shock wave |
| 2 | behind reflected shock wave |
| c | at point c |
| d | at point d, the origin of the disturbance ray |
| g | at ground level |
| i | incident wave |
| k | x net point location |
| l | y net point location |
| p | at point P on the wall |
| r | reflected wave |
| t | at the tropopause, or at the time a ray passed the tropopause |
| v | at the vertex of the shock cone |

CHAPTER I

INTRODUCTION

The prospect of commercial flight at supersonic speeds served for
the last decade as a stimulus to aeronautical research in the United
States and abroad.  Several complex problems such as configurations,
propulsion, stability and control, and structures are involved in the
supersonic transport design.  But at present the problem of sonic
booms, the shock waves that are generated by supersonic aircraft and
extended from the flight altitude to the ground, is of utmost im-
portance and is indeed the main obstacle to feasible operation of the
supersonic transport.  In addition to complaints of the unpleasant
noise, several instances of structural damage have been recorded in
the past decade.

To investigate the people's reaction and the property damage
caused by sonic booms, the Federal Aviation Agency conducted a six-
month series of tests from February 3 to July 30, 1964, in which
Air Force jets simulating future SSTs carried out supersonic flights
over Oklahoma City eight times a day in various atmospheric and flight
conditions.  Of the total 12,558 complaints received, 8,335 alleged
damage to property.

In view of the proposed SST program, and the conclusions that
were drawn from the sonic boom tests conducted in Oklahoma City,
analytical methods are needed to predict the structural response and

damage to an arbitrary structure when it is subjected to typical sonic boom type inputs. The pressure wave, striking the ground when a supersonic aircraft passes, is the result of a conical pressure field pulled along by the aircraft. Shock waves, which are popularly known as sonic booms, extend outward and backward from the nose and tail regions of the plane as shown in Figure 1. Between the two shocks, the expansion around the convex body produces a gradual pressure drop. The general shape of the pressure profile on a region of a flat, open ground is shown in Figure 2. The resulting N-wave is not, however, the pressure history felt by a wall. The wall receives the N-wave plus a wave reflected from the ground and from any other nearby surfaces. The displacement in time of these two waves is $\Delta T_{ir}$. The resulting change in wave shape should have a significant effect on those parts of the structure having certain natural frequencies. A few possibilities are shown in Figure 3. In case (a) the overpressure would be doubled, and in cases (b), and (c), four nearly equally spaced pulses would cause a vibration of large amplitude in structural members having a natural frequency near that of pulses.

Not much theoretical work has been done in the area of wave/structure interaction in the past. Zumwalt (1) pointed out the importance of time intervals between the bow and tail shock waves, in causing structural damage. Lowery (1) identified the various vibrational modes of both structural panels and cavities which are likely to be excited for sonic boom wave inputs. Recently, a few investigators, Simpson (2), Whitehouse (3), and Reddy (4), have developed analytical methods to estimate the response of cavities and panels for sonic boom type inputs. These investigations can be applied to
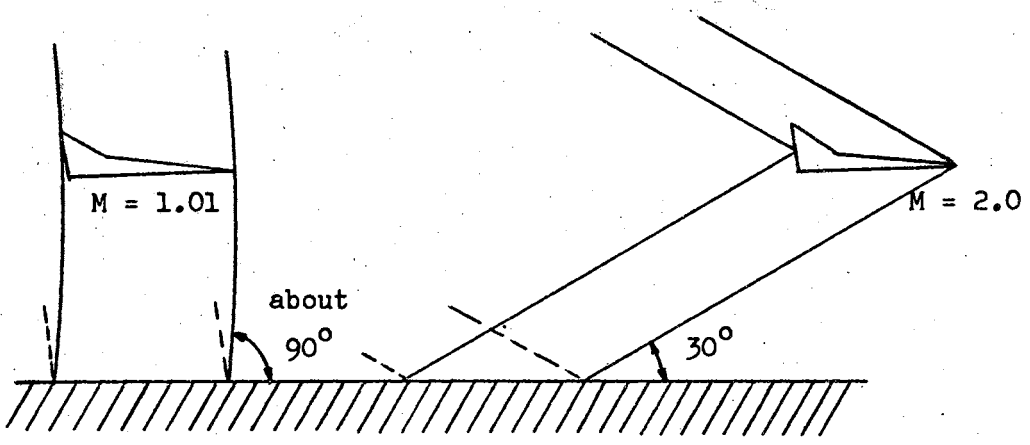
Figure 1.  Typical Sonic Boom Waves
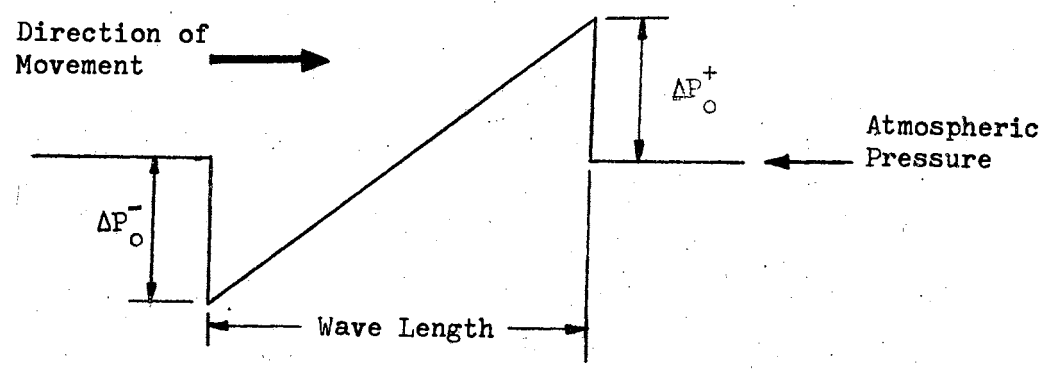


Figure 2.  Typical Pressure Wave of a Sonic Boom
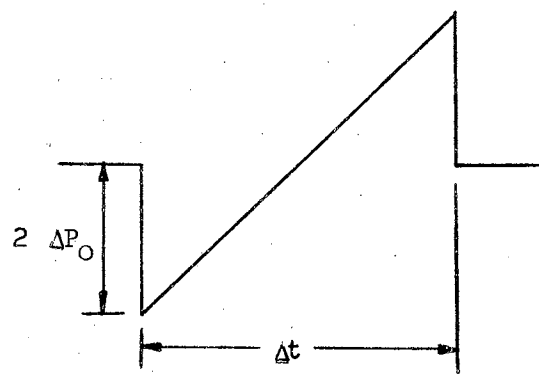
(a)  Wall Position Near the Ground:  $\Delta T_{ir} = 0$
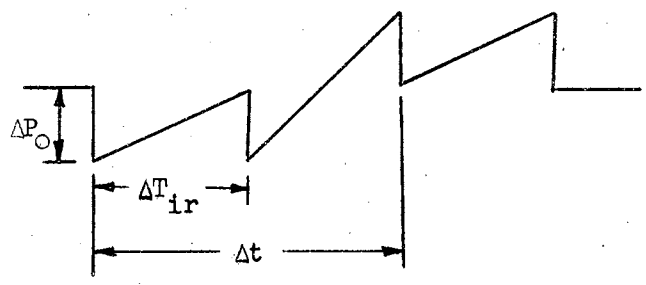
(b)  Intermediate Wall Height Position:  $\Delta T_{ir} = \Delta t/2$
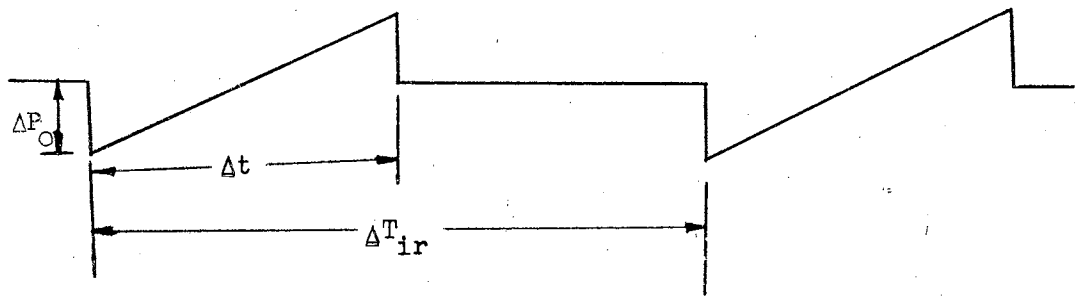
(c)  Very High Wall Position:  $\Delta T_{ir} = 2 \Delta t$

Figure 3.  A Few Incident and Ground Reflected Sonic Boom Waves

predict the structural response of a structure for a given pressure-
time history on the structure due to the passage of a sonic boom wave.
For evaluation of the structural response due to the passage of the
sonic boom, it is necessary to predict the pressure-time history on
the structure including the effect, of the diffractions and reflections
caused by the corners of the structure on the original sonic boom wave.

The present investigation can be divided into three phases:

1. Three methods, ranging from a simple, highly idealized model
   to a rather realistic, but complex, analysis, were developed to
   estimate the time-of-arrival of an incident wave and its re-
   flection on a structure. The applicability and the validity
   of the three methods were investigated for several flight
   altitude and Mach number ranges. In this, only plane walls
   facing the aircraft were considered, so that wave diffractions
   and reflections by walls were eliminated.

2. Two-dimensional analytical and numerical solutions using a super-
   position and mesh-field computation with Rusanov's (5) blurring
   techniques, respectively, were developed to predict the effects
   of diffraction and reflection of sonic boom waves by corners and
   walls.

3. The analyses developed in phases 1 and 2, were applied to a
   particular problem: The window, on the north wall and under a
   roof canopy of the Kinney Shoe Store, which was broken during
   a sonic boom test in Oklahoma City.

IBM 1620 and IBM 7040 computers were used to perform the compu-
tations.

The techniques developed here make possible the prediction of

the pressure-time history on wall due to sonic booms when the wave reflections and diffractions by the walls are essentially two-dimensional. The numerical method is directly extendable to permit three-dimensional solutions with no geometric limitations.

CHAPTER II

LITERATURE REVIEW

Literature reviewed for this investigation may be divided into
three categories.  The first category is the literature in which the
general equations were developed to predict the time history of a
sonic boom bow wave.  The second category is the literature in which
analytical methods were developed for the problem of diffraction and
reflection of weak shock waves by corners of structures.  The third
category is the literature in which numerical solutions were sought
for problems associated with shock wave phenomena.

Randall (6) derived the equations of the ballistic wave and its
ray-lines in an inhomogenous atmosphere assuming the speed of sound
decreases linearly with altitude up to the tropopause.  He justified
the assumption of the linear speed of sound variation in view of its
close approximation to the I. C. A. O. Standard atmosphere.  Lansing (7)
applied Randall's work to the problem of determining the location of
the shock wave produced by a maneuvering aircraft.

Tyler and Walker (8, 9, 10) conducted a thorough literature survey
of the analytical methods of shock diffraction and reflection problems.
Busemann (11) conceived the general idea of the conical flow field,
that is, a flow in which all fluid properties are uniform on rays
through a common vertex.  Busemann pointed out the frequent existence
of conical fields in supersonic flow.  In conical fields, the governing

equations for the velocity components or pressure distribution can be reduced to a Laplace equation of two independent variables. The propagation of plane discontinuities was investigated by Luneberg (12) in electromagnetic theory and by Keller (13) in acoustics. In both these investigations, it was found that the discontinuity surface satisfied a first order differential equation, the "eiconal equation" in a homogenous media, and that the magnitude of the discontinuity varied in a simple manner as the surface moved. Keller and Blank (14) obtained solutions, for the problems of diffraction and reflection of pulses by wedges and corners, as explicit closed expressions in terms of elementary functions. They accomplished this work, utilizing the investigations of Luneberg and Keller to convert the initial-boundary value problem into a characteristic-boundary value problem in xyt-space and applying Busemann's conical flow concept.

Von Neumann (15) conducted extensive research in both analytical and experimental investigations of oblique-shock reflection. He developed a mathematical analysis to evaluate the upper limits of "regular" reflection as a function of shock strength and discussed the physical phenomena of "Mach" reflection. Ting (16) studied the problem of a weak shock hitting a two-dimensional rectangular barrier. The solutions were sought to satisfy all boundary conditions at suitably divided time intervals for two structures, a very thin barrier, and a rectangular barrier of finite width. A few reflected wave patterns were shown for the two structures mentioned above. Whitham (17) presented a method for treating the propagation and ultimate decay of the shocks by explosions and by bodies in supersonic flight. Ting (18), as an extension to his earlier work (16), solved the problem of the

diffraction of a two-dimensional disturbance by a convex right angle corner by a method which permits final results to be obtained conveniently. The analysis was applied to the two-dimensional unsteady flow field associated with the diffraction of a weak shock by a rectangular barrier and also to the equivalent three dimensional steady supersonic flow field produced by the interference of wings and prismatic bodies of rectangular cross section. Filippov (19) considered the problem of a diffraction of a plane weak shock wave at contours of arbitrary shapes. Filippov treated the plane unsteady problem of diffraction as an auxiliary three-dimensional steady problem, where the third coordinate is proportional to the time. The problems were linearized in the whole region of the diffraction field and this assumption was justified since it fails to be valid in only small regions of the diffracted flow field and for very short durations.

The literature review of the numerical methods for shock wave problems would constitute a text book by itself. For this reason, literature of these methods is omitted here. The interested reader may refer to the works of Tyler and Walker (8, 9, 10) who presented a detailed discussion of the numerical methods. However, a brief discussion is given in Chapter V, while deriving finite difference equations.

CHAPTER III

COMPUTATION OF SONIC BOOM WAVE ARRIVAL TIMES ON A WALL

The purpose of this section is to develop a method for estimating
the time of arrival of incident and reflected sonic boom waves at any
point on a building wall facing the flight track. To determine the
time of arrival between bow and tail waves and their reflections, the
geometric relations between wall and wave must be known for a given
aircraft altitude, direction, and speed. Three methods, ranging from
highly idealized to rather realistic analyses, were attempted. The
assumptions made here were (a) that no wind effects are present, and
(b) that the sonic booms are produced by an aircraft in steady, level
flight.

The coordinate axis system for an arbitrarily oriented plane wall
is shown in Figure 4 and the model of a conical wave intersecting the
wall is shown in Figure 5. Special notation which is used in this
Chapter is as follows:

$D_{gv}$    horizontal distance between the vertex of the sonic boom and
its ground intersection point, g.

$D_{pv}$    horizontal distance between a wall point, P, and the vertex of
the sonic boom wave, at the instant P is intersected by the
incident wave.

m    coefficient of acoustic velocity variation with altitude.

S    projected distance of the wave from the flight path in the YZ
plane (see Figure 5).
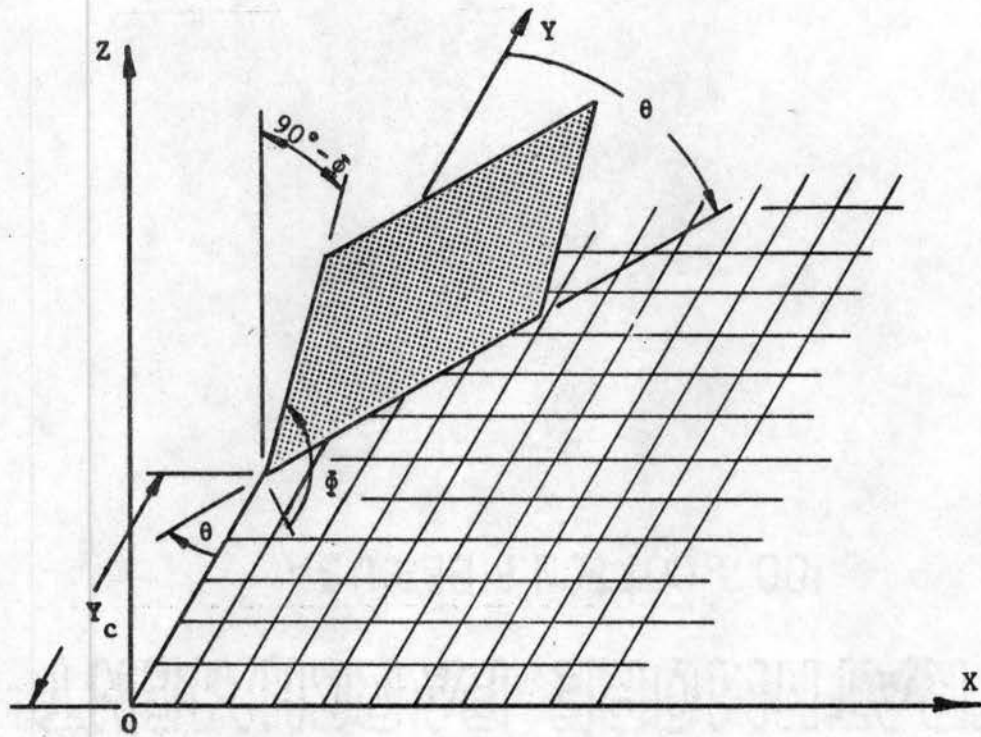
Figure 4.   Coordinate System for an Arbitrarily Oriented Plane,
Rectangular Wall
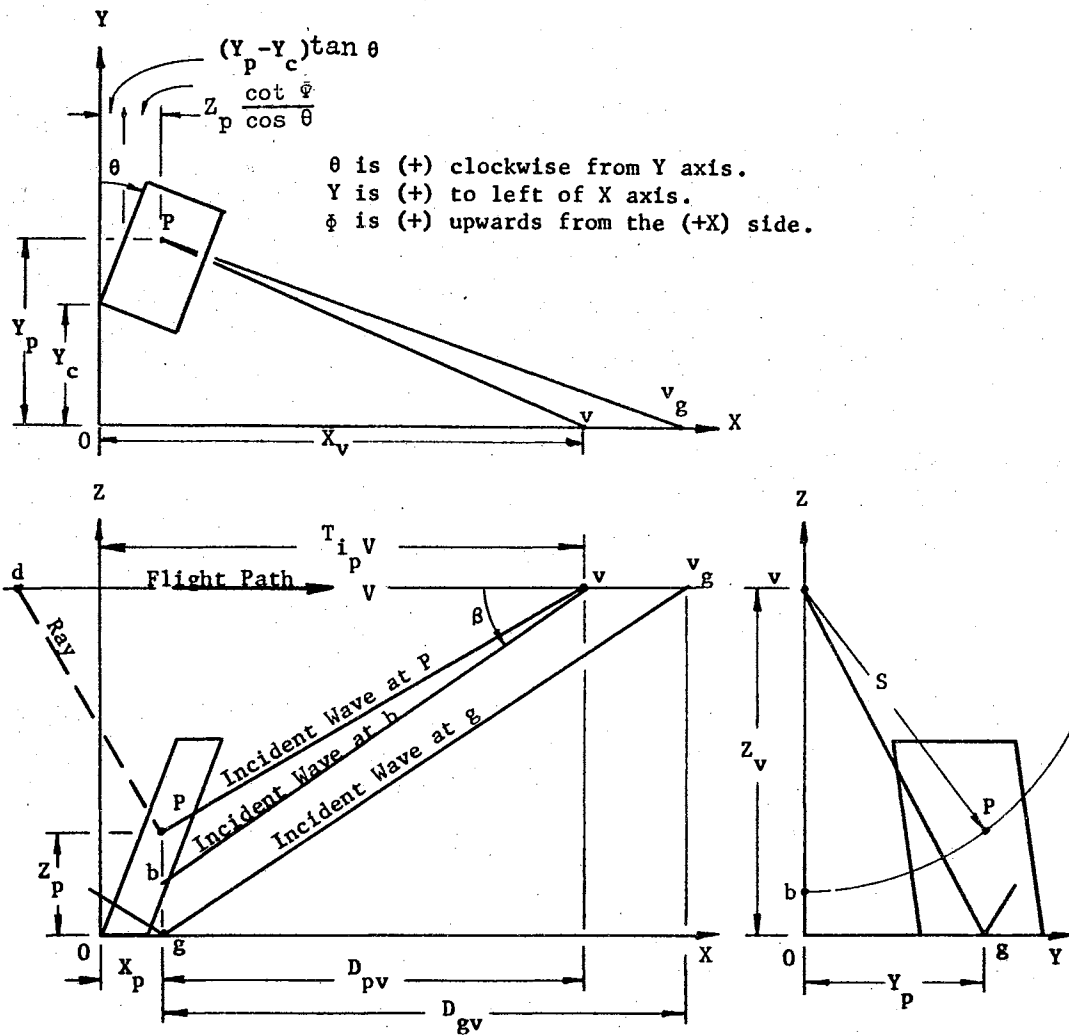
Figure 5. Model for the Analysis of a Conical Wave Intersecting
a Plane, Rectangular, Sloping Wall

T         time for a wave to pass a point after the aircraft passes the coordinate origin (subscripts indicate incident or reflected wave; second subscript indicates the point).

$\Delta T_{ir_p}$   time interval between the arrival of the incident and reflected waves at a point, P, on a wall.

X         coordinate axis, horizontal and along the flight track on the ground.

Y         coordinate axis, horizontal and perpendicular to the flight track on the ground.

$Y_c$       distance along the Y-axis to the nearest corner point, c, of the wall on the ground.

Z         coordinate axis, vertical.

$\beta$         Mach angle or incident wave angle measured from the horizontal.

$\theta$         angle between the wall and the Y-axis, measured clockwise from the Y-axis in the horizontal plane.

$\tau$         time at which a pressure disturbance wave was emitted.

$\Phi$         angle between the wall and the horizontal (XY) plane.


## Method I


An approximate method was developed to predict the arrival times of incident and reflected sonic boom waves on a plane wall. The simplifying assumption made here was that the speed of sound of the conical wave is constant and equal to that at ground level. The wave then can be considered to be conical if the aircraft is in steady, level flight.

The bow and tail waves are assumed to have been produced by an aircraft in steady, level flight at altitude $Z_v$, flying with a velocity V parallel to the X-axis (see Figure 5). The horizontal distance of the effective vertex of the cone from a fixed origin "0", at the time the wave passes a given location on the wall, can be estimated. This

distance is designated as $X_v$. For a known geometry and forward speed of the aircraft, the arrival time of an incident wave on a plane wall can then be computed from the geometric relations shown in **Figure 5**:

$$T_{i_p} = \frac{X_v}{V} , \qquad (3\text{-}1)$$

$$X_v = \left(X_p + D_{pv}\right) , \qquad (3\text{-}2)$$

$$X_p = (Y_p - Y_c) \tan \theta + Z_p \left(\frac{\cot \Phi}{\cos \theta}\right) , \qquad (3\text{-}3)$$

$$D_{pv} = \frac{\sqrt{Y_p^2 + (Z_v - Z_p)^2}}{\tan \beta} . \qquad (3\text{-}4)$$

The above four equations can be combined to give the time the incident wave reaches P:

$$T_{i_p} = \frac{1}{V} (Y_p - Y_c) \tan \theta + Z_p \left(\frac{\cot \Phi}{\cos \theta}\right) + \frac{\sqrt{Y_p^2 + (Z_v - Z_p)^2}}{\tan \beta} , \qquad (3\text{-}5)$$

where the time $T_{i_p}$ is referenced to the passing of the aircraft over the origin, O.

The time interval between the incident and reflected waves passing P is twice the time interval from P to the ground directly beneath:

$$\Delta T_{ir_p} = 2 \left(T_{i_g} - T_{i_p}\right) ; \qquad (3\text{-}6)$$

where

$$T_{i_g} = \frac{1}{V} (X_p + D_{gv}) , \qquad (3\text{-}7)$$

$$D_{gv} = \frac{\sqrt{Y_p^2 + Z_p^2}}{\tan \beta} . \qquad (3\text{-}8)$$

Equations (3-1), (3-2), (3-4), (3-6), (3-7), and (3-8) are combined and simplified:

$$\Delta T_{ir_p} = \frac{2}{V} (D_{gv} - D_{pv}) , \qquad (3\text{-}9)$$

$$\Delta T_{ir_p} = \frac{2}{V} \cot \beta \left[ \sqrt{Y_p^2 + Z_p^2} - \sqrt{Y_p^2 + (Z_v - Z_p)^2} \right] \quad . \quad (3\text{-}10)$$

The time of arrival of the incident wave, $T_{i_p}$, and the time interval between incident and reflected waves, $\Delta T_{ir_p}$, at any point P is thus given in terms of the location of the point and the velocity and altitude of the aircraft. $T_{i_p}$ and $\Delta T_{ir_p}$ values for a large number of points, P, on a wall give a clear picture of the time-history of the incident and reflected waves for a wall which is struck by an undisturbed wave. This does not, of course, apply to a wall which would be in the "shadow".

$\Delta T_{ir_p}$ plays an important role in the structural response. From Equation (3-10), it can be seen that this time interval increases with height of the wall point above ground level and decreases as the offset distance from the flight track increases.

## Method II

A more exact method, based on the ballistic wave analysis of references (6) and (7), was developed. In this, the speed of sound was assumed to decrease linearly with altitude up to the tropopause (assumed as 36,000 feet), and to be constant at 972 ft/sec above the tropopause.

$$c = c_g - mZ \quad . \quad\quad\quad\quad\quad\quad (3\text{-}11)$$

For $c_g = 1116$ ft/sec and $m = 0.004$ ft/sec-ft, the speed of sound is found to be very near that of the standard atmosphere (see Figure 6).

## Flight Altitudes Below the Tropopause

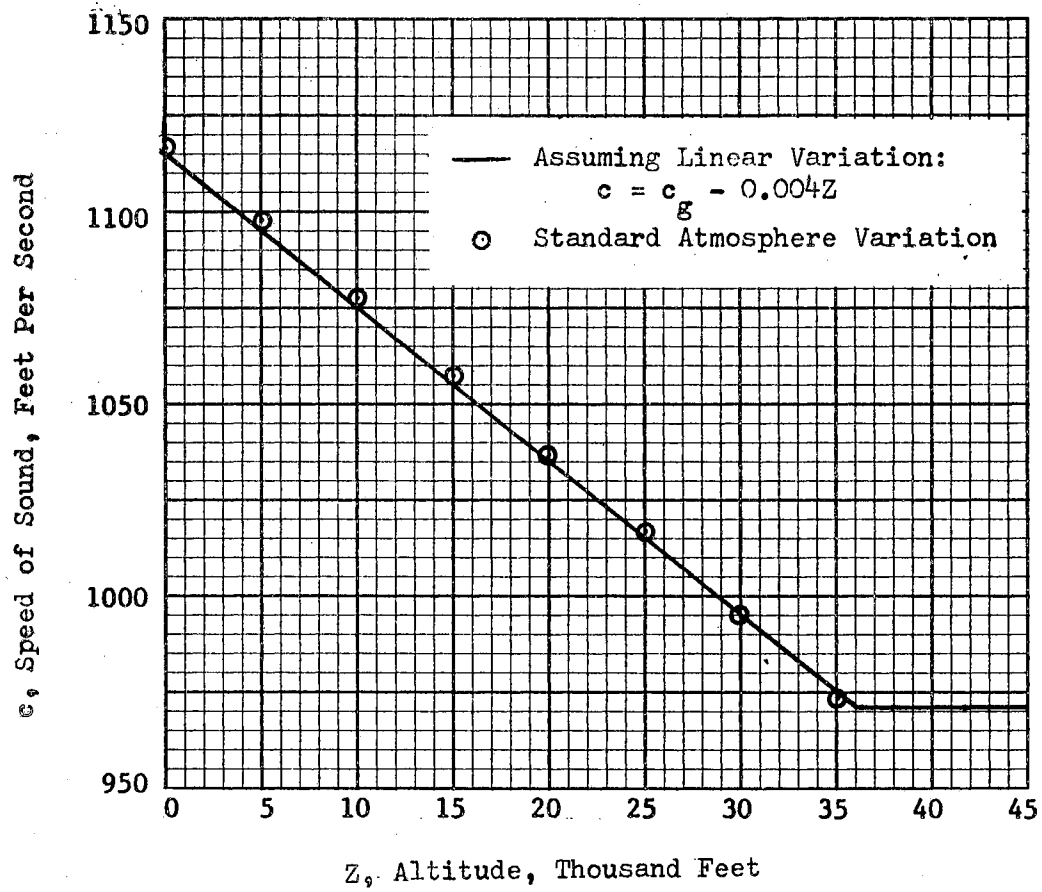The shape of the wave fronts produced by a point disturbance was

16



Figure 6. Speed of Sound Versus Altitude

obtained by finding the system of surfaces which are orthogonal to rays from that point. By following that disturbance as it propagates from a point along a given ray, it is possible to relate the shape of the wave fronts to the growth of these fronts. In an atmosphere in which the sonic speed decreases linearly with altitude, the disturbance front coordinates $(X, Y, Z)$ are given by:

$$(X-X_d)^2 + (Y-Y_d)^2 + [Z-Z_d + \frac{c_d}{m}(\cosh mt-1)]^2 = \left|\frac{c_d}{m}\right|^2 \sinh^2 mt. \tag{3-12}$$

The coordinates are as shown in Figure 5, except that, for a non-constant-temperature atmosphere, the ray and wave lines are not straight. In Equation (3-12), t is the time since the disturbance was initiated. For a fixed coordinate system as shown in Figure 5, the disturbance origin, point d, becomes a function of time. Then at time t, the position of the wave front $(X, Y, Z)$ emitted by the aircraft at an earlier time $\tau$ is given by:

$$(X-X_d)^2 + (Y-Y_d)^2 + \left(Z-Z_d + \frac{c_d}{m}[\cosh m(t-\tau)-1]\right)^2 = \left|\frac{c_d}{m}\right|^2 \sinh^2 m(t-\tau), \tag{3-13}$$

where $c_d = c_g - mZ_d$, and $X_d$, $Y_d$, and $Z_d$ are functions of $\tau$.

The envelope of this system of wave fronts is obtained by eliminating $\tau$ between Equation (3-13) and its partial derivative with respect to $\tau$. This differentiation gives

$$- 2(X-X_d)\dot{X}_d - 2(Y-Y_d)\dot{Y}_d - 2\left(Z-Z_d + \frac{c_d}{m}[\cosh m(t-\tau)-1]\right)$$

$$\left(\dot{Z}_d + \dot{Z}_d[\cosh m(t-\tau)-1] + c_d \sinh m(t-\tau)\right) =$$

$$- 2\frac{c_d}{m}\sinh m(t-\tau)[c_d \cosh m(t-\tau) + \dot{Z}_d \sinh m(t-\tau)]. \tag{3-14}$$

For steady, level flight:

$$Y_d = 0 \text{ (by coordinate system)}, \quad Z_d = \text{constant} = Z_v,$$

$$c_d = c_v, \quad \dot{X}_d = V, \quad \dot{Y}_d = 0, \quad \dot{Z}_d = 0. \tag{3-15}$$

Equations (3-14) and (3-15) are combined and simplified to give

$$(X - X_d) = \frac{1}{M} \left( Z - Z_v - \frac{c_v}{m} \right) \sinh m(t - \tau). \tag{3-16}$$

Equations (3-13), (3-15), and (3-16) are combined and simplified:

$$\frac{1}{M^2} \left( Z - Z_v - \frac{c_v}{m} \right)^2 \cosh^2 m(t - \tau) + \frac{2c_v}{m} \left( Z - Z_v - \frac{c_v}{m} \right) \cosh m(t - \tau)$$

$$+ Y^2 + \left( Z - Z_v - \frac{c_v}{m} \right)^2 \left( 1 - \frac{1}{M^2} \right) + \left( \frac{c_v}{m} \right)^2 = 0. \tag{3-17}$$

The roots of equation (3-17) are contained in

$$\cosh m(t - \tau) = \frac{M}{\left( Z - Z_v - \frac{c_v}{m} \right)} \left\{ - \frac{Mc_v}{m} \pm \sqrt{ \left( 1 - \frac{1}{M^2} \right) \left[ \left( \frac{Mc_v}{m} \right)^2 - \left( Z - Z_v - \frac{c_v}{m} \right)^2 \right] - Y^2 } \right\}. \tag{3-18}$$

For positive Z and $Z_d$ values, the (+) sign applies before the inner bracket in Equation (3-18).

For given values of $Y = Y_p$, $Z = Z_p$, $Z_v$, and M values, $(t - \tau)$ can be calculated by Equation (3-18). The time of arrival of an incident wave is then given by:

$$T_{i_p} = \frac{1}{V} (X_p + D_{pv})$$

$$= \frac{1}{V} (Y_p - Y_c) \tan \theta + Z_p \left| \frac{\cot \Phi}{\cos \theta} \right| + (t - \tau)_p - \frac{(X_p - X_d)}{V}. \tag{3-19}$$

For this linearly-varying-speed-of-sound atmosphere, the time interval between incident and reflected waves is

$$\Delta T_{ir_p} = \frac{2}{V} (D_{gv} - D_{pv})$$

$$= \frac{2}{V} \left( [(t-\tau)_p V - (X_p - X_d)] - [(t-\tau)_g V - (X_g - X_{dg})] \right) . \quad (3-20)$$

The $(X_g - X_{dg})$ term can be obtained from Equation (3-16); one can solve Equation (3-18) for $(t-\tau)_g$ with $Y = Y_g = Y_p$ and $Z = Z_g = 0$.

As in the first method, values of $T_{i_p}$ and $\Delta T_{ir_p}$ can thus be computed from geometric relations and flight and atmospheric information.

## Flight Altitudes Above the Tropopause

An explicit solution is not possible for a given offset distance from the flight track. A method will be proposed, however, which will permit the computation of local positions and arrival times of the wave.

For $Z_v \geq Z \geq Z_t$, where $Z_t$ is the altitude of the tropopause, the speed of sound is assumed to be constant. The disturbance envelope at time $t$ for a point disturbance emitted by the aircraft at $\tau$ is a cone:

$$(X - X_d)^2 + (Y - Y_d)^2 + (Z - Z_d)^2 = c_d^2 (t-\tau)^2 . \quad (3-21)$$

Differentiation of Equation (3-21) with respect to $Z$, and recognition of the identies for steady, level flight,

$$Y_d = 0, \ Z_d = Z_v, \ c_d = c_v, \ \dot{X}_d = V, \ \dot{Y}_d = 0, \ \dot{Z}_d = 0, \ \text{and} \ \dot{c}_d = 0,$$

gives

$$(X - X_d) = \frac{c_v (t-\tau)}{M} . \quad (3-22)$$

Equations (3-21) and (3-22) are combined and the result is

$$Y^2 + (Z - Z_v)^2 = c_v^2 (t-\tau)^2 \left( 1 - \frac{1}{M^2} \right) . \quad (3-23)$$

Differentiation of Equation (3-23) with respect to $Z$, and recognition of the orthogonal property between any ray and the disturbance envelope, gives

$$\frac{\partial Y}{\partial Z}\bigg|_{ray} = constant = \frac{Y}{(Z-Z_v)} . \tag{3-24}$$

When the tropopause conditions, $Y = Y_t$, and $Z = Z_t$, are substituted into Equations (3-23) and (3-24), the resulting expressions are

$$Y_t^2 + (Z_t - Z_v)^2 = c_v^2 (t_t - \tau)^2 \left(1 - \frac{1}{M^2}\right) , \tag{3-25}$$

and

$$\frac{\partial Y}{\partial Z}\bigg|_{ray} = \frac{Y_t}{(Z_t - Z_v)} . \tag{3-26}$$

For $Z_t \geq Z \geq 0$, the cone is "warped" by the temperature gradients and no exact analysis is available. For local wave positions and arrival times, however, it is sufficient to consider only the ray which reaches the given point. If the ray at the tropopause plane is considered to be a point disturbance, the previously developed equations will describe its path. Then the location of the wave can be found as a function of time, working point-by-point with a ray tracing procedure.

The equation for the disturbance envelope at time $t$ of a point disturbance emitted at time $t_t$ at the tropopause plane is

$$\cosh m(t-t_t) = \frac{M}{\left(Z-Z_t - \frac{c_t}{m}\right)} \left[ -\frac{Mc_t}{m} + \sqrt{\left(1 - \frac{1}{M^2}\right)\left[\left(\frac{Mc_t}{m}\right)^2 - \left(Z-Z_t - \frac{c_t}{m}\right)^2\right] - (Y-Y_t)^2} \right] . \tag{3-27}$$

Equation (3-27) can be solved as before, except that now the value of $Y_t$ is not known. An iterative method must be used:

1.    A value is assumed for $Y_t$.

2.    $t_t$ and $\frac{\partial Y}{\partial Z}\bigg|_{ray}$ at the tropopause are calculated by Equations (3-25)

and (3-26).

3.  The slope is assumed to be constant for a selected Z interval:

$$Y-Y_t = \frac{\partial Y}{\partial Z} \Delta Z \; ; \tag{3-28}$$

$$Z = Z_t - \Delta Z \; . \tag{3-29}$$

4.  $(t-t_t)$ is calculated from Equation (3-27) by the techniques explained earlier. The new-wave slopes are calculated as follows: From Equation (3-17), $\frac{\partial Y}{\partial Z}$ can be evaluated for the disturbance envelope which is everywhere perpendicular to the rays. For a point disturbance at the point $(X_t, Y_t, Z_t)$, Equation (3-17) is differentiated with respect to $Z$, after replacing Y with $Y-Y_t$, and the resulting expression is

$$\frac{2}{M^2} \left(Z-Z_t - \frac{c_t}{m}\right) \sinh^2 m(t-t_t) + 2(Y-Y_t) \left.\frac{\partial Y}{\partial Z}\right|_{\substack{\text{dist.}\\ \text{envel.}}}$$

$$+ 2\left(Z-Z_t - \frac{c_t}{m}\right) + 2\frac{c_t}{m} \cosh m(t-t_t) = 0 \; . \tag{3-30}$$

Since the disturbance and the ray are orthogonal,

$$\left.\frac{\partial Y}{\partial Z}\right|_{\substack{\text{dist.}\\ \text{envel.}}} \quad \left.\frac{\partial Y}{\partial Z}\right|_{\text{ray}} = -1 \; . \tag{3-31}$$

Equations (3-30) and (3-31) are simplified, and the result is

$$\left.\frac{\partial Y}{\partial Z}\right|_{\text{ray}} = (Y-Y_t) \left[\left(Z-Z_t - \frac{c_t}{m}\right)\left(1 + \frac{\sinh^2 m(t-t_t)}{M^2}\right) + \frac{c_t}{m} \cosh m(t-t_t)\right]^{-1}$$

$$\tag{3-32}$$

5.  Steps 3 and 4 are repeated until the desired Z value is obtained. If the computed Y does not give the desired location $Y_p$, a new $Y_t$ is selected and the procedure is repeated till the desired value is obtained.

6.  When the desired Y location is obtained to sufficient accuracy,

the $T_{i_p}$ value is computed by Equation (3-19) with the new intervals:

$$(t-\tau)_p = (t_t-\tau)_p + (t-t_t)_p \ , \tag{3-33}$$

and

$$(X_p-X_d) = (X_p-X_t) + (X_t-X_d) \ . \tag{3-34}$$

For the proper $Y_t$ value, Equations (3-33) and (3-34) can be solved from Equations (3-25), (3-27), (3-16), and the relation,

$$(X_t-X_d) = \frac{c_t}{m} (t_t-\tau)_p \ . \tag{3-35}$$

7. For the g location, steps 1 through 5 must be performed again, with all p subscripts replaced by g. $D_{gv}$ can now be found with $(t-\tau)_g$ and $(X_g-X_{dg})$ as was done for p in step 6.

8. $\Delta T_{ir_p}$ is computed with Equation (3-9).

With an IBM 1620 computer and 500 feet intervals for Z, about 70 seconds was required for each complete iteration for a 50,000 foot altitude.

This method is considered to be the most accurate prediction method available without specific meteorological information along the wave path for each flight.

## Method III

A third method was developed which attempted to reduce the computer time of Method II without sacrificing too much accuracy. The simplifying assumption added was that $\frac{dY}{dZ}$ of the ray was constant at the value of the flight altitude, while the linear variation of speed of sound with altitude below the tropopause was retained. The time of arrival of an incident wave is then given by:

$$T_{i_p} = \frac{1}{V}(X_p + D_{pv}) = \frac{1}{V}\left[X_p + \int_0^{S_p} \frac{dS}{\tan\beta}\right] . \tag{3-36}$$

S is the projected distance of the wave from the flight path in the YZ plane (see Figure 5), and

$$dS = \sqrt{(dY^2 + dZ^2)} = -dZ\sqrt{1 + \left(\frac{dY}{dZ}\right)^2} . \tag{3-37}$$

## Flight Altitudes Below the Tropopause

The assumptions and geometry give the following:

$$\frac{dY}{dZ}\bigg|_{ray} = \text{constant} = \frac{Y-Y_v}{Z-Z_v} , \quad Y_v = 0 ,$$

$$dS = -dZ\sqrt{1 + \left(\frac{Y}{Z-Z_v}\right)^2} , \tag{3-38}$$

$$c = c_g - mZ, \quad dZ = -\frac{dc}{m} ,$$

and

$$\tan\beta = \frac{1}{\sqrt{(M^2-1)}} = \frac{c}{\sqrt{(V^2-c^2)}} .$$

From Equations (3-3), (3-36), (3-37), and (3-38), the time interval from aircraft passage over the origin, O, until wave arrival at point P can be calculated:

$$T_{i_p} = \frac{1}{V}\left[X_p + \sqrt{1 + \left(\frac{Y_p}{Z_p-Z_v}\right)^2}\int_{c_v}^{c_p} \frac{V^2-c^2}{mc} dc\right]$$

$$= \frac{1}{V}\left[(Y_p-Y_c)\tan\theta + Z_p\left|\frac{\cot\Phi}{\cos\theta}\right|\right] + \frac{1}{mV}\sqrt{1 + \left(\frac{Y_p}{Z_p-Z_v}\right)^2}$$

$$\left[\sqrt{V^2-c_p^2} - \sqrt{V^2-c_v^2} + V\ln\left(\frac{V+\sqrt{V^2-c_v^2}}{V+\sqrt{V^2-c_p^2}}\frac{c_p}{c_v}\right)\right] , \tag{3-39}$$

$$T_{i_g} = \frac{1}{V}\left[(Y_p - Y_c)\tan\theta + Z_p\left(\frac{\cot\Phi}{\cos\theta}\right)\right] + \frac{1}{mV}\sqrt{1 + \frac{Y_p}{Z_p}^2}$$

$$\left[\sqrt{V^2 - c_g^2} - \sqrt{V^2 - c_v^2} + V\ln\left(\frac{V + \sqrt{V^2 - c_v^2}}{V + \sqrt{V^2 - c_g^2}}\frac{c_g}{c_v}\right)\right] \, . \qquad (3\text{-}40)$$

Equations (3-39), (3-6), and (3-40), permit $T_{i_p}$ and $\Delta T_{ir_p}$ to be computed.

## Flight Altitudes Above the Tropopause

The assumption of constant $\frac{dY}{dZ}$ eliminates the iterative solution which was required in Method II. The time of arrival of an incident wave be expressed as

$$T_{i_p} = \frac{1}{V}\left[X_p + \int_0^{S_p}\frac{dS}{\tan\beta}\right] = \frac{1}{V}\left[X_p + \int_0^{S_t}\frac{dS}{\tan\beta} + \int_{S_t}^{S_p}\frac{dS}{\tan\beta}\right] \, . \qquad (3\text{-}41)$$

In view of the assumptions,

$$c = \text{constant in the region } Z_v \geq Z \geq Z_t \, ,$$

$$\frac{Y_t}{Z_t - Z_v} = \text{constant} = \frac{Y_p}{Z_p - Z_v} \, ,$$

the integral terms in equation (3-41) become

$$\int_0^{S_t}\frac{dS}{\tan\beta} = \frac{Z_v - Z_t}{c_v}\sqrt{V^2 - c_v^2}\sqrt{1 + \left(\frac{Y_t}{Z_t - Z_v}\right)^2} \, , \qquad (3\text{-}42)$$

and

$$\int_{S_t}^{S_p}\frac{dS}{\tan\beta} = \frac{1}{m}\sqrt{1 + \frac{Y_p}{Z_p - Z_v}^2}\left[\sqrt{V^2 - c_p^2} - \sqrt{V^2 - c_v^2} + V\ln\left(\frac{V + \sqrt{V^2 - c_v^2}}{V + \sqrt{V^2 - c_p^2}}\frac{c_p}{c_v}\right)\right] \, . \qquad (3\text{-}43)$$

Equations (3-41), (3-42), and (3-43) are combined and the resulting expressions for $T_{i_p}$ and $T_{i_g}$ are:

$$T_{i_p} = \frac{1}{V}\left[(Y_p - Y_c)\tan\theta + Z_p\left(\frac{\cot\Phi}{\cos\theta}\right)\right] + \frac{1}{V}\sqrt{1 + \left(\frac{Y_p}{Z_p - Z_v}\right)^2}\left[\frac{Z_v - Z_t}{c_v}\right.$$

$$\left.\sqrt{V^2 - c_v^2} + \frac{\sqrt{V^2 - c_p^2}}{m} - \frac{\sqrt{V^2 - c_v^2}}{m} + \frac{V}{m}\ln\left(\frac{V + \sqrt{V^2 - c_v^2}}{V + \sqrt{V^2 - c_p^2}}\frac{c_p}{c_v}\right)\right], \qquad (3\text{-}44)$$

and

$$T_{i_g} = \frac{1}{V}\left[(Y_p - Y)\tan\theta + Z_p\left(\frac{\cot\Phi}{\cos\theta}\right)\right] + \frac{1}{V}\sqrt{1 + \left(\frac{Y_p}{Z_p}\right)^2}\left[\frac{Z_v - Z_t}{c_v}\sqrt{V^2 - c_v^2}\right.$$

$$\left.+ \frac{\sqrt{V^2 - c_g^2}}{m} - \frac{\sqrt{V^2 - c_v^2}}{m} + \frac{V}{m}\ln\left(\frac{V + \sqrt{V^2 - c_v^2}}{V + \sqrt{V^2 - c_g^2}}\frac{c_g}{c_v}\right)\right]. \qquad (3\text{-}45)$$

From Equations (3-44), (3-6), and (3-45), $T_{i_p}$ and $\Delta T_{ir_p}$ can be computed.

Method III is much more straight forward for computation than Method II, but the assumption of constant ray angle places its accuracy in doubt. Therefore, a number of typical cases were computed by the three methods to provide a comparison of the results.

### Computed Results by the Three Methods and Observations

In order to compare the three methods, computations were performed for a vertical wall location of 100 feet above ground level. The ground level was assumed to be at sea level, and flight altitudes of 70,000, 36,000, and 20,000 feet were used. For flight Mach numbers of 1.5, 2.0, and 3.0 and offset distances, $Y_p$, from 0 to 70,000 feet, the three methods gave values of incident wave arrival time, $T_{i_p}$, and time interval between incident and reflected waves, $\Delta T_{ir_p}$. The results are plotted in Figures 7 and 8.

For small offset distances, the three methods give almost identical results. The differences are greatest at low Mach numbers and

large $Y_p$ values. Method I, the conical wave analysis, gives the poorest accuracy, if it is assumed that Method II is the most exact of the three. Method III, which is considerably easier to calculate, appears to be nearly equivalent to Method II, and is the one rec-commended for use.

The computation methods developed in this Chapter provide a means of establishing geometric relationships between an incident sonic boom bow wave and its ground reflection and a plane wall. This knowledge can be used as the starting point for further computations of the whole sonic boom wave pattern as it proceeds around, over, or past a complete structure.
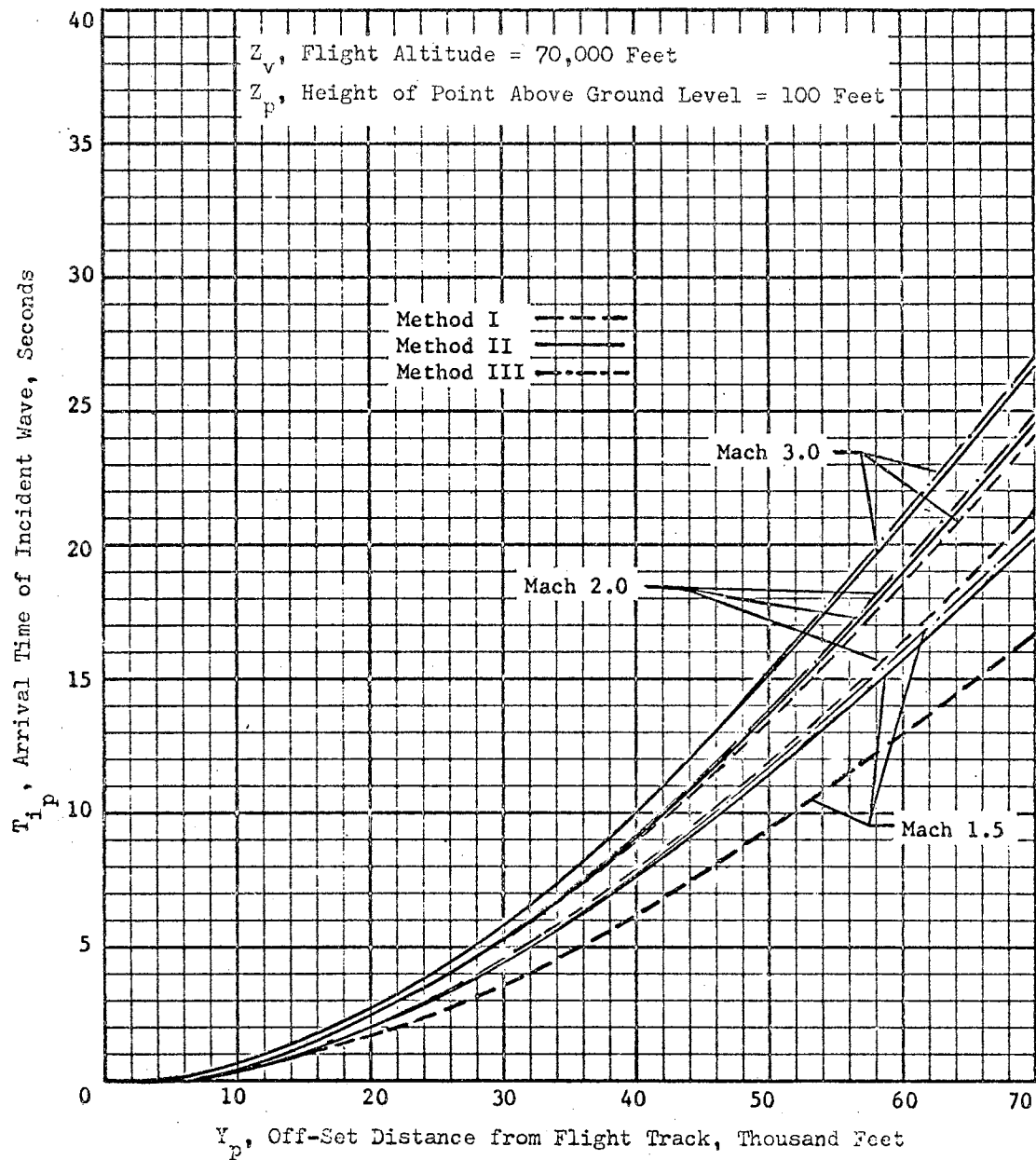
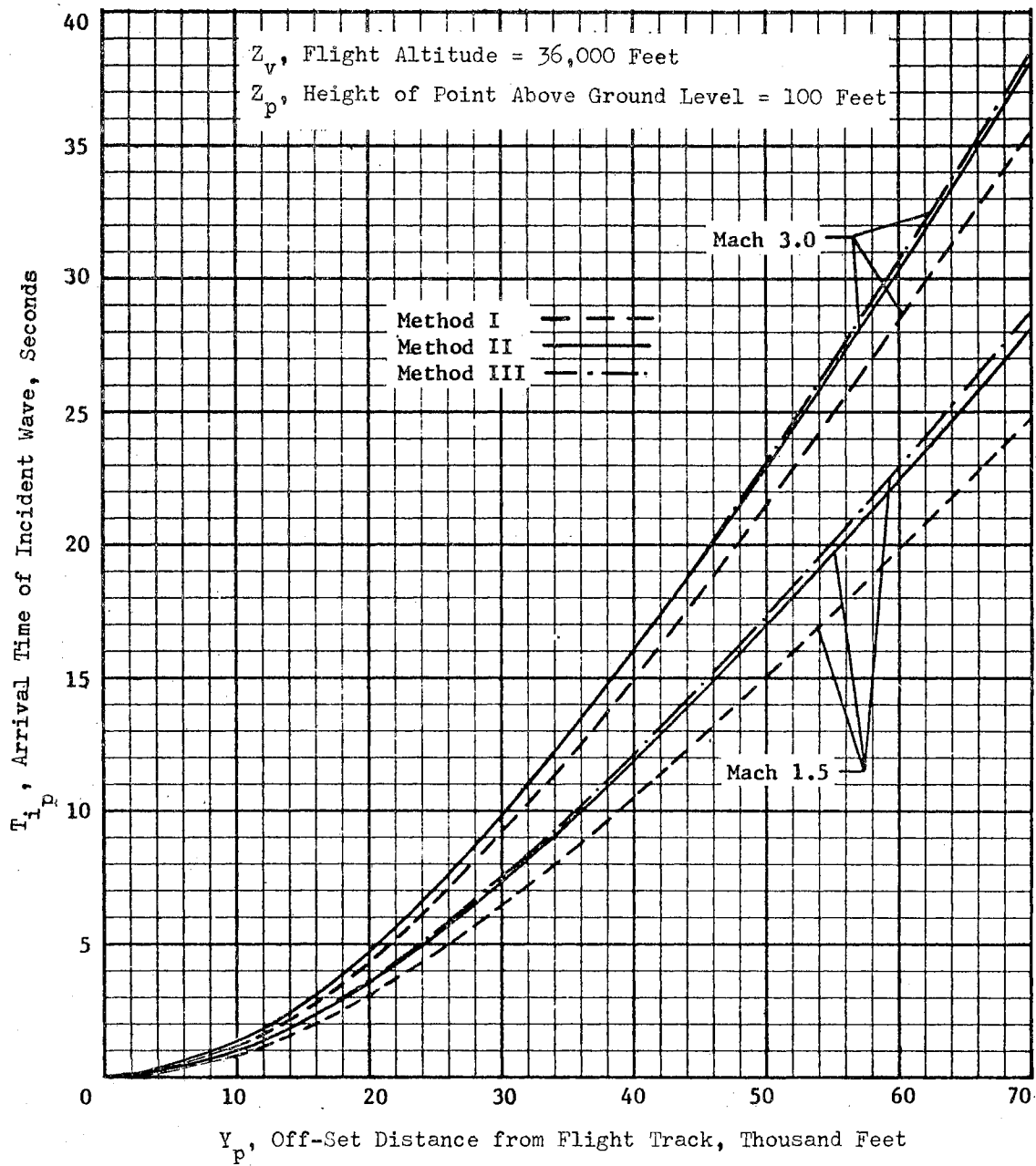Figure 7. Comparison of Incident Wave Arrival Times by the Three Methods
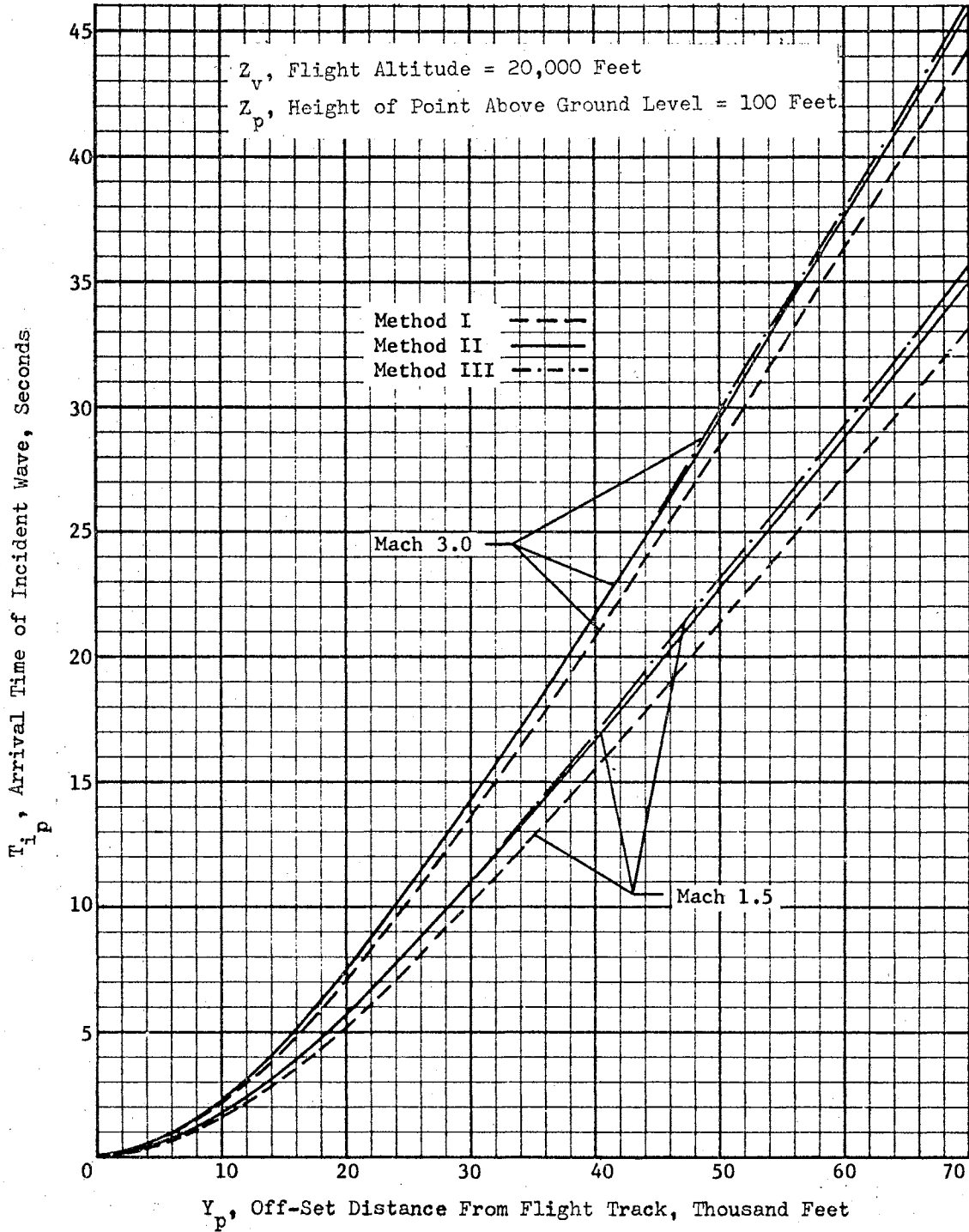
Figure 7. (continued)
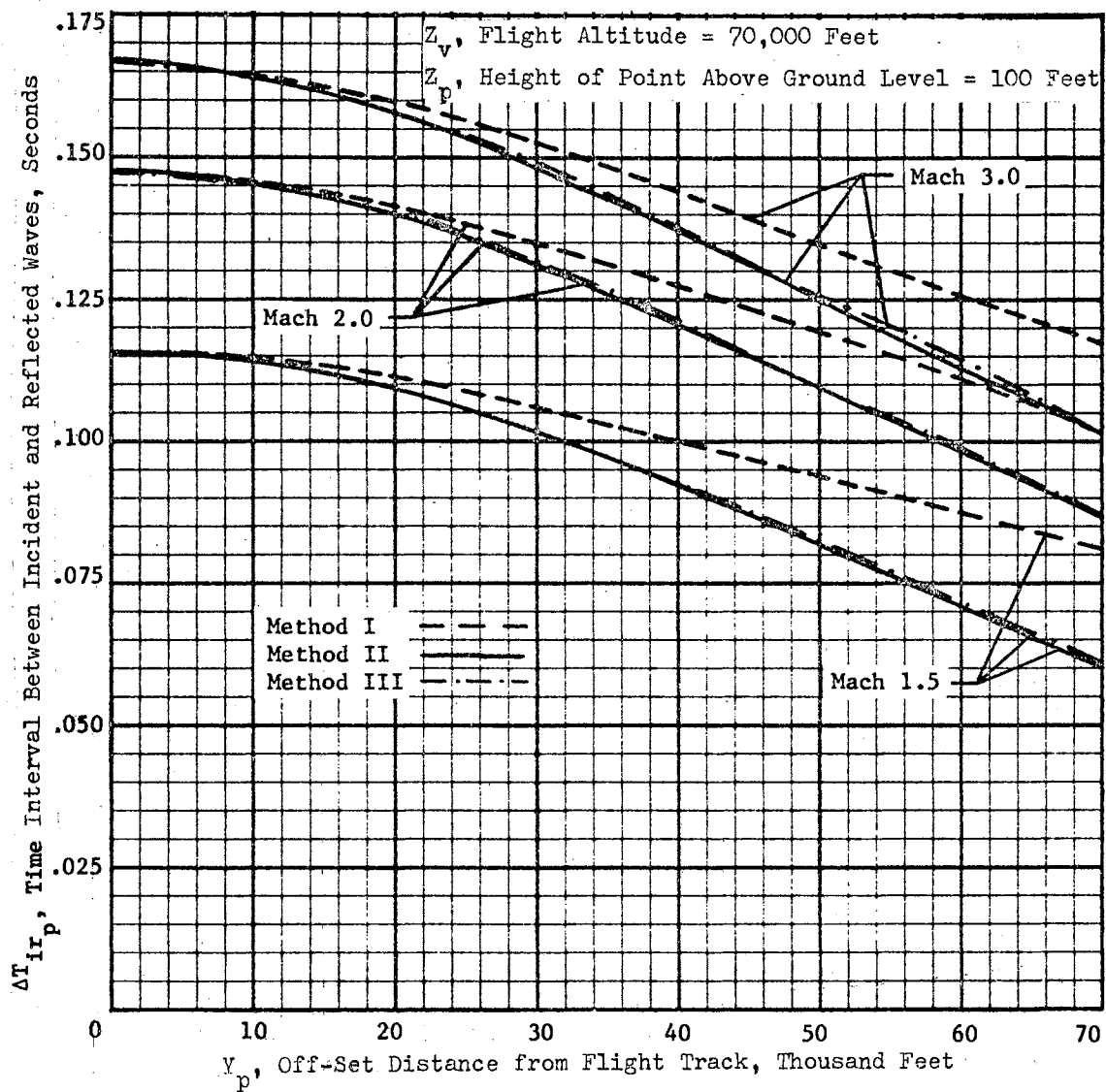
Figure 7. (continued)

Figure 8. Comparison of the Time Intervals Between Incident
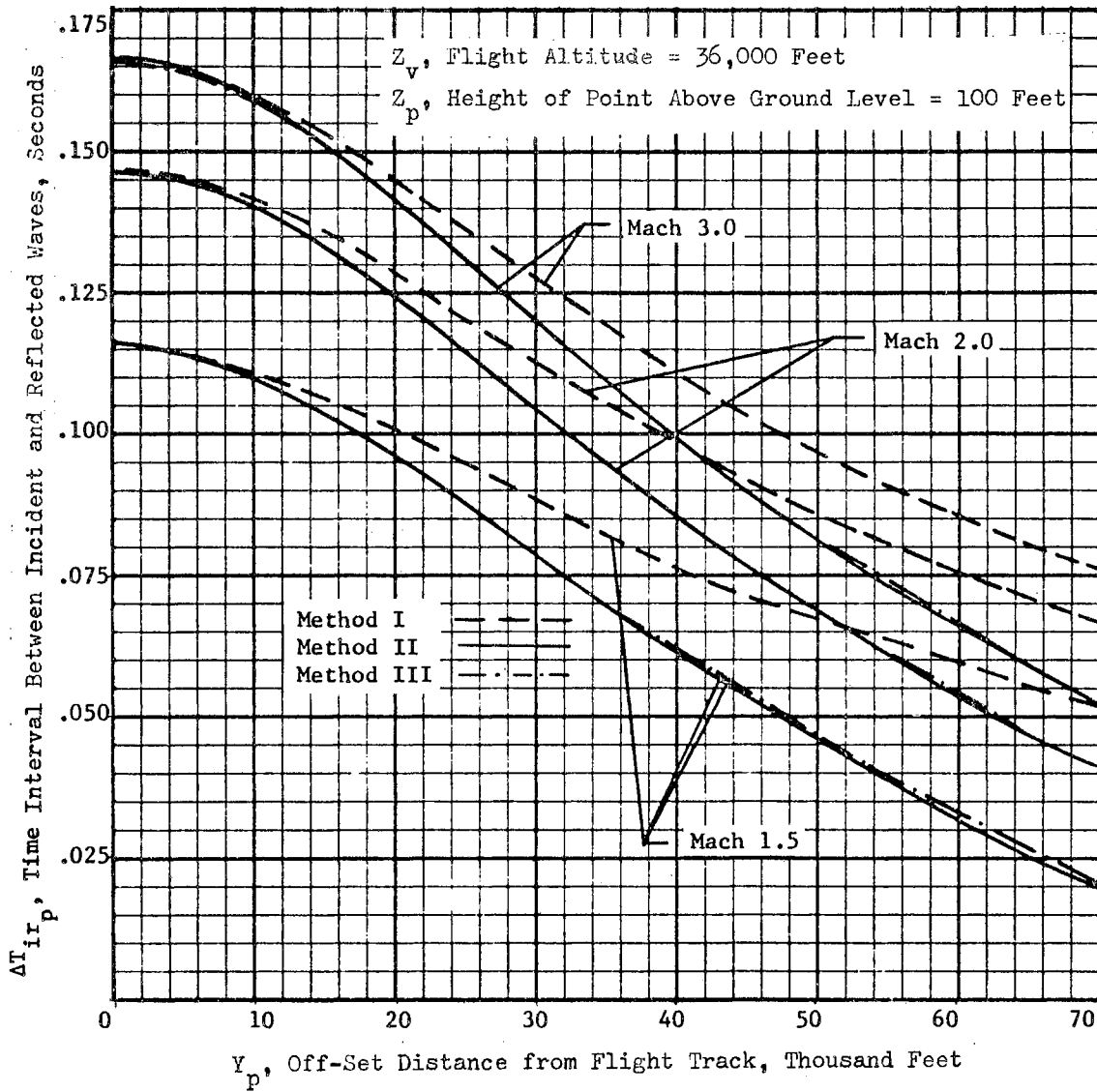and Reflected Waves computed by the Three
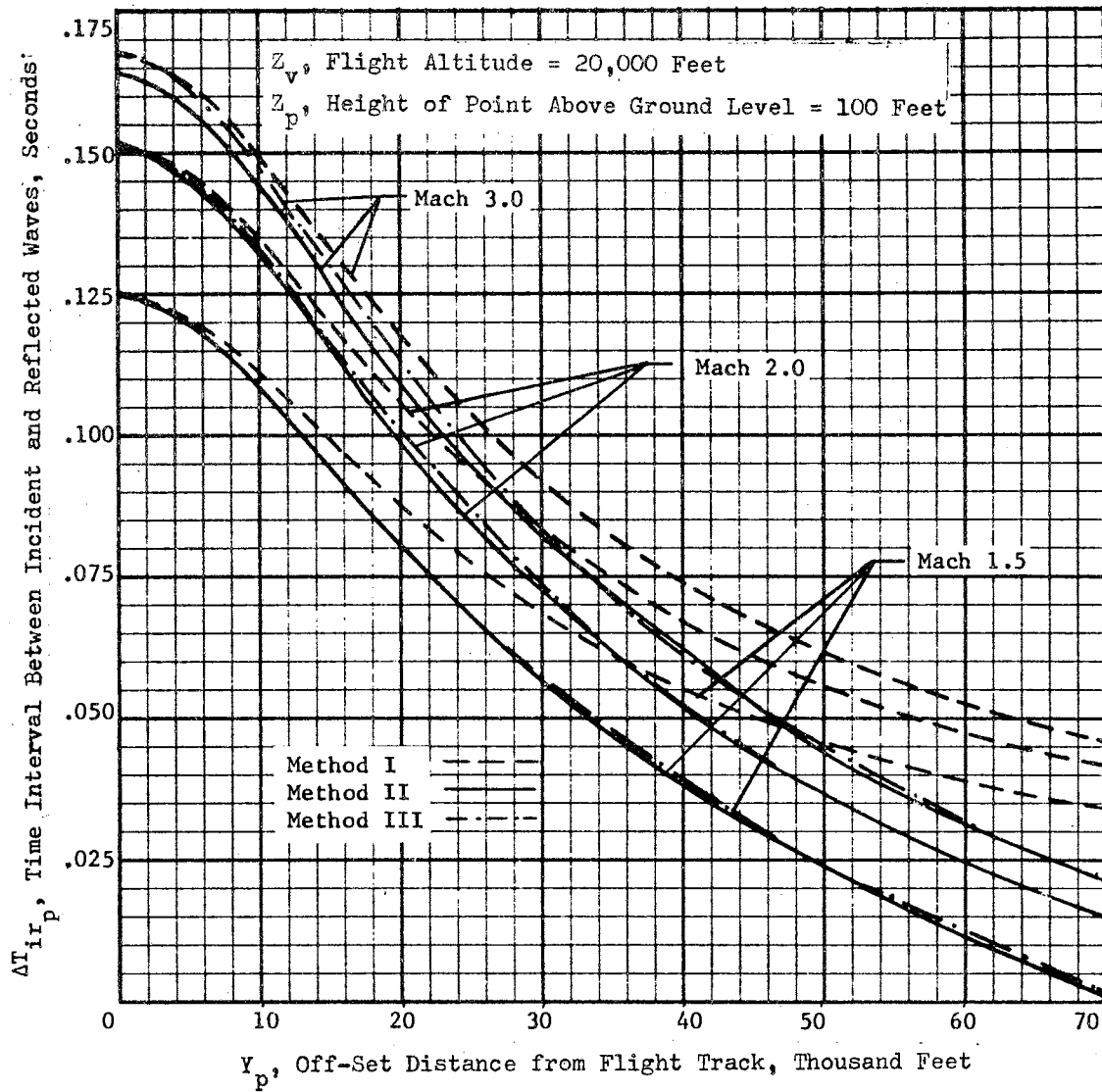Methods

Figure 8. (continued)

Figure 8. (continued)

CHAPTER IV

DIFFRACTION AND REFLECTION OF SONIC BOOM

WAVES - ANALYTICAL METHOD

The preceding chapter presented three methods for predicting the

wave histories of walls which were hit directly by a sonic boom wave.

For walls which are in the "shadow" or which receive the reflected

effects of nearby walls or corners, a further development is required.

As an example, the broken window in the Kinney Shoe Store, whose

solution is presented in Chapter VI, was both in the shadow region and

beneath an overhanging canopy. In the time interval between bow and

tail shock waves, there was sufficient time for about twenty wave

reflections between the ground and the overhanging roof. It is

obviously hopeless to attempt to predict the pressure history on the

window without reliance on a computer programmed analysis to include

both wave input and proper boundary conditions. In this section, an

analytical solution for diffraction and reflection of weak pulses or

weak shocks, developed by Keller and Blank (14), is described. This

solution is then extended to a sonic boom problem by making use of

weak shock reflection principles.

Sonic booms may be considered to act as acoustic waves, or plane

weak pulses, since they are weak shock waves. In Reference 14, the

diffraction and reflection of an incident plane pulse by wedges and

corners were treated and explicit, closed-form expressions were

obtained in terms of elementary functions. For this geometry the
solution is "conical" and independent of "radial" distance in the xyt
space. This allows separation into appropriate coordinates, as is
done in Busemann's conical flow method which is widely used in super-
sonic aerodynamics. The propagation of plane discontinuities was
investigated by Luneberg (12) in electromagnetic theory, and by Keller
(13) in acoustics. It was found in both cases that the discontinuity
surface satisfies a first order differential equation, the eiconal
equation, in a homogenous media, and that the magnitude of the dis-
continuity varies in a simple manner. Making use of these results,
Blank and Keller (14) converted the initial-boundary value problem
into a characteristic-boundary value problem in xyt space and then
used the conical flow method to obtain the solution. A similar pro-
cedure will be followed here.

A solution is sought to the acoustic wave equation in the two-
dimensional geometry of Figure 9: (subscripts represent differentiation)

$$p_{xx} + p_{yy} = \frac{1}{c^2} p_{tt} \qquad \text{for } \Phi \leq \theta \leq 2\pi - \Phi \qquad (4\text{-}1)$$

where

$$p = \frac{P - P_o}{P_1 - P_o} \quad ,$$

$$\theta = \arctan y/x .$$

By definition, the half-plane at $\theta = \pm \Phi$ form either a wedge or a
corner, depending on whether $\Phi$ is less or greater than $90^o$.

The solution to be considered will have jump discontinuities on
a certain moving surface representing a shock wave, say $r(x,y) = ct$.
It is required that r should satisfy the eiconal equation:

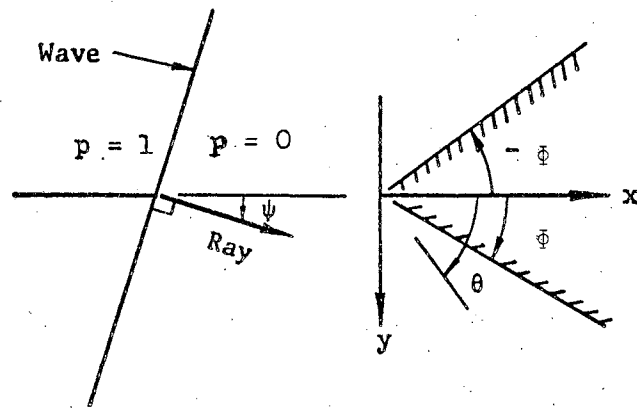$$r_x^2 + r_y^2 = 1 . \qquad (4\text{-}2)$$

Figure 9.  Incident Wave on a Wedge

This implies that the surface can be constructed by Huygen's principle, i.e., that it moves with velocity c along its normal, and that it is reflected from the wall in accordance to the simple reflection law. A further assumption is that the reflected discontinuity value is twice the incident discontinuity value for a rigid wall. The orthogonal trajectories of a family of discontinuity surfaces S(t) are straight lines called "rays". The set of rays through a small closed curve on a discontinuity surface is called a "tube". The areas of the tubes at $S(t_o)$ and at S(t), are denoted by $dS_o$ and dS respectively. Also, the pressure discontinuities at $S(t_o)$ and S(t) are denoted as $p_o$ and p respectively. Then, for plane geometry, the magnitudes of the discontinuities must vary inversely as $\sqrt{dS}$ :

$$\lim_{dS \to 0} \left(\frac{dS}{dS_o}\right)^{\frac{1}{2}} = \frac{p_o}{p} .$$ (4-3)

Equation (4-3) permits p to be computed from $p_o$ on the same ray, once the geometry of the discontinuity surfaces are known.

In Figure 9, the ray direction is normal to the discontinuity plane and is positive in the direction of motion. The angle between the ray direction and the x axis is $\psi$, and it is always positive. It follows from Equation (4-2) that a plane discontinuity surface moves parallel to itself with velocity c along its normal and from Equation (4-3) that a pressure jump, p = 1, across the wave does not change. This situation continues until the wave front reaches the wedge. Then reflected and diffracted discontinuity surfaces may originate. These surfaces can be obtained from the configuration at the instant of contact. Then the incident plane progresses to itself, and one (for $\psi \geq \Phi$) or two (for $\psi < \Phi$) reflected plane discontinuity surfaces,

plus a cylindrical surface with the wedge as its axis, are produced as shown in Figures 10a and 10b.

The pressure jump across the original plane is unchanged and the jump across the reflected wave is equal to that of the incident wave, making p = 2. The pressure jump across the cylindrical wave is zero, however, since all rays reaching it come from the axis where $dS_o$ vanishes. Thus, p is not discontinuous across the cylinder. The value of p everywhere outside the cylinder is known (either 0, 1, or 2). Since $\frac{\partial p}{\partial n} = 0$ on the wedge and p is continuous across the circular arc, the values on the boundary are known. From these values it is possible to determine the p values within the cylinder.

The wave patterns are self-similar with respect to time, and so can be represented in $\frac{x}{ct}$ and $\frac{y}{ct}$ coordinates, as in Figures 11a and 11b. Solutions are to be sought inside the circle along radial lines from the origin. A set of special coordinates in xyt space will be used for this solution, which follows the method of Keller and Blank (14). The coordinates are

$$r = [c^2 t^2 - (x^2 + y^2)]^{\frac{1}{2}} ,$$
$$s = \frac{ct}{r} , \tag{4-4}$$
$$\theta = \arctan y/x .$$

The boundary of the circle is given by r = 0 and s = ∞. Then Equation (4-1) becomes

$$(r^2 p_r)_r + [(1 - s^2)p_s]_s + \frac{1}{1 - s^2} p_{\theta\theta} = 0 . \tag{4-5}$$

In accordance with the assumption of similarity, p = p(s, θ), Equation (4-5) becomes

$$[(1 - s^2)p_s]_s + \frac{1}{1 - s^2} p_{\theta\theta} = 0 . \tag{4-6}$$
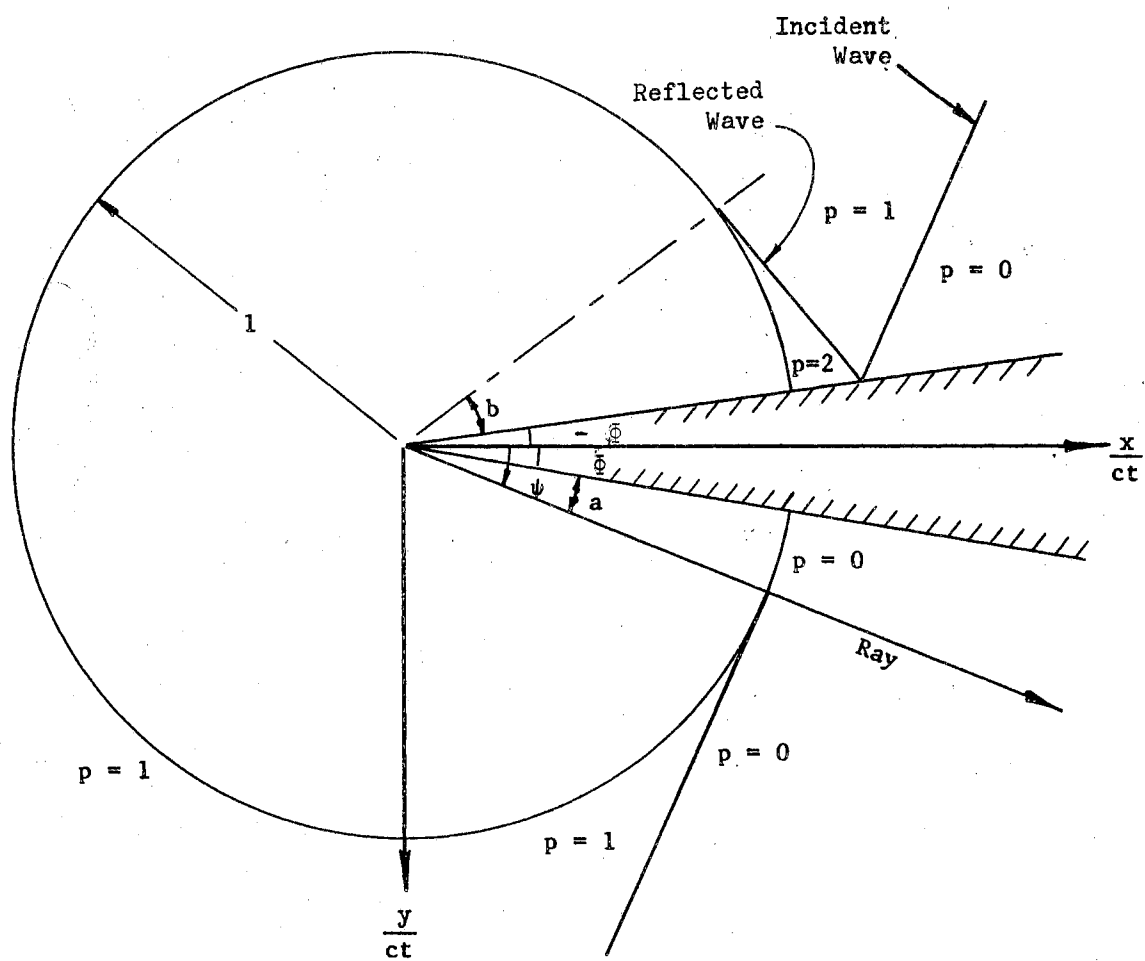
(a)  $\psi \geq \bar{\phi}$  (One Reflected Wave)

Figure 10. Diagram of a Plane Wave Intersecting a Wedge
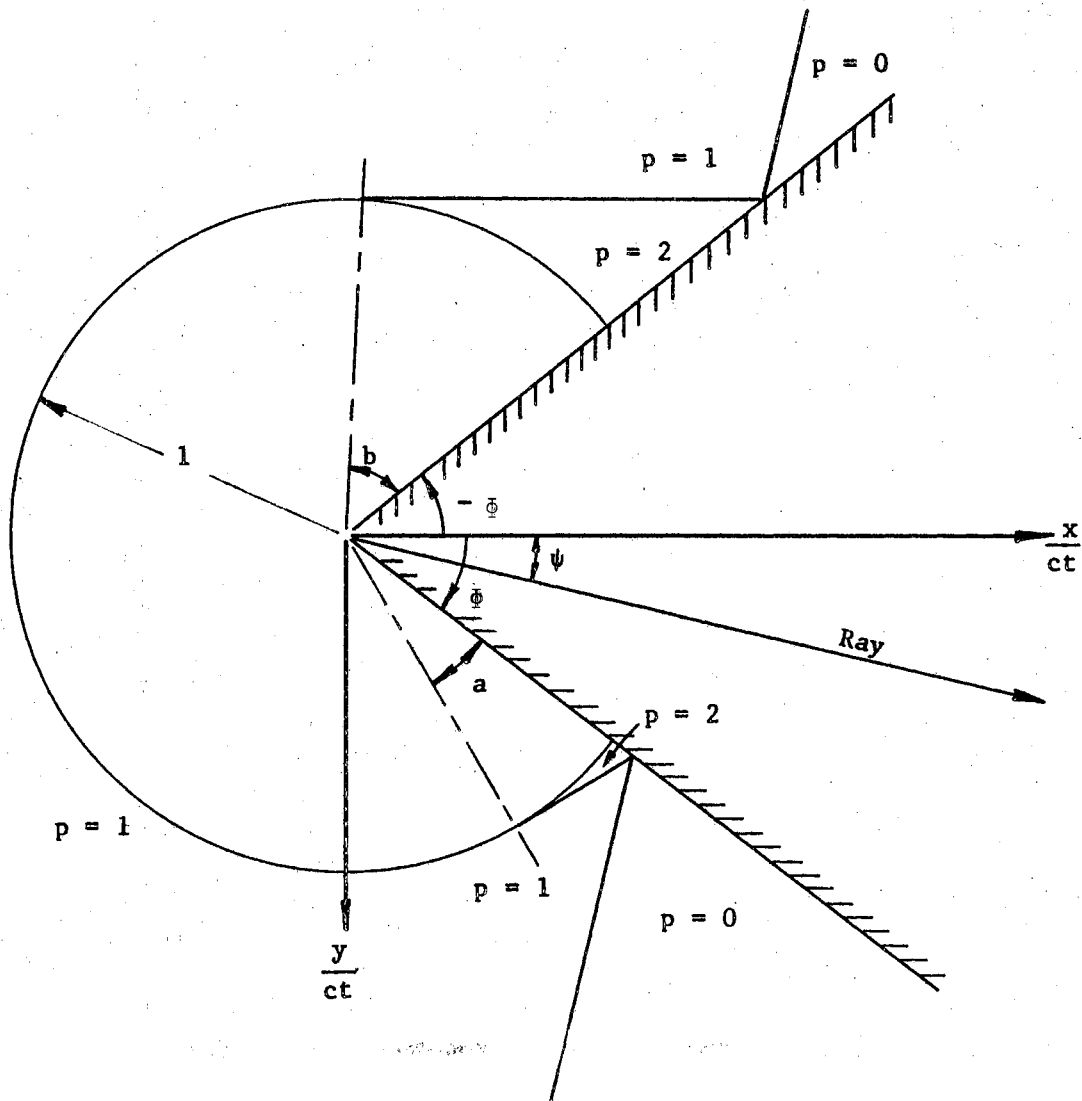
(b)  $\psi < \phi$ (Two Reflected Waves)

Figure 10.  (continued)

(a)  $\psi \geq \Phi$



(b)  $\psi < \Phi$

Figure 11.  Complex Plane Wedge/Shock Representation

If $\rho$ is defined as

$$\rho = \left(\frac{s - 1}{s + 1}\right)^{\frac{1}{2}} , \tag{4-7}$$

then Equation (4-6) reduces to a Laplace equation:

$$\rho \frac{\partial}{\partial \rho} \left(\rho \frac{\partial p}{\partial \theta}\right) + \frac{\partial^2 p}{\partial \theta^2} . \tag{4-8}$$
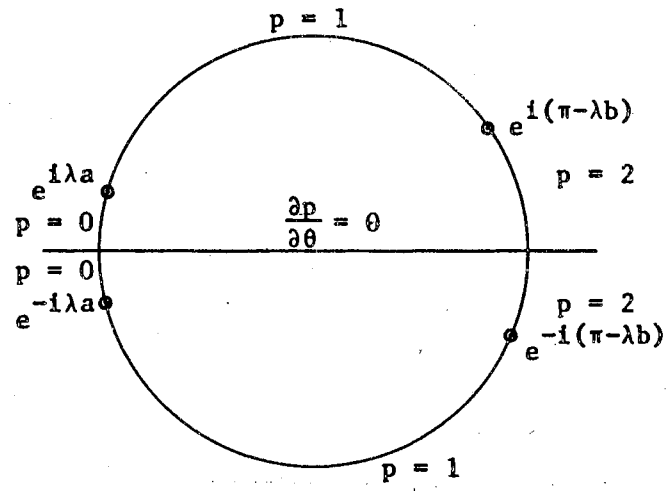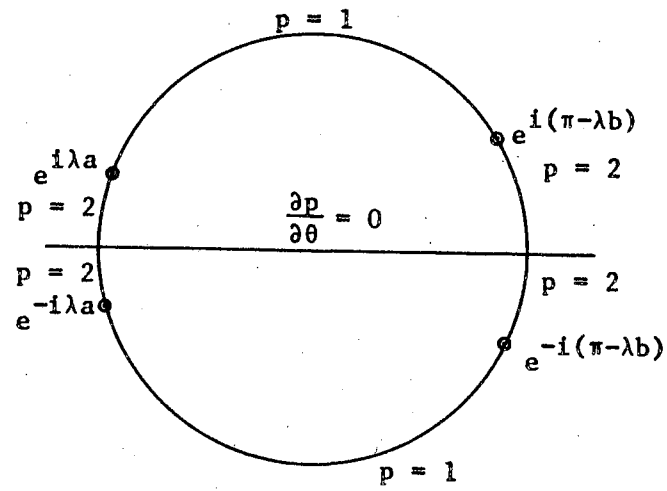
The solution to Equation (4-8) may be written in the form

$$p = \text{Im } f(z) , \tag{4-9}$$

where $f(z)$ is an analytic function of the complex variable, $z = \rho e^{i\theta}$ . Lettering $R = (x^2 + y^2)^{\frac{1}{2}}$ , and combining Equations (4-4) and (4-7), gives

$$z = \rho e^{i\theta} = \frac{x + iy}{ct + (c^2 t^2 - R^2)^{\frac{1}{2}}} , \tag{4-10}$$

and

$$\rho = \frac{R}{ct + (c^2 t^2 - R^2)^{\frac{1}{2}}} . \tag{4-11}$$

The cone $R \leq ct$ is thus mapped into the unit circle $\rho \leq 1$. The problem has been reduced to that of finding the function which is analytic in an appropriate sector of the unit circle with the pre-scribed imaginary part of the boundary.

The values of p on the boundary of the circle in Figure 10a, for $\psi \geq \Phi$ , are

$$\begin{aligned}
p &= 0 \text{ on } \rho = 1, \quad \Phi \leq \theta \leq \Phi + a , \\
p &= 1 \text{ on } \rho = 1, \quad \Phi + a < \theta \leq 2\pi - \Phi - b , \\
p &= 2 \text{ on } \rho = 1, \quad 2\pi - \Phi - b < \theta \leq 2\pi - \Phi , \\
\frac{\partial p}{\partial \theta} &= 0 \text{ on } 0 \leq \rho \leq 1, \quad \theta = \Phi \text{ and } \theta = 2\pi - \Phi .
\end{aligned} \tag{4-12}$$

For Figure 10b, where $\psi < \Phi$, the boundary values are

$$p = 2 \text{ on } \rho = 1, \quad \Phi \leq \theta \leq \Phi + a ,$$

$$p = 1 \text{ on } \rho = 1, \quad \Phi + a < \theta \leq 2\pi - \Phi - b ,$$

$$p = 2 \text{ on } \rho = 1, \quad 2\pi - \Phi - b < \theta \leq 2\pi - \Phi ,$$

$$\frac{\partial p}{\partial \theta} = 0 \text{ on } 0 \leq \rho \leq 1, \quad \theta = \Phi \text{ and } \theta = 2\pi - \Phi .$$

(4-13)

In order to solve for p, the exterior wedge will be mapped from the z plane onto the upper half of the w plane by the transformation

$$w = \rho_1 e^{i\omega} = (e^{-i\Phi} z)^\lambda ,$$

(4-14)

where

$$\lambda = \frac{\pi}{2(\pi - \Phi)} .$$

If the value for z is substituted in Equation (4-14), the resulting relations are

$$\rho_1 = \rho^\lambda , \quad \omega = \lambda(\theta - \Phi) = \lambda(\theta - \pi) + \frac{\pi}{2} .$$

(4-15)

The circular sector in which p is to be determined becomes a semi-circle in the w plane with $\frac{\partial p}{\partial \theta} = 0$ on the diameter (into which the sides of the wedge transform). By the reflection principle one may extend p into the whole plane, and obtain a boundary value problem in the unit circle as shown in Figure 11.

The next step is the determination of a harmonic function p with piecewise constant boundary values. The solution of the problem may be obtained as the sum of the solutions, each of which takes on a specified constant value on the arc of the circle and is zero on all other arcs. If $\omega_2 > \omega_1$ with $\omega_2 - \omega_1 < 2\pi$ and p is a constant, K, on the arc $\omega_2 \geq \omega \geq \omega_1$ and p = 0, then p can be shown in take the form (Reference 14)

$$p = \frac{K}{\pi} \left[ \arg \left| \frac{w - \exp(i\omega_2)}{w - \exp(i\omega_1)} \right| - \frac{\omega_2 - \omega_1}{2} \right] ,$$

(4-16)

and in terms of real variables it becomes

$$p = \frac{K}{\pi} \arctan \left[ \frac{(1-\rho_1^2)\,\sin\left(\frac{\omega_2-\omega_1}{2}\right)}{(1+\rho_1^2)\cos\left(\frac{\omega_2-\omega_1}{2}\right) - 2\rho_1\cos\left(\omega - \frac{\omega_2-\omega_1}{2}\right)} \right] \, . \qquad (4\text{-}17)$$

The arctangent is taken in the interval between 0 and $\pi$. The solutions may then be written explicitly as follows:

Case 1, $\Phi \leqslant \psi \leqslant \frac{\pi}{2} - \Phi$ ,

$$p = 1 - \frac{1}{\pi} \arctan \left[ \frac{-(1-\rho^{2\lambda})\cos\lambda(\psi-\pi)}{(1+\rho^{2\lambda})\sin\lambda(\psi-\pi) - 2\rho^\lambda\sin\lambda(\theta-\pi)} \right]$$

$$+ \frac{1}{\pi} \arctan \left[ \frac{-(1-\rho^{2\lambda})\cos\lambda(\psi+\pi)}{(1+\rho^{2\lambda})\sin\lambda(\psi+\pi) - 2\rho^\lambda\sin\lambda(\theta-\pi)} \right] \, , \qquad (4\text{-}18)$$

Case 2, $0 \leqslant \psi \leqslant \Phi$

$$p = 1 + \frac{1}{\pi} \arctan \left[ \frac{(1-\rho^{2\lambda})\cos\lambda(\psi-\pi)}{(1+\rho^{2\lambda})\sin\lambda(\psi-\pi) - 2\rho^\lambda\sin\lambda(\theta-\pi)} \right]$$

$$+ \frac{1}{\pi} \arctan \left[ \frac{-(1-\rho^{2\lambda})\cos\lambda(\psi+\pi)}{(1+\rho^{2\lambda})\sin\lambda(\psi+\pi) - 2\rho^\lambda\sin\lambda(\theta-\pi)} \right] \, . \qquad (4\text{-}19)$$

## Application to a Sonic Boom Wave Incident on a Building

Using Equations (4-18) or (4-19), one can compute the pressure distribution in a circular arc of radius ct surrounding a corner of a structure struck by a sonic boom wave. The circle defines the region in which the wave is diffracted and reflected due to the presence of the corner.

Let:   t — time elapsed since the wave hit the corner of the structure,

H — height of the structure.

Then, if $ct > H$, the circular sector has reached the ground and has been reflected; the previous formulae cannot be applied directly. Sonic boom waves are always associated with incident bow and tail waves with an expansion region in between them (the "N" wave). In addition, both bow and tail waves have ground-reflected waves. The pressure distribution of a sonic boom can be computed as the algebraic sum of the pressure distributions of each of these elements: bow wave (incident and reflected), expansion wave region, and tail wave (incident and reflected). A few multiple reflected disturbance regions of a sonic boom wave past a right angled corner are shown in Figure 12. For this case, $\psi = 0$ and $\Phi = \dfrac{\pi}{4}$. So Equation (4-19) may be used to compute the pressure distribution of a diffracted incident wave at point $(x_1, y_1)$ in the neighborhood of the corner. Pressure distribution at any time is a function of the height of the point above ground level and the geometry of the reflected disturbance regions.

In the interval $0 \leq ct \leq \sqrt{x_1^2 + y_1^2}$, (Figure 12a), $p(x_1, y_1) = 0$, 1, or 2; the value depends on the wave location at the time.

In the interval $\sqrt{x_1^2 + y_1^2} < ct \leq \sqrt{x_1^2 + (2H-y_1)^2}$, (Figure 12b), $p(x_1, y_1)$ can be computed from the equation for disturbance $C_1$ only. Thus, $p_1$, the pressure disturbance at $p$ due to $C_1$, is computed by means of

$$\theta = \arctan (y_1/x_1) - \Phi, \text{ and } R = \sqrt{x_1^2 + y_1^2} \; ; \; p = p_1 .$$

In the interval $\sqrt{x_1^2 + (2H-y_1)^2} < ct \leq 2H + \sqrt{x_1^2 + y_1^2}$, (Figure 12c), $p(x_1, y_1)$ can be computed by treating the point as affected by $C_1$ and its ground reflected disturbance $C_2$, where $C_2$ is treated as a mirror image of $C_1$:
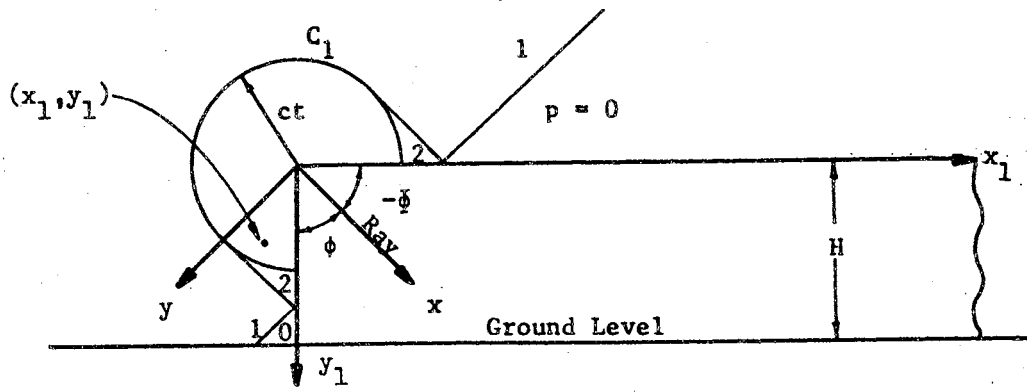
(a)  Phase I:  $0 \leq ct \leq \sqrt{x_1^2 + y_1^2}$
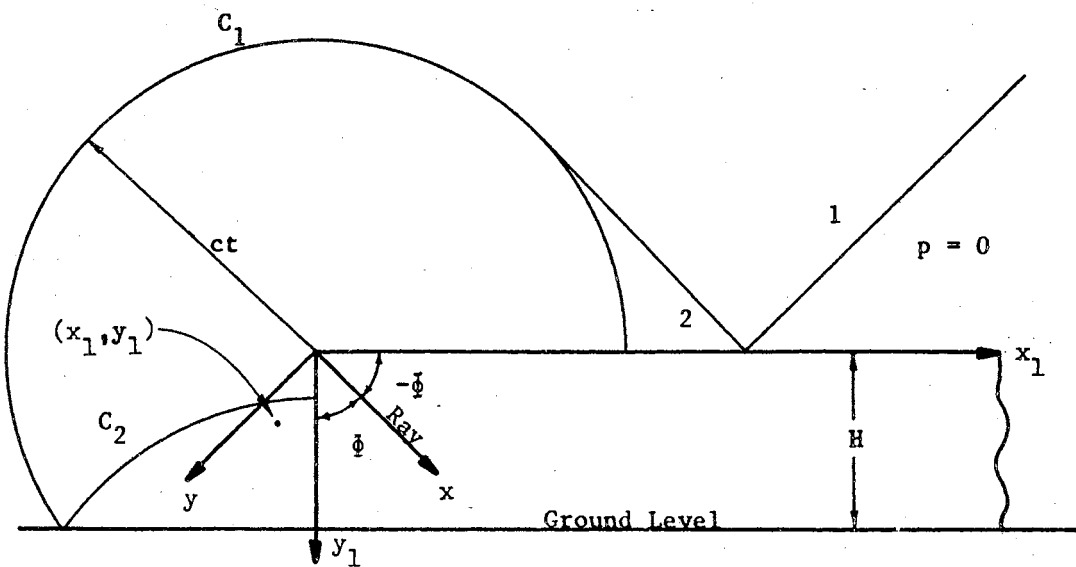
(b)  Phase II:  $\sqrt{x_1^2 + y_1^2} < ct \leq \sqrt{x_1^2 + (2H - y_1)^2}$

Figure 12.  Wave Reflection by a building

(c)  Phase III:  $\sqrt{x_1^2 + (2H - y_1)^2} < ct \leq 2H + \sqrt{x_1^2 + y_1^2}$

Figure 12. (continued)

(d)   Phase IV:   $2H + \sqrt{x_1^2 + y_1^2} < ct \leq 2H + \sqrt{x_1^2 + (2H - y_1)^2}$

Figure 12. (continued)

$$p_2(x_1,y_1) = p_1(x_1, 2H-y_1).$$

$p_{2b}(x_1,y_1)$ is the pressure at the boundary of the region $C_2$, which may be calculated as the boundary pressure of $C_1$ with

$$\theta = \arctan\left[(2H-y_1)/x_1\right] - \Phi .$$

Then:

$$p(x_1,y_1) = p_1(x_1,y_1) + p_2(x_1,y_1) - p_{2b}(x_1,y_1),$$

where

for $p_1$, $R = \sqrt{x_1^2 + y_1^2}$ and $\theta = \arctan(y_1/x_1) - \Phi,$

for $p_2$, $R = \sqrt{x_1^2 + (2H-y_1)^2}$ and $\theta = \arctan\left[(2H-y_1)/x_1\right] - \Phi,$

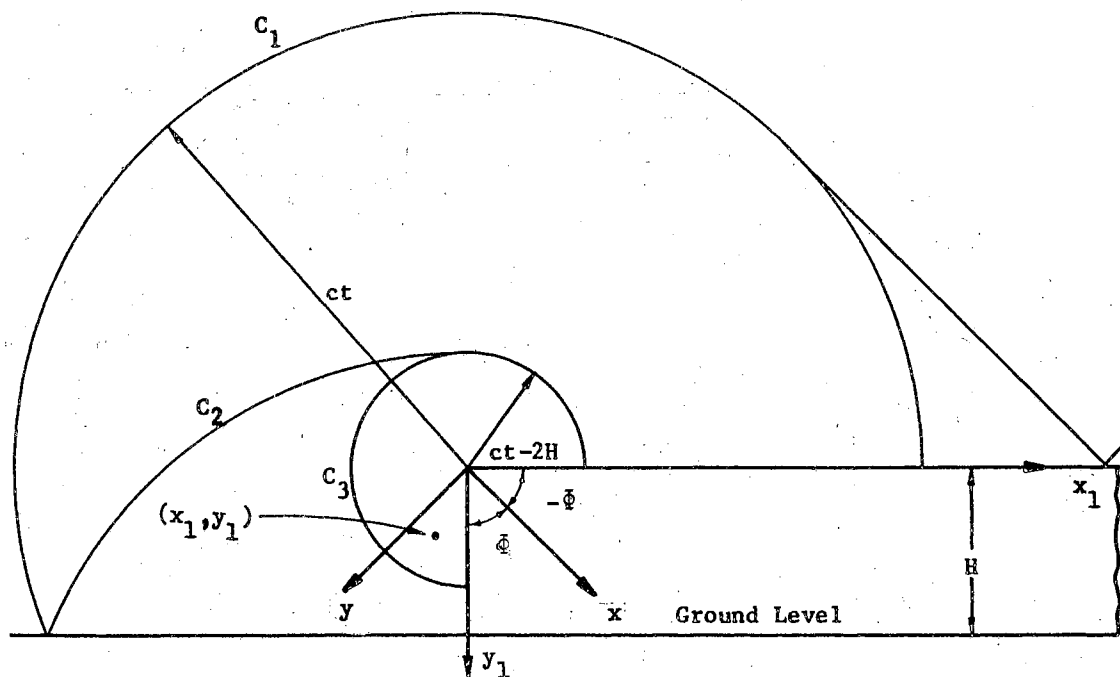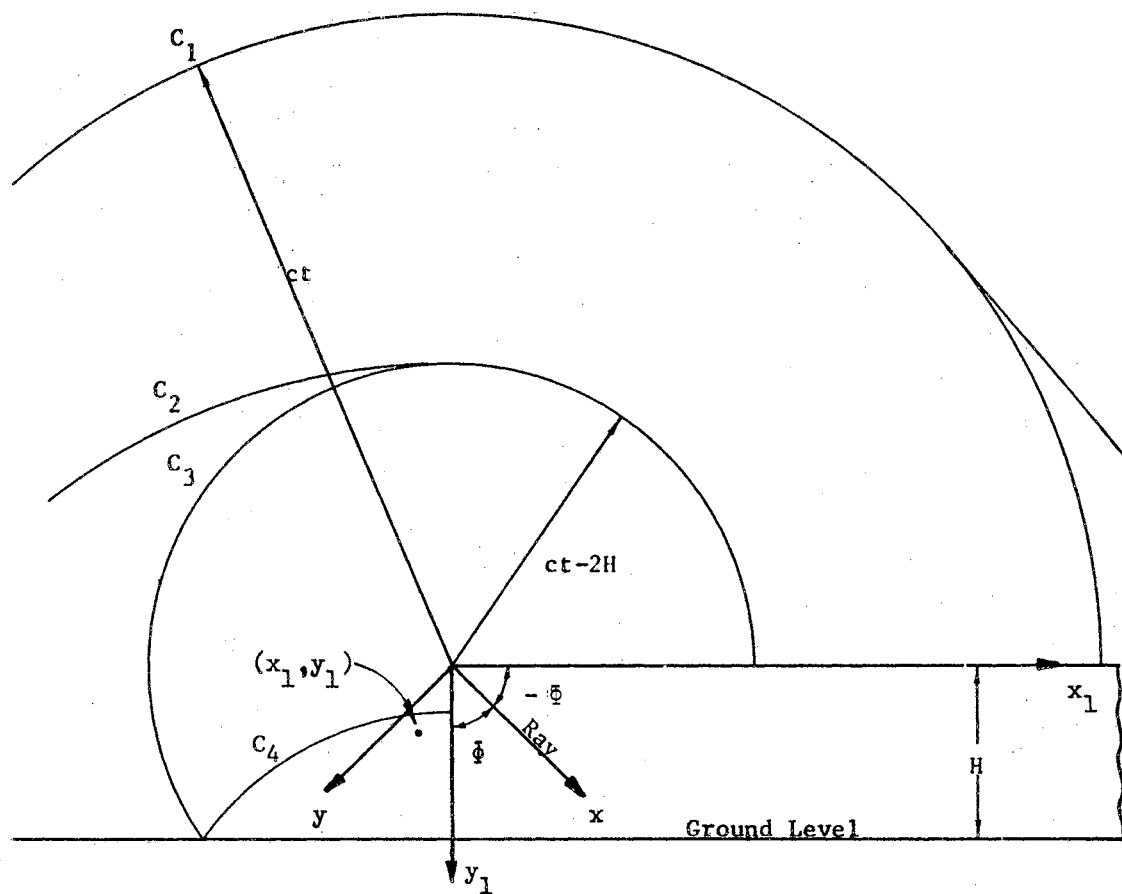for $p_{2b}$, $R = ct$ and $\theta = \arctan\left[(2H-y_1)/x_1\right] - \Phi .$

In the interval $\sqrt{x_1^2 + y_1^2} + 2H < ct \le 2H + \sqrt{x_1^2 + (2H - y_1^2)}$ , (Figure 12d), $p(x_1,y_1)$ is affected by the regions of $C_1$, $C_2$, and $C_3$. An exact method would be to compute the boundary values on $C_3$, with the assumption that it is affected by regions $C_1$ and $C_2$ for $\frac{\pi}{4} \le \Phi \le \frac{5\pi}{4}$ and $C_1$ only for $\frac{5\pi}{4} \le \Phi \le \frac{7\pi}{4}$ , and then to find an exact solution for the pressure at $x_1, y_1$ consistent with these boundary conditions. This method is very difficult, if indeed possible, because it requires satisfying variable boundary conditions involving complex expressions. The influence of region $C_3$ is small compared to that of $C_1$ and $C_2$. It is therefore suggested that an easier, and perhaps fairly accurate, method is to assume that the influence of region $C_3$, on the point is due to a weak normal shock of strength equal to the difference of $p_2(0,ct-2H)$ and $p_2(0,\sqrt{x_1^2 + y_1^2})$ at $\frac{5\pi}{4}$ . Then $p(x_1,y_1)$ is the sum of the pressures due to $C_1$, $C_2$, and $C_3$:

$$p(x_1,y_1) = p_1(x_1,y_1) + p_2(x_1,y_1) - p_{2b}(x_1,y_1) + p_2(0,\sqrt{x_1^2 + y_1^2})$$

$$- p_2(0, ct-2H) ,$$

where

for $p_1$, $R = \sqrt{x_1^2 + y_1^2}$ and $\theta = \arctan(y_1/x_1) - \Phi$ ,

for $p_2$, $R = \sqrt{x_1^2 + (2H-y_1)^2}$ and $\theta = \arctan[(2H-y_1)/x_1] - \Phi$ ,

for $p_{2b}$, $R = ct$ and $\theta = \arctan[(2H-y_1)x_1] - \Phi$ ,

for $p_2(0, \sqrt{x_1^2 + y_1^2})$, $R = 2H + \sqrt{x_1^2 + y_1^2}$ and $\theta = \pi$,

for $p_2(0, ct-2H)$, $R = ct$ and $\theta = \pi$ .

This simplification was not used, however, in this study, and its effect on accuracy is therefore not known.

In the interval $\sqrt{x_1^2 + (2H-y_1)^2} + 2H < ct \leq 4H + \sqrt{x_1^2 + y_1^2}$ , $p(x_1, y_1)$ is computed as affected by regions $C_1$, $C_2$, $C_3$, and $C_4$, with the first three treated as in the previous time interval. For $p_4$, $C_4$ can be considered as the ground reflection of $C_3$.

By the use of a digital computer, this process can be extended to large numbers of reflection and the pressure distributions can be predicted as functions of time for given wall geometries and wave incident angles. The method developed in this chapter will be applied to the Kinney Shoe Store geometry in Chapter VI.

CHAPTER V

DIFFRACTION AND REFLECTION OF SONIC BOOM

WAVES – NUMERICAL METHOD

The analytical method described earlier has several limitations.
Firstly, for the solution of any particular problem of sonic boom wave
interaction with a structure, it is necessary to visualize the shock
wave patterns around the structure, which may be difficult in certain
cases of complicated structures. Secondly, this method is useful only
in a two-dimensional case and cannot be extended to three-dimensional
problems. In this section, a numerical method has been developed so
that more general sonic boom wave/structure interaction problems can
be handled.

Tyler (8) and Walker (10) obtained numerical solutions for two-
dimensional and axisymmetric problems associated with shock wave
phenomena utilizing Rusanov's (5) difference technique in which
"dissipative" terms were used to obtain a numerically stable solution
for shock diffraction.

Governing Equations

The conservation forms of the general flow equations for a
two-dimensional case for a plane flow, derived in Reference (8)
by assuming the fluid to be an inviscid and ideal gas, are:

Continuity,

$$\frac{\partial \rho}{\partial t} + \frac{\partial (\rho u)}{\partial x} + \frac{\partial (\rho v)}{\partial y} = 0 \; ; \tag{5-1}$$

x-Momentum,

$$\frac{\partial (\rho u)}{\partial t} + \frac{\partial}{\partial x} (P+\rho u^2) + \frac{\partial}{\partial y} (\rho uv) = 0 \; ; \tag{5-2}$$

y-Momentum,

$$\frac{\partial (\rho v)}{\partial t} + \frac{\partial}{\partial x} (P+\rho u^2) + \frac{\partial}{\partial y} (\rho uv) = 0 \; ; \tag{5-3}$$

Energy,

$$\frac{\partial \rho}{\partial t} + \frac{\partial}{\partial x} (e+P)u + \frac{\partial}{\partial y} (e+P)v = 0 \; . \tag{5-4}$$

The fluid energy, e, is defined as

$$e = \frac{\rho(u^2 + v^2)}{2} + \frac{P}{\gamma-1} \; . \tag{5-5}$$

Definitions for the above equations are

$\rho$ - density,

u - x-component of velocity,

v - y-component of velocity,

P - pressure,

$\gamma$ - ratio of specific heats,

t - time,

x,y - space coordinates.

If Equation (5-1) is substituted into Equations (5-2) and (5-3), the resulting momentum equations are,

x-Momentum,

$$\frac{\partial u}{\partial t} + u \frac{\partial u}{\partial x} + v \frac{\partial u}{\partial y} + \frac{1}{\rho} \frac{\partial P}{\partial x} = 0 \; ; \tag{5-6}$$

y-Momentum,

$$\frac{\partial v}{\partial t} + u \frac{\partial v}{\partial x} + v \frac{\partial v}{\partial y} + \frac{1}{\rho} \frac{\partial P}{\partial y} = 0 \; . \tag{5-7}$$

If Equations (5-1), (5-5), (5-6), and (5-7) are substituted into Equation (5-4), the resulting energy equation is,

$$\frac{\partial P}{\partial t} + u\frac{\partial P}{\partial x} + v\frac{\partial P}{\partial y} + \gamma P\left(\frac{\partial u}{\partial x} + \frac{\partial v}{\partial y}\right) = 0 \ . \tag{5-8}$$

Sonic Boom Wave Approximations Applied to Conservation Laws

In Figure 13, a shock wave making an angle $\theta$ with the x axis is shown. Von Neumann (15) and (20) derived equations relating the
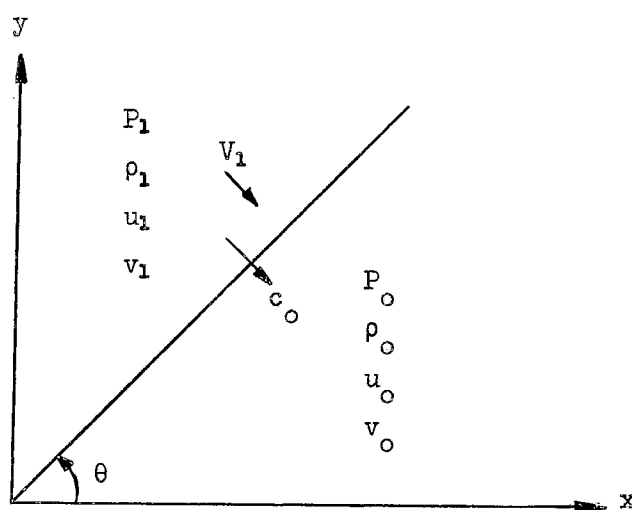


Figure 13. Geometry of a Shock Wave

downstream-to-upstream properties of a weak shock wave; these are:

$$V_1 = \frac{c_o\ 2(\xi-1)}{\sqrt{2\gamma[(\gamma+1)\xi + (\gamma-1)]}} \ ; \tag{5-9}$$

$$\rho_1 = \rho_o\left[\frac{(\gamma+1)\xi + (\gamma-1)}{(\gamma-1)\xi + (\gamma+1)}\right] ; \tag{5-10}$$

where     V — velocity in the direction perpendicular to the shock wave,

        $\xi$ — shock strength, $P_1/P_o$ ,

        o — refers to conditions upstream of the shock wave,

$_1$ - refers to conditions downstream of the shock wave,

and     $\rho_0 = \dfrac{\gamma P_0}{c_0^2}$ .

Velocity components in Figure 13, are

$$u_1 = V_1 \sin \theta$$
$$v_1 = V_1 \cos \theta .$$

<div align="right">(5-12)</div>

For a typical sonic boom wave, the values for $\theta$, $c_0$, $P_0$, and $P$ are assumed as

$$\theta = 45^\circ ,$$
$$c_0 = 1100 \text{ ft/sec},$$
$$P_0 = 2000 \text{ psf},$$
$$\Delta P = 1 \text{ psf},$$
$$P_1 = 2001 \text{ psf},$$
$$\xi = \frac{P_1}{P_0} = 1.0005 .$$

<div align="right">(5-13)</div>

For the above $\xi$ value, Equations (5-9), and (5-10) can be approximated as,

$$V_1 \cong \frac{c_0 (\xi - 1)}{\gamma}$$

<div align="right">(5-14)</div>

$$\rho_1 \cong \rho_0 = \text{constant} .$$

<div align="right">(5-15)</div>

If the values in Equation (5-13) for $\theta$, $c_0$, and $P_0$ are substituted in Equations (5-11), (5-12), (5-14), and (5-15), the resulting values are

$$\rho_1 = \rho_0 = 0.002315 \text{ slugs/ft}^3$$
$$V_1 = 0.393 \text{ ft/sec}$$
$$u_1 = 0.281 \text{ ft/sec}$$
$$v_1 = 0.281 \text{ ft/sec} .$$

<div align="right">(5-16)</div>

Now, the orders of magnitudes for various terms in Equations (5-6), (5-7), and (5-8) are evaluated here :

$$\frac{\partial u}{\partial x} = \frac{\partial u}{\partial y} = \frac{\partial v}{\partial x} = \frac{\partial v}{\partial y} = 0 \ [10^0]$$

$$u \frac{\partial u}{\partial x} = v \frac{\partial u}{\partial y} = u \frac{\partial v}{\partial x} = v \frac{\partial v}{\partial y} = 0 \ [10^0]$$

$$\frac{\partial P}{\partial x} = \frac{\partial P}{\partial y} = 0 \ [10^0]$$

$$\frac{1}{\rho} \frac{\partial P}{\partial x} = \frac{1}{\rho} \frac{\partial P}{\partial y} = 0 \ [10^3]$$

(5-17)

$$\gamma P \frac{\partial u}{\partial x} = \gamma P \frac{\partial v}{\partial y} = 0 \ [10^3]$$

$$\frac{\partial u}{\partial t} = \frac{\partial v}{\partial t} = \frac{\partial P}{\partial t} = 0 \ \left[ c \ \frac{\partial P}{\partial x} \right] = 0 \ [10^3] \ .$$

Comparison of the orders of the magnitudes of various terms in Equation (5-17), Equations (5-6), (5-7), and (5-8) leads to these approximations:

x-Momentum,

$$\frac{\partial u}{\partial t} + \frac{1}{\rho} \frac{\partial P}{\partial x} = 0$$

(5-18)

y-Momentum,

$$\frac{\partial v}{\partial t} + \frac{1}{\rho} \frac{\partial P}{\partial y} = 0$$

(5-19)

Energy,

$$\frac{\partial P}{\partial t} + \gamma P \left( \frac{\partial u}{\partial x} + \frac{\partial v}{\partial y} \right) = 0 \ .$$

(5-20)

For reduction of the energy Equation (5-20) to a more general form, which will be presented later, two terms, $\gamma u \frac{\partial P}{\partial x}$, and $\gamma v \frac{\partial P}{\partial x}$ were added to it. This is permissible since comparison of the orders of the magnitudes of these two terms with the other terms in the energy equation indicate that this will change the equation by a negligible amount. The modified energy equation is

$$\frac{\partial P}{\partial t} + \gamma \left[ \frac{\partial}{\partial x} (Pu) + \frac{\partial}{\partial y} (Pv) \right] \ .$$

(5-21)

Equations (5-18), (5-19), and (5-21) are the conservation laws after the proper approximations of a typical sonic boom wave are included.

With the assumption of constant $\gamma$ and $\rho$, the flow Equations (5-18), (5-19), and (5-21) may be written as a single equation:

$$\frac{\partial f}{\partial t} + \frac{\partial F^x}{\partial x} + \frac{\partial F^y}{\partial y} = 0 , \qquad (5-22)$$

where $f$, $F^x$, and $F^y$ are treated as three component vectors:

$$f = \left\{ \begin{array}{c} u \\ v \\ p \end{array} \right\} ; \qquad F^x = \left\{ \begin{array}{c} P/\rho \\ 0 \\ \gamma Pu \end{array} \right\} ; \qquad F^y = \left\{ \begin{array}{c} 0 \\ P/\rho \\ \gamma Pv \end{array} \right\} . \qquad (5-23)$$

## Finite Difference Equations

The Equation (5-22) was solved numerically by the method of finite differences. Tyler (8) discussed in detail the properties of conservation laws applied to a gas dynamics problem and has made a brief survey of several difference techniques developed to solve problems associated with shock wave phenomena. The concept of a weak solution, which has been discussed in mathematical journals (21), (22), and (23), allows the solution to be discontinuous. Therefore, a weak solution may have jump discontinuities and hence it can be used to solve problems associated with shock wave phenomena. A method of obtaining physically relevant weak solutions for the conservation equations has been described in (24), (25), and (26). Von Neumann and Richtmeyer (24) suggested that the inviscid flow equations should be altered by adding dissipative terms so that the surfaces of discontinuity would be "blurred" into regions where all the flow variables would be continuous,

but rapidly changing. In view of the similarity of its effect to that of viscosity in accomplishing the blurring process, this method is known as the method of artificial viscosity. Since the time of Von Neumann's work, most of the significant theories are based on the blurring technique. Tyler and Walker have applied a difference technique developed by Rusanov (5).

The addition of blurring terms to the general partial differential Equation (5-22) results in the expression:

$$\frac{\partial f}{\partial t} + \frac{\partial F^x}{\partial x} + \frac{\partial F^y}{\partial y} = \frac{\partial}{\partial x} \left[ A(x,y,t)\frac{\partial f}{\partial t} \right] + \frac{\partial}{\partial y} \left[ B(x,y,t)\frac{\partial f}{\partial y} \right] \qquad (5-24)$$

where $A(x,y,t)$ and $B(x,y,t)$ are the blurring terms whose values are obtained from the stability analysis in Appendix. Von Neumann and Richtmeyer (24) have given four requirements that must be satisfied in the selection of the blurring terms:

1. The equation with blurring terms must possess solutions without discontinuities.

2. The thickness of the shock must be of the same order as the length $\Delta x$, and $\Delta y$ in the numerical calculations.

3. The effect of the blurring terms must be negligible outside the shock region.

4. The Rankine-Hugoniot equations must be satisfied across the shock region.

The finite difference equation corresponding to the partial difference Equation (5-24) is obtained by using forward differences for time derivatives, and central differences for first-order space derivatives. Use of a scheme like this permits evaluation of the values of $f$, at any instant explicitly from the values $f$, $F^x$, and $F^y$

at the preceding time.

The finite difference net notation is shown in Figure 14. The rectangular net has steps $\Delta x = h_1$, $\Delta y = h_2$, and $\Delta t = \tau$ in the $(x, y, t)$ space. The angle $\chi$ is the angle between $h_1$ and $h$ where

$$h = (h_1^2 + h_2^2)^{\frac{1}{2}} . \tag{5-25}$$

At some net intersection, a quantity q with coordinates $(kh_1, \ell h_2, n\tau)$ is denoted by $q_{k,\ell}^n$. For purposes of discussion, n is referred as the nth time plane.

One can see that the form of the difference equations will vary depending upon the location of the net point in the flow field. Thus, the difference equations for net points lying entirely within the flow field, "field points", will be different from the difference equations for the net points lying on walls and on flow plane boundaries, "boundary points". This difference is due to the requirement of satisfying the boundary points, and their lack of surrounding points.

## Difference Equations for Field Points

With the use of the difference techniques and the difference net notation discussed above, the complete difference approximation to the general partial differential Equation (5-24) may be written as

$$f_{k,\ell}^{n+1} = f_{k,\ell}^n - \frac{\tau}{2h_1} \left[ F_{k+1,\ell}^x - F_{k-1,\ell}^x \right]^n - \frac{\tau}{2h_2} \left[ F_{k,\ell-1}^y - F_{k,\ell+1}^y \right]^n$$

$$+ \frac{\tau}{h_1^2} \left[ A_{k+\frac{1}{2},\ell} (f_{k+1,\ell} - f_{k,\ell}) - A_{k-\frac{1}{2}} (f_{k,\ell} - f_{k-1,\ell}) \right]^n \tag{5-26}$$

$$+ \frac{\tau}{h_2^2} \left[ B_{k,\ell+\frac{1}{2}} (f_{k,\ell+1} - f_{k,\ell}) - B_{k,\ell-\frac{1}{2}} (f_{k,\ell} - f_{k,\ell-1}) \right]^n .$$

$$X = \tan^{-1} \frac{h_2}{h_1}$$

$$h = (h_1^2 + h_2^2)^{\frac{1}{2}}$$

(k-1, ℓ+1)   (k, ℓ+1)   (k+1, ℓ+1)

(k-1, ℓ)   (k, ℓ)   (k+1, ℓ)

h   $h_2$

$h_1$

(k-1, ℓ-1)   (k, ℓ-1)   (k+1, ℓ)
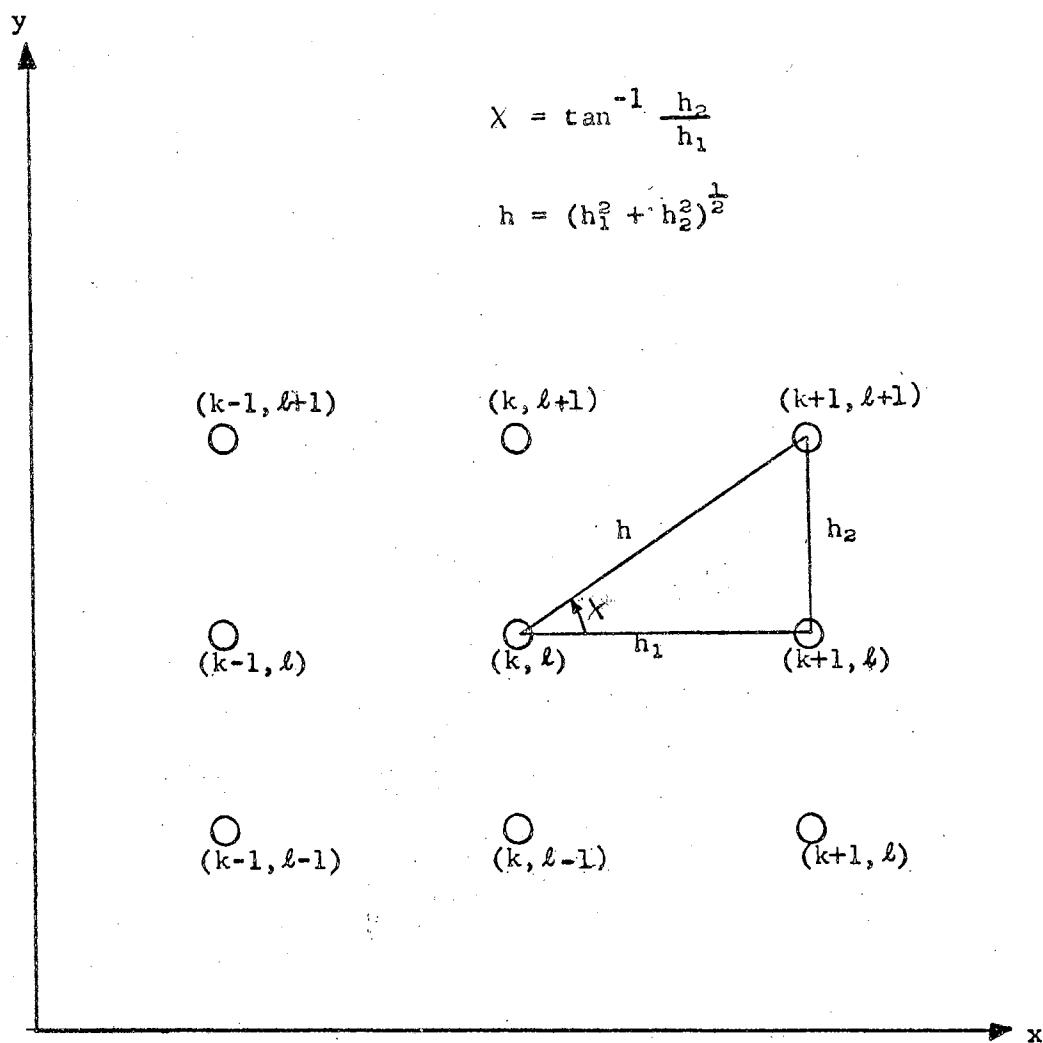
Figure 14.   Finite Difference Net Notation

Equation (5-26) may be simplified by defining

$$K_1 = \frac{\tau}{h_1},$$

$$K_2 = \frac{\tau}{h_2},$$

$$A^n_{k,\ell} = \frac{h_1^2}{2\tau} \alpha^n_{k,\ell},$$

$$B^n_{k,\ell} = \frac{h_2^2}{2\tau} \beta^n_{k,\ell},$$

(5-27)

and Equation (5-26) is then written as

$$f^{n+1}_{k,\ell} = f^n_{k,\ell} - \frac{K_1}{2}\left[F^x_{k+1,\ell} - F^x_{k-1,\ell}\right]^n - \frac{K_2}{2}\left[F^y_{k,\ell+1} - F^y_{k,\ell-1}\right]^n$$

$$+ \frac{1}{2}\left[\alpha_{k+\frac{1}{2},\ell}(f_{k+1,\ell} - f_{k,\ell}) - \alpha_{k-\frac{1}{2},\ell}(f_{k,\ell} - f_{k-1,\ell})\right]^n \quad (5-28)$$

$$+ \frac{1}{2}\left[\beta_{k,\ell+\frac{1}{2}}(f_{k,\ell+1} - f_{k,\ell}) - \beta_{k,\ell-\frac{1}{2}}(f_{k,\ell} - f_{k,\ell-1})\right]^n.$$

A new parameter K is defined as

$$K = \left[K_1^2 + K_2^2\right]^{\frac{1}{2}}.$$

(5-29)

From Equations (5-27) and (5-29), K may be expressed as

$$K = \frac{\left[h_1^2 + h_2^2\right]^{\frac{1}{2}}}{h_1 h_2}\tau.$$

(5-30)

The geometry of the Figure 14 and Equations (5-25), (5-27), and (5-30), permit $K_1$ amd $K_2$ to be expressed as

$$K_1 = K \sin \chi, \quad K_2 = K \cos \chi.$$

(5-31)

In Appendix stability analysis is performed to evaluate the required values of $\alpha^n_{k,\ell}$ and $\beta^n_{k,\ell}$ for the difference equations of the conservation laws, in a manner similar to that of Rusanov. The needed values for $\alpha^n_{k,\ell}$ and $\beta^n_{k,\ell}$ are found to be

$$\alpha^n_{k,\ell} = \alpha = K\omega c \sin^2 \chi,$$

(5-32)

$$\beta^n_{k,\ell} = \beta = K\omega c \cos^2 \chi,$$

whereas the inequality

$$0 \leq \omega c \leq 1 , \qquad (5\text{-}33)$$

must be satisfied.

The time increment between any two successive time steps is given by

$$K \leq \frac{1}{c_{max}} . \qquad (5\text{-}34)$$

## Boundary Points on Walls

Walker (10) discussed in detail the possible boundary conditions that can be applied for points lying on walls or planes of symmetry. Walker considered three possible methods:

1.  Ideal boundary conditions that must exist at the boundary in question are forcefully imposed on the boundary. Strict usage of this condition, without due regard for the physical problem, can lead to erraneous results.

2.  Either forward or backward differences for the appropriate space derivatives are applied to the boundary points. This method is not sufficient to satisfy the complete set of realistic boundary conditions at the wall.

3.  A reflection technique, discussed by Burstein (27), assumes that the points adjacent to plane walls are imaged by virtual points that lie within the wall. In the present analysis, this method has been applied because of its merits explained below.

For a wall parallel to the x-axis such as that shown in Figure 15, the relations of the variables at the field point (k, $\ell$+1) to the

variables at the virtual point $(k, \ell{-}1)$ are:

$$P_{k, \ell+1} = P_{k, \ell-1} \; ,$$

$$u_{k, \ell+1} = u_{k, \ell-1} \; ,$$

$$v_{k, \ell+1} = -v_{k, \ell-1} \; .$$

(5-35)

This representation allows boundary points to be treated by central differences in the same way as the field points. Thus, for a wall parallel to the x-axis the difference Equation (5-26) can be modified by using the conditions of Equation (5-35).

For a net point lying on a wall parallel to the y-axis the relations of the variables at the field point $(k+1, \ell)$ to the variables at the virtual point $(k{-}1, \ell)$ are

$$P_{k-1, \ell} = P_{k+1, \ell} \; ,$$

$$u_{k-1, \ell} = -u_{k+1, \ell} \; ,$$

$$v_{k-1, \ell} = v_{k+1, \ell} \; ,$$

(5-36)

and the difference equation can be obtained by using the conditions of Equation (5-36) in Equation (5-26).

The advantage of the image point method for treating boundary points is that it is not necessary to dictate the values of derivatives at a surface and it allows the derivatives to assume whatever the boundary conditions are not imposed in such a manner that they negate the possibility of certain phenomenon occurring in the vicinity of a wall.

## Boundary Points on a Flow Plane

For any finite difference solution, the "flow plane" corresponds the boundary of the finite difference net. The net points on $k = 1$, $k = k_{max}$, and $\ell = \ell_{max}$ in Figure 16 are the boundary points on the
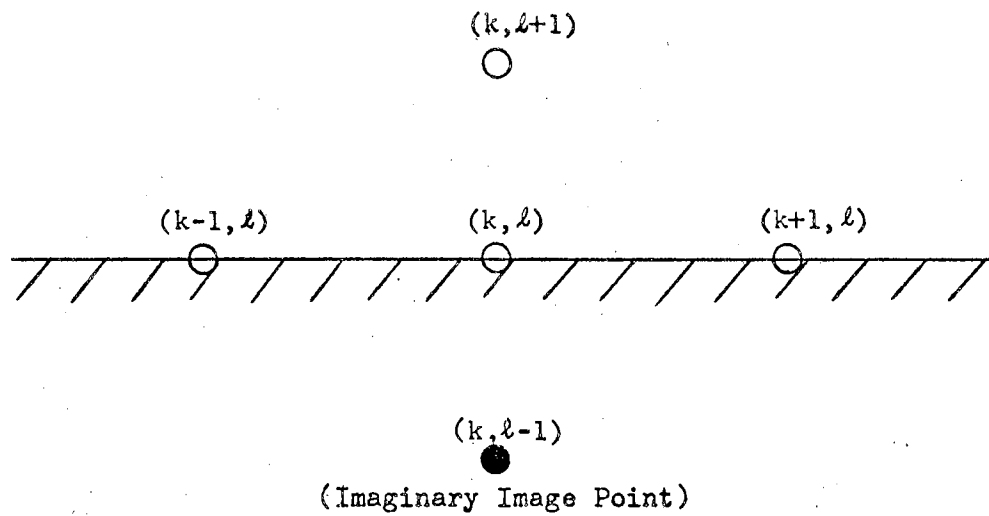
(k,ℓ+1)

○

(k-1,ℓ)          (k,ℓ)          (k+1,ℓ)

○          ○          ○

(k,ℓ-1)

●

(Imaginary Image Point)

Figure 15.   Image Point Principle for wall Point

(y,ℓ)

$k_{max}$

○    o    o    o    o    o    o —— $\ell_{max}$

○    o    o    o    o    o

○    o    o    o    o    o

○    o    o    o    o    o

○    o    o    o    o    o

○    o    o    o    o    o

(1,1)  ○    o    o    o    o    o    o          (x,k)
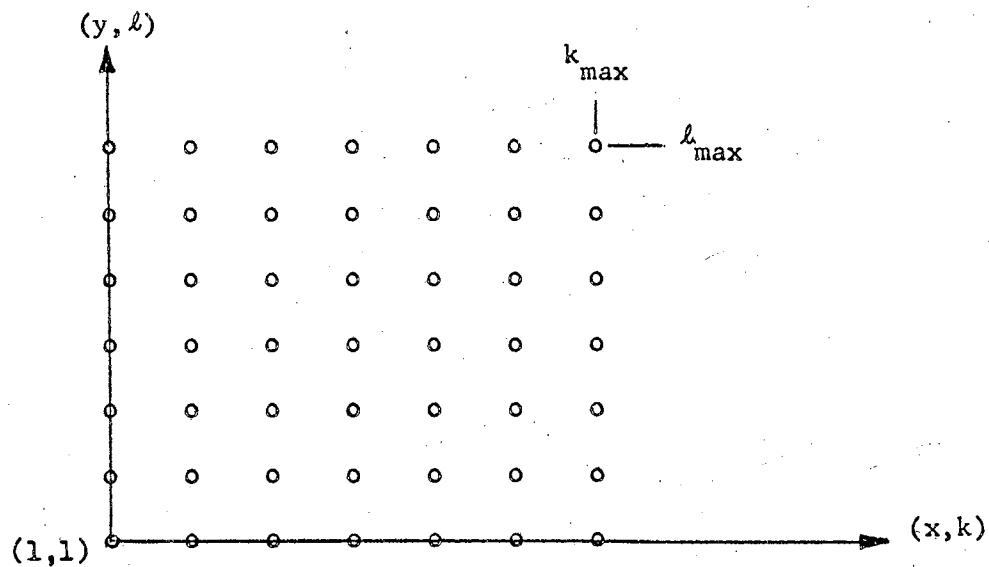
Figure 16.   Boundary Points on a Flow Plane

flow plane.

There is no general technique for handling the points on the flow plane boundaries. Each particular problem has to be treated separately and proper boundary conditions to represent the physical problem should be imposed.

The method developed in this chapter will be used in the succeeding chapter to compute pressure-time histories for the Kinney Shoe Store geometry. This will permit a direct comparison to be made between the analytical and numerical results.

CHAPTER VI

PRESSURE-TIME HISTORY OF A SONIC BOOM WAVE ACTING ON WINDOW

IN A BUILDING

During the series of sonic boom test flights conducted in the

Oklahoma City area during 1964, an 8' x 10' x $\frac{1"}{4}$ plate glass window

in the north wall of the Kinney Shoe Store, a single-story commercial

building, was broken with the occurrence of one of the sonic booms.

This particular sonic boom occurred at about 1:20 p.m. on May, 1964,

and was produced by an F-101 aircraft at 37,742 feet altitude on a

scheduled steady-state course at a scheduled speed of Mach number 1.4.

Orientation and distance of aircraft course with respect to the

building are shown in Figure 17. In this chapter the methods de-

veloped in Chapters III, IV, and V will be applied to this building,

and to the window region in particular, for the flight conditions

which produced the breakage.

Conversion of Wave Time-Histories into Wave Geometry

For the Kinney Shoe Store, the predicted position of the wave

relative to the building was needed, as well as the time-of-arrival

of the waves at specific locations. The wave geometry was estimated

from the computed time values as described below.

To determine the angle between wave and wall in a horizontal

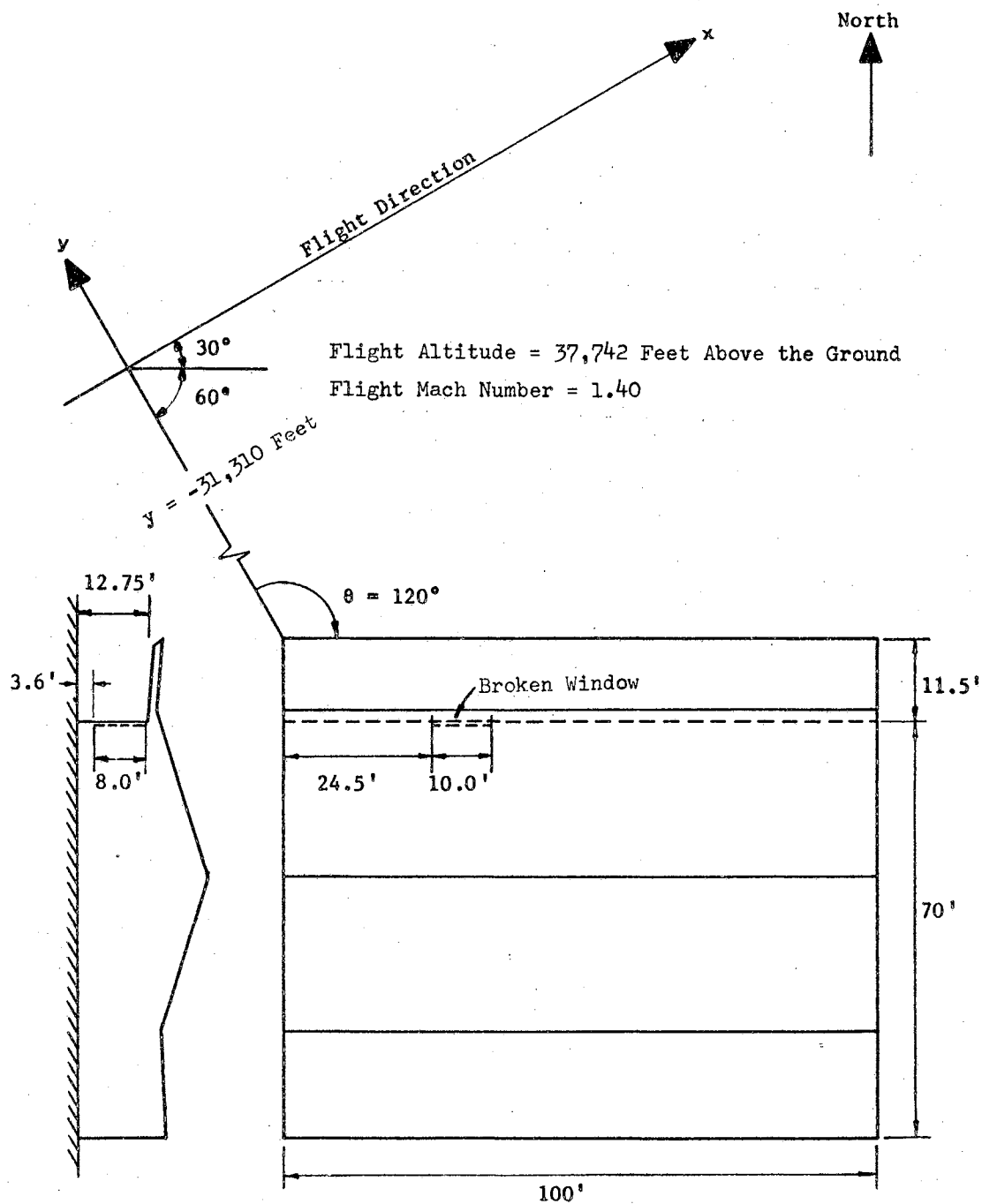plane, two points on the wall in the horizontal plane, such as the

Figure 17. Geometry Used in the Arrival Time Computations for the Kinney Shoe Store

lower corners of a building, were selected and the $T_i$ values computed using one of the methods described in Chapter III. With reference to Figure 18, the distance between these two selected points is L, and the point having the smaller y-coordinate is point 1 and the larger is point 2; xy is the horizontal plane. It can be shown, by use of the law of sines, that the wave angle is

$$\tan \theta_w = \tan \theta - \frac{V}{L} (T_{i2} - T_{i1}) \sec \theta . \qquad (6\text{-}1)$$

Similarly, two points were chosen on a vertical line, such as the upper and lower corner points of the corner of a building, with the upper designated as 3 and the lower as 4. A vertical plane containing points 3 and 4 and perpendicular to the wave line on the ground (i.e., at an angle $\theta_w + 90^\circ$ from the y-axis) was as shown in Figure 19. Then, for a wall height H, the wave angle in the vertical plane was

$$\phi_w = \frac{c}{H} (T_{i4} - T_{i3}) . \qquad (6\text{-}2)$$

These relations were applied to the Kinney Shoe Store conditions. For this, the flight path geometry is shown in Figure 17, and L = 70 feet, H = 12.75 feet. Values of $(T_{i2}-T_{i1})$ and $(T_{i4}-T_{i3})$ were computed by the Method II of Chapter III, and were found to be 0.0031 and 0.0038 seconds, respectively. These values, in combination with Equations (6-1) and (6-2), gave wave angles $\theta_w$ and $\phi_w$ of 26.8° and 70.1°, respectively. The resulting wave-building relationship is shown in Figure 20. Some wave-time positions are depicted in Figure 21, in which $T_{iR}$ is the time for a wave to pass a point after it has passed the reference point, the south-west corner at the ground level.

From test data for the F-101 aircraft at the flight Mach number, altitude and y-distance, the bow-to-tail wave time interval was estimated to be 0.135 seconds and the incident ground overpressure to
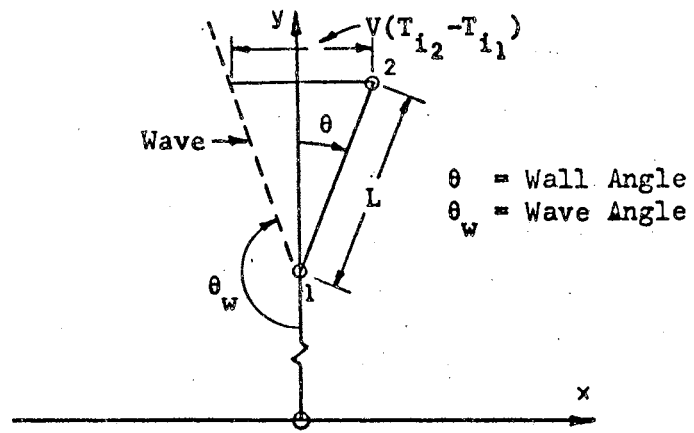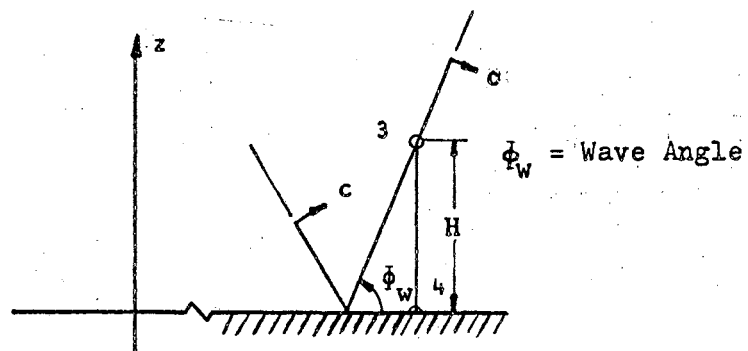
Figure 18. Wave in the Horizontal Plane
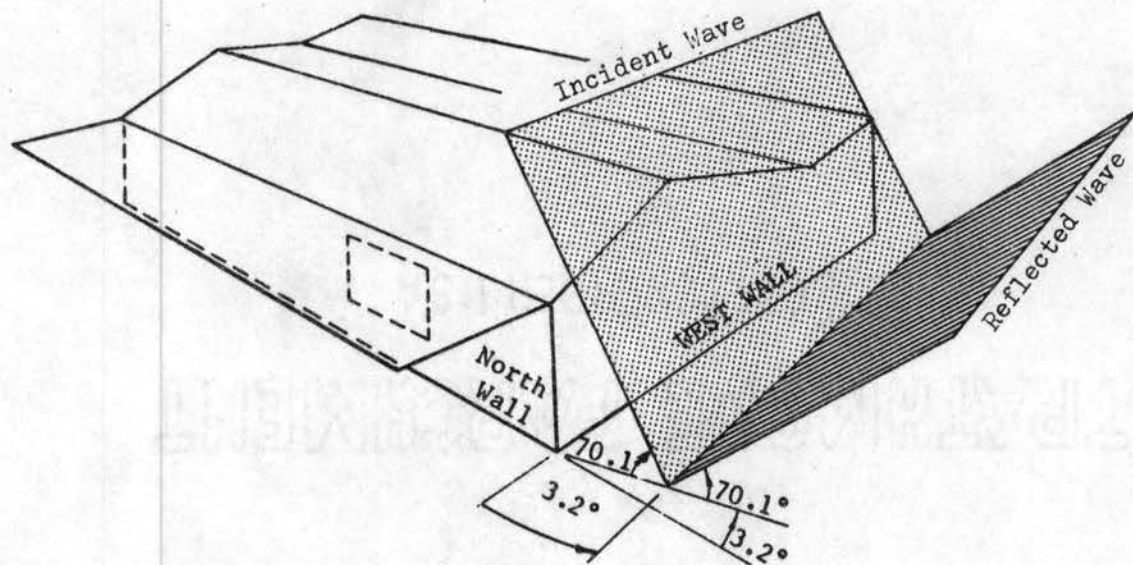


Figure 19. Wave in the Vertical Plane

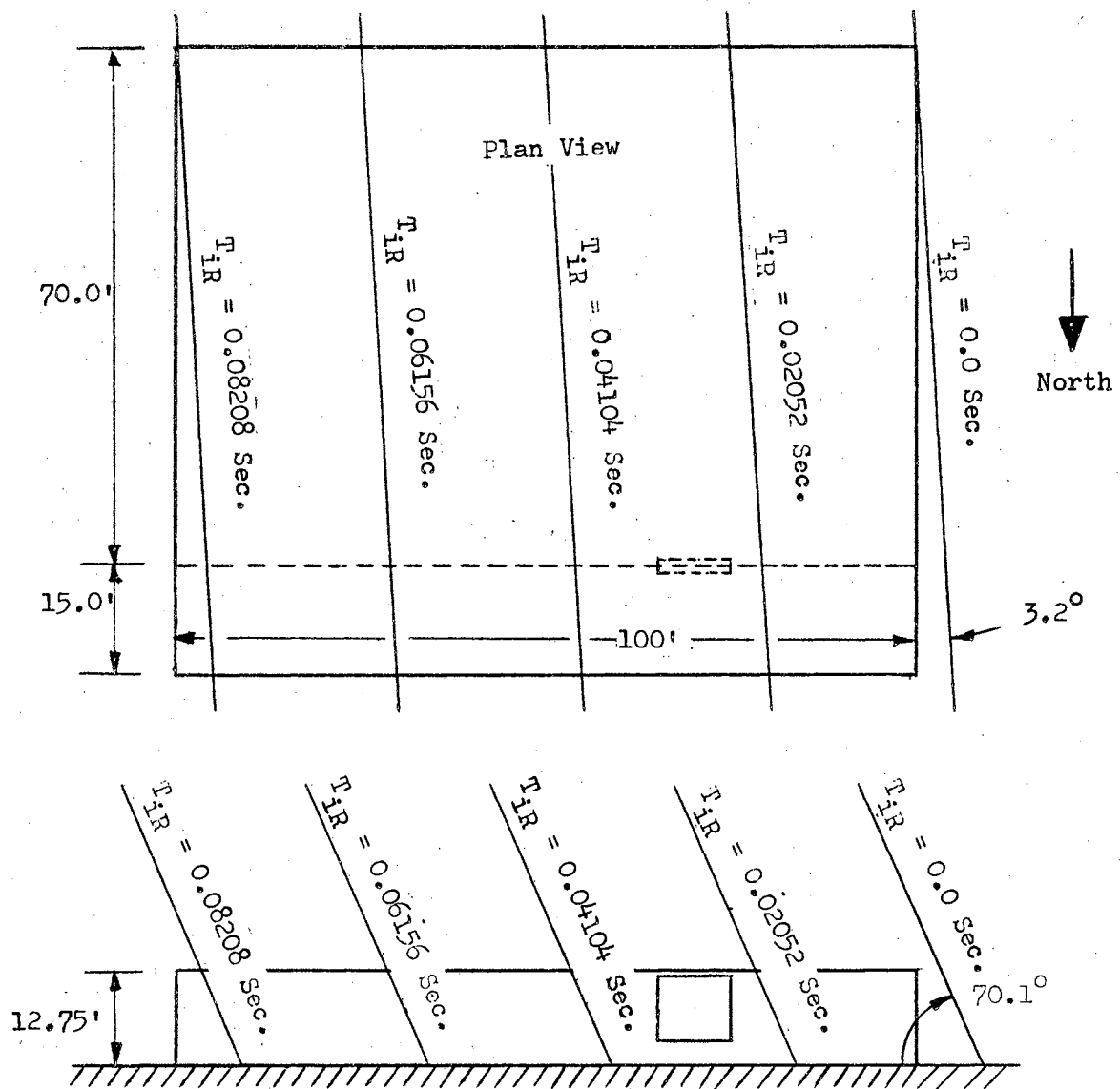Figure 20.  Geometric Relationship of Building and Wave

Figure 21. Arrival Times of Incident Wave of Sonic Boom Wave on Kinney Shoe Store

be 1.65 psf (Reference 1). Upon computing the incident-to-reflected wave time interval, $\Delta T_{ir}$, for 6.0 and 12.75 feet heights, the pressure histories on the west wall were predicted as shown in Figure 22.

### Pressure History on the Window of the Kinney
### Shoe Store - Analytical Method

Figure 23 depicts the window on the north wall of the Kinney Shoe Store, under the roof overhang, that was broken during the seventh flight of a F-101 aircraft on May 17, 1964. The position of the sonic boom wave for the particular conditions was determined in the previous section and is shown in Figure 23. For the two-dimensional analysis, the wave was assumed to be parallel to the west wall, neglecting the $3.2^{\circ}$ angle that was estimated in the previous analysis. As shown in Figures 24a and 24b, the incident and reflected waves (with the bow wave considered only as a step input at present) were diffracted by the roof overhang and reflected by the ground and roof overhang. The sonic boom wave was considered as a two-dimensional wave and the effects of the north edge of the roof overhang and south-extending west wall were neglected. The wave-history for the window and for some of the points on the north-west corner were estimated by the analytical method developed in Chapter IV, including the effects of the reflected disturbance regions on the rigid walls (the ground and the roof over-hang). The x and y axes were selected as shown in Figure 23. For this particular geometry, $\Phi = 0$, and $\psi = 19.9$. If these values are sub-stituted into Equations (4-14) and (4-18), the resulting expressions are
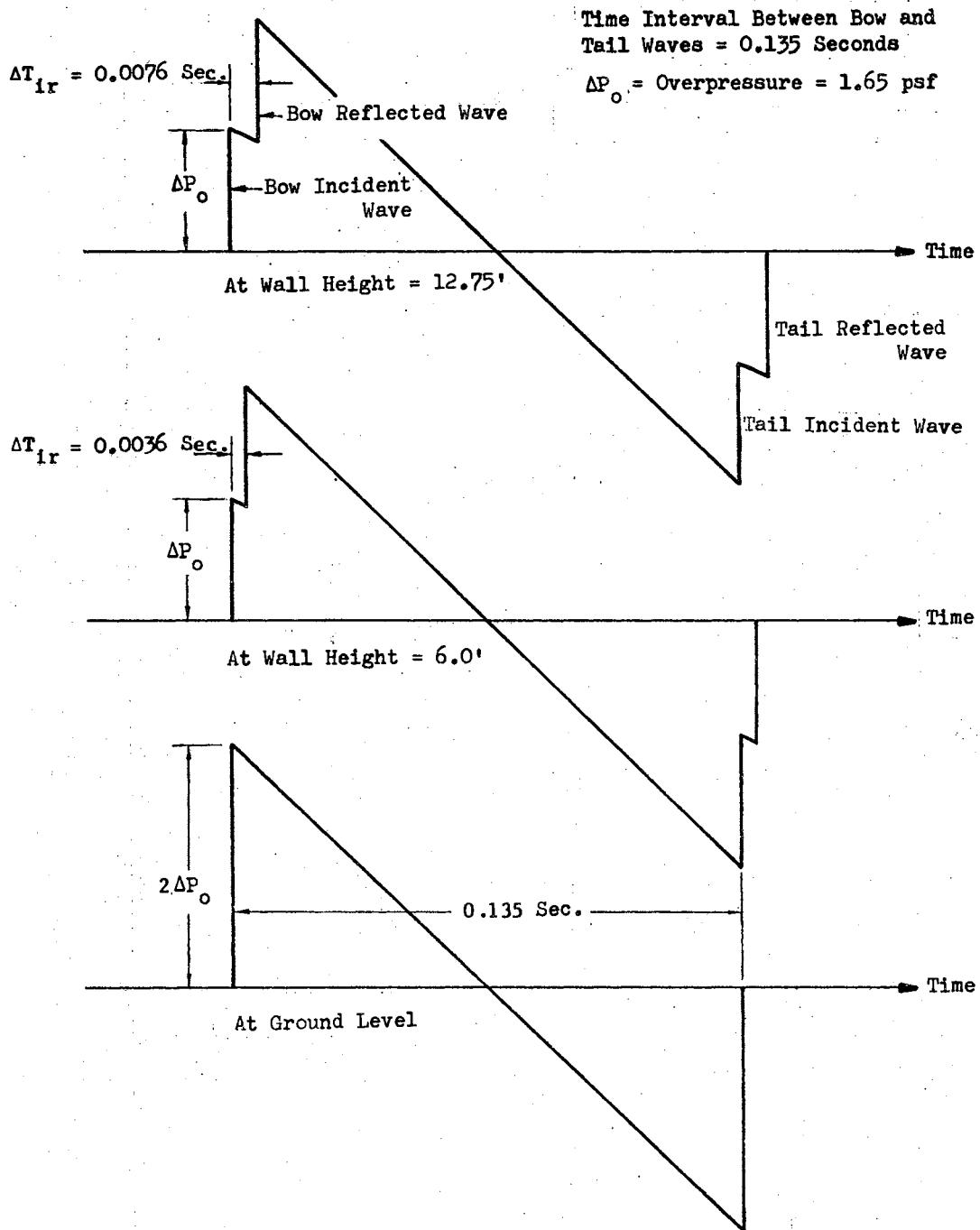
$\Delta T_{ir} = 0.0076$ Sec.

Time Interval Between Bow and
Tail Waves = 0.135 Seconds

$\Delta P_o$ = Overpressure = 1.65 psf

Bow Reflected Wave

$\Delta P_o$  Bow Incident
Wave

Time

At Wall Height = 12.75'

Tail Reflected
Wave

Tail Incident Wave

$\Delta T_{ir} = 0.0036$ Sec.

$\Delta P_o$

Time

At Wall Height = 6.0'

$2 \Delta P_o$

0.135 Sec.

Time

At Ground Level

Figure 22. Sonic Boom Wave Pressure Histories on the Kinney
Shoe Store West Wall

Incident Wave

Ground Reflected
Wave

p = 0

p = 1

p = 2

$\psi$ = 19.9°

Roof Overhang

x

(x,y)

A      C

10'

E

11.6'

H = 12.75'

B      D

3.6'

24.5'

70.1°

F

Ground Level

(View Facing North From Interior)

Ray

y
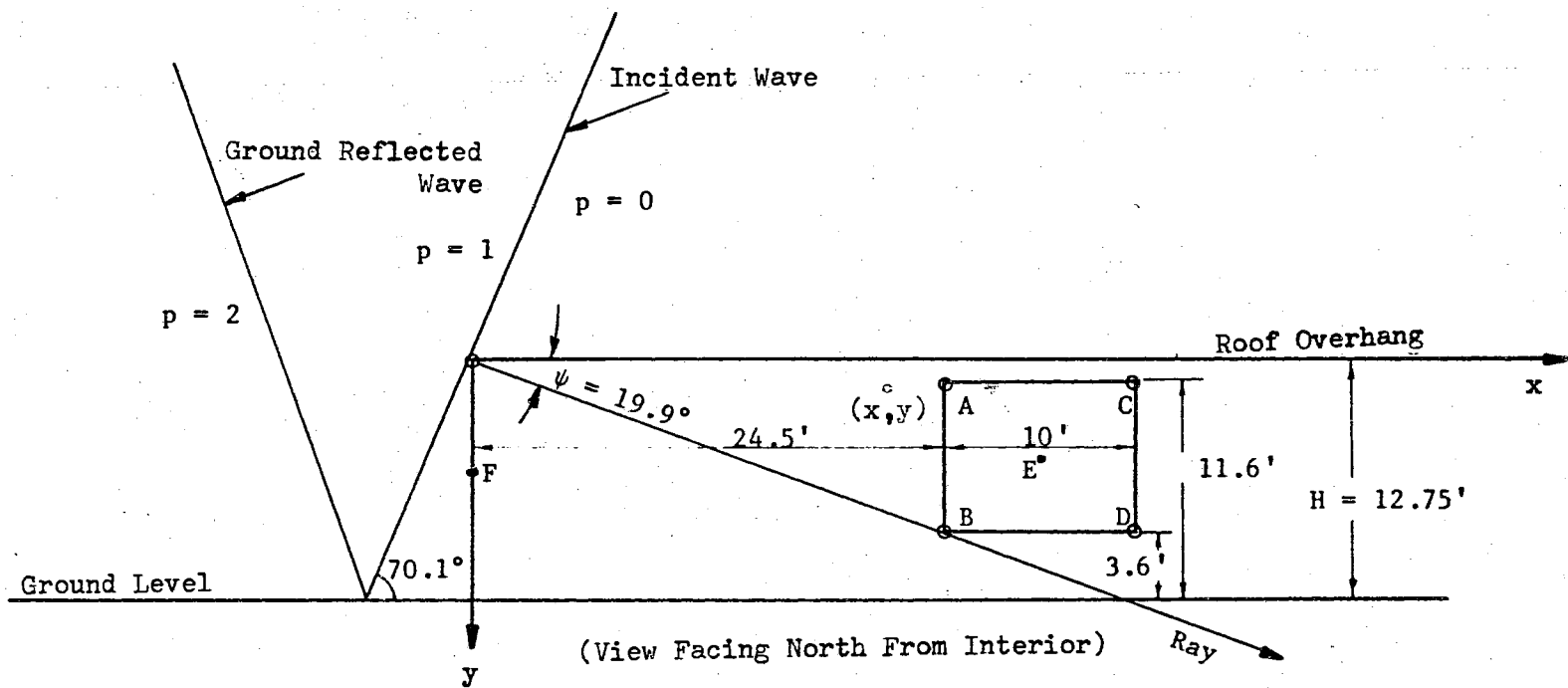
Figure 23.  Geometry of Sonic Boom Wave and Front of Kinney Shoe Store
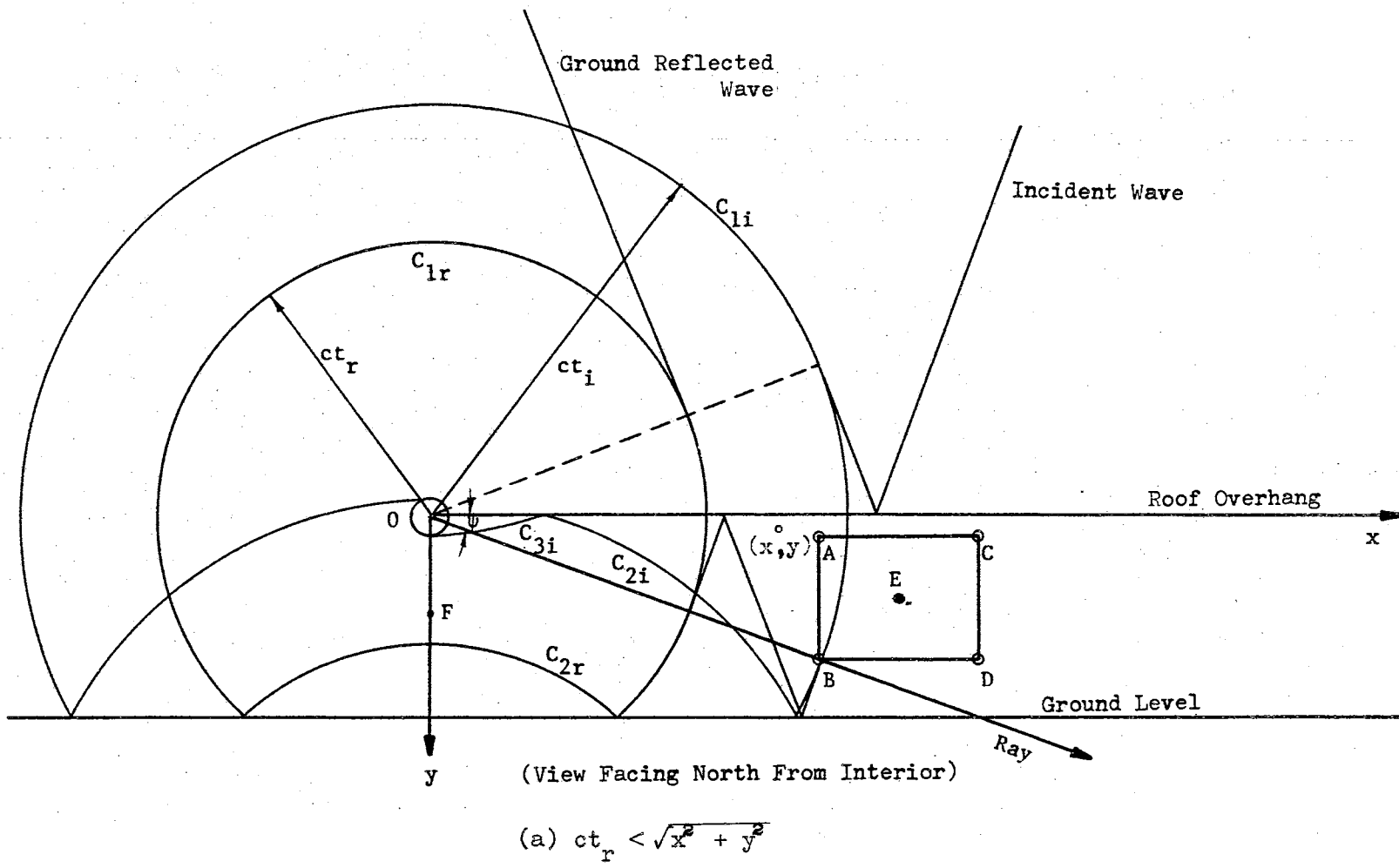Used in the Two-Dimensional Analysis

Ground Reflected Wave
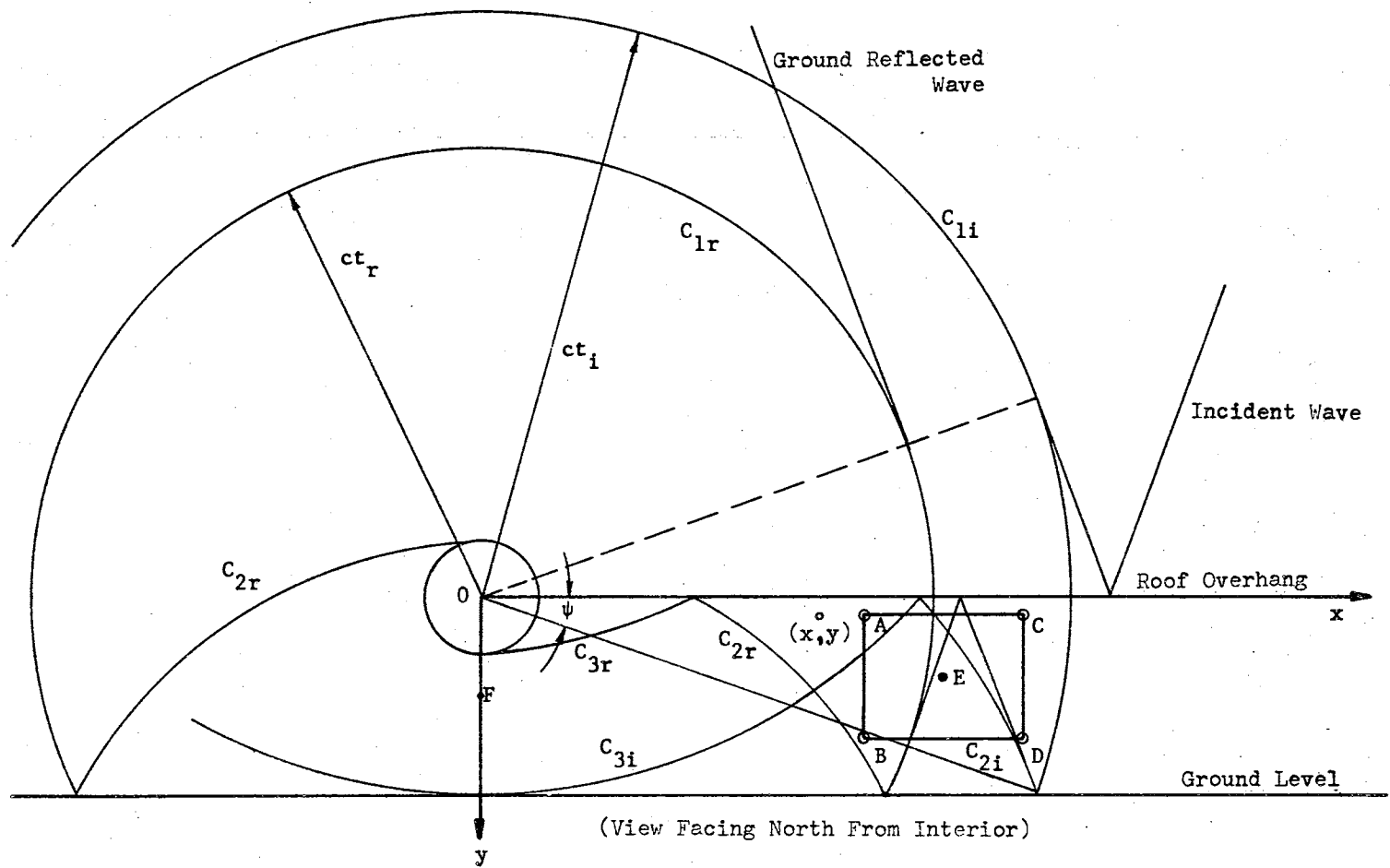
Incident Wave

$C_{1i}$

$C_{1r}$

$ct_r$

$ct_i$

Roof Overhang

x

0

$\psi$

$C_{3i}$

$(\overset{o}{x,y})$ A

C

$C_{2i}$

E

F

B

D

$C_{2r}$

Ground Level

Ray

y

(View Facing North From Interior)

(a) $ct_r < \sqrt{x^2 + y^2}$

Figure 24. Incident and Reflected Wave Patterns on the North Wall of the Kinney Shoe Store

73

Ground Reflected Wave

Incident Wave

Roof Overhang

Ground Level

(View Facing North From Interior)

(b) $ct_r > \sqrt{x^2 + y^2}$

Figure 24. (continued)

$$\lambda = \frac{\pi}{2(\pi-\Phi)} = \frac{1}{2} \text{ ,}$$

$$p = 1 - \frac{1}{\pi} \arctan \left[ \frac{- (1-\rho) \cos \frac{1}{2}(\psi-\pi)}{(1+\rho) \sin \frac{1}{2}(\psi-\pi) - 2\sqrt{\rho} \sin \frac{1}{2}(\theta-\pi)} \right]$$

$$+ \frac{1}{\pi} \arctan \left[ \frac{- (1-\rho) \cos \frac{1}{2}(\psi+\pi)}{(1+\rho) \sin \frac{1}{2}(\psi+\pi) - 2\sqrt{\rho} \sin \frac{1}{2}(\theta-\pi)} \right] \text{ .} \qquad (6\text{-}3)$$

Equation (6-3) can be simplified to become

$$p = 1 - \frac{1}{\pi} \arctan \left[ \frac{(1-\rho) \sin \frac{\psi}{2}}{(1+\rho) \cos \frac{\psi}{2} - 2\sqrt{\rho} \cos \frac{\theta}{2}} \right]$$

$$+ \frac{1}{\pi} \arctan \left[ \frac{(1-\rho) \sin \frac{\psi}{2}}{(1+\rho) \cos \frac{\psi}{2} + 2\sqrt{\rho} \cos \frac{\theta}{2}} \right] \text{ .} \qquad (6\text{-}4)$$

A computer method was developed for the wave history at any point $x,y$ in the coordinate system shown in Figures 23 and 24. The time $t = 0$ corresponds to the condition at which the incident wave of the sonic boom has reached the origin of the chosen coordinate axes (west edge of the roof overhang). The special notation used in this method is expanded as follows:

C     disturbance region.

$p = \dfrac{p-P_o}{P_1-P_o}$ ,   dimensionless overpressure at the point $x,y$ due to the sonic boom.

$p_i$     p at the point $x,y$ at any time $t_i$ due to the incident wave.

$p_r$     p at the point $x,y$ at any time $t_i$ due to the reflected wave.

$p_{np}$     p at the point $x,y$ at any time $t_i$ due to the disturbance region $C_n$.

$p_{nb}$     p at any time $t_i$ at the boundary of the disturbance region at the angle $\theta_n$.

$\Delta P = P-P_o$ ,   overpressure at the point $x,y$ at any time $t_i$ due to the sonic boom.

$R_1 = (x^2+y^2)^{\frac{1}{2}}$ ,   the distance of the point $x,y$ from the origin "0".

$R_n = (x^2 + y_n^2)^{\frac{1}{2}}$, the distance of the point $x,y$ from the origin of the disturbance region $C_n$.

$t_i$    time elapsed since the incident wave passed over the origin "O".

$t_r$    time elapsed since the reflected wave passed over the origin "O".

$y_n = (n-1)H + y$, if $n$ is odd,

     $= nH - y$, if $n$ is even; $y$ coordinate of the disturbance region $C_n$.

$\theta_n = \arctan \left(\dfrac{y_n}{x}\right)$, inclination of the point $x,y$ in the vertical plane (positive in clockwise direction from the x-axis).

With reference to Figure 28, a relation between $t_i$ and $t_r$ is established as

$$t_r = t_i - \frac{2H \tan \psi \cos \psi}{c} = t_i - \frac{2H \tan \psi}{c} \quad . \qquad (6\text{-}5)$$

The pressure history at the point $x,y$ due to the passage of a sonic boom is a function of the geometry of the incident and reflected waves and the several disturbance regions at any time $t_i$. Computational procedure is presented below to predict the overpressure due to the incident and reflected waves. At any time $t_i$, the overpressure at the point $x,y$ is the algebraic sum of the overpressures due to the incident and reflected waves.

Computation of Overpressure Due to the Incident Wave

Condition 1: $ct_i \leq R_1$

     (a) If $\theta_1 \leq \psi$; $p_i = 0$.

     (b) If $\theta_1 > \psi$;

$$(6\text{-}6)$$

$$\text{for } \frac{ct_i}{\cos (\theta_1 - \psi)} > R_1, \quad p_i = 1,$$

$$\text{and for } \frac{ct_i}{\cos (\theta_1 - \psi)} \leq R_1, \quad p_i = 0 .$$

Condition 2: $ct_i > R_1$, n was computed for

$$R_n < ct_i \leq R_{n+1} \; ; \qquad (6\text{-}7)$$

where

$$R_n = (x^2 + y^2)^{\frac{1}{2}} \; , \qquad (6\text{-}8)$$

and

$$y_n = (n\text{-}1)H + y, \text{ if n is odd,}$$
$$= nH - y, \text{ if n is even.} \qquad (6\text{-}9)$$

Then $p_i$ was the algebraic sum of the overpressures contributed by the regions $C_{1i}$, $C_{2i}$, --------, $C_{(n\text{-}1)i}$, and $C_{ni}$. So,

$$p_i = p_{1i} + p_{2i} + p_{3i} + - - - - - - - - + p_{(n\text{-}1)i} + p_{ni}; \qquad (6\text{-}10)$$

where

$$p_{1i} = p_{1pi},$$

and for $n > 1$,

$$p_{ni} = p_{npi} - p_{nbi} \; .$$

$p_{npi}$ was computed from Equation (6-4) and the values for $\rho$ and $\theta$ as follows:

$$\rho = \frac{R_n}{R_n + \sqrt{(c^2 t_i^2 - R_n^2)}} \; , \qquad (6\text{-}11)$$

$$\theta = \theta_n = \arctan\left(\frac{y_n}{x}\right) \; . \qquad (6\text{-}12)$$

$p_{nbi}$ depends on the value of $\theta_n$ and the value is always 0 or 1 or 2 depending on the geometry of the point in consideration. In this particular case, it was always 1. Hence,

$$p_{nbi} = 1 \; . \qquad (6\text{-}13)$$

At any time $t_i$, $p_i$ was computed by Equations (6-7) to (6-13).

Computation of Overpressures Due to the Reflected Wave

For any time $t_i$, the $t_r$ value was computed from Equation (6-5).

Condition 1: $ct_r \leq R_1$

If $x \geq \dfrac{ct_r}{\cos \theta} + y \tan \psi$ ; $p_r = 0$ .

If $x < \dfrac{ct_r}{\cos \theta} + y \tan \psi$ , and

(a) $R_1 \geq \dfrac{ct_r}{\cos (\psi-\theta_1)}$ , $p_r = 1$ ,

(b) $R_1 < \dfrac{ct_r}{\cos (\psi-\theta_1)}$ , and $\theta_1 \leq \psi$ ; $p_r = 2$ ,

(c) $R_1 < \dfrac{ct_r}{\cos (\psi-\theta_1)}$ , and $\theta_1 > \psi$ ; $p_r = 1$ .

Condition 2: $ct_r > R_1$, n was computed such that

$$R_n < ct_r \leq R_{n+1} . \qquad (6-14)$$

Then $p_r$ was the algebraic sum of the overpressure contributed by the regions $C_{1r}$, $C_{2r}$, ———, $C_{(n-1)r}$, and $C_{nr}$. $p_r$ was computed by the same procedure of Condition 2 of the incident wave after replacing $t_i$ by $t_r$ and changing the subscripts "i" to "r" in the overpressure terms.

Computational Technique for an N-Wave

A sonic boom ordinarily will have a shape similar to an N-wave. The time interval, $\Delta t$, between the bow and tail waves of the sonic boom that caused the broken window has been estimated from related test data to be 0.135 seconds. An N-wave can be treated as two shocks of equal strength ($p_i = p_r = \frac{1}{2}\Delta P_o$) with a series of expansion waves between them. An N-wave of strength $p_i = 1.0$ and $p_r = 1.0$ at bow and tail waves separated by 0.135 seconds was assumed. Then 135 small

expansion waves were assumed of strength $p_i = p_r = 2/135$, each separated by a time interval of 0.001 seconds. Overpressure at any time $t_i$ was then the algebraic sum of all the overpressures due to all the step waves, effective at that time. The input to the region beneath the canopy was thus an N-wave of 0.5 psf incident pressure for an unit overpressure sonic boom wave and a period of 0.135 seconds. The resulting pressure at any point considered the reflection/diffraction effects and the height of the point.

## Computations and Results of the Analytical Method

The pressure distribution due to the subject sonic boom was computed at six points, A through F, as shown in Figure 25, on the north wall of the Kinney Shoe Store. Computer programs were written both for a step input and for an N-wave utilizing the technique described above. About 15 minutes were required to obtain the pressure history of each point from $t_i = 0$ to 0.16 seconds on an IBM 7040 computer for an N-wave.

In Figures 26 and 27, the pressure distribution at points A through F are plotted for a step input wave and for an N-wave respectively. The dotted lines represent the input waves if there were no corner or overhang effects.

## Pressure History on the Window of the Kinney Shoe
## Store - Numerical Method

The finite difference net (140 x 23) used is shown in Figure 28. The roof overhang was treated as a thin wall of negligible thickness, located between the two rows of net points $\ell = 9$ and $\ell = 10$, starting
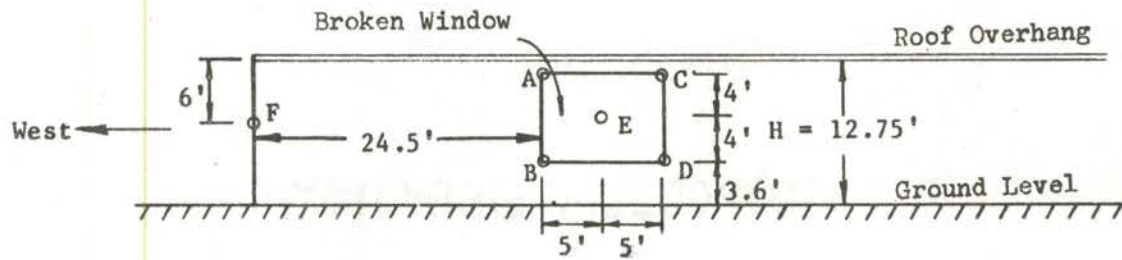
Figure 25. The Chosen Six Points on the North Wall of the Kinney Shoe Store for Overpressure Computations
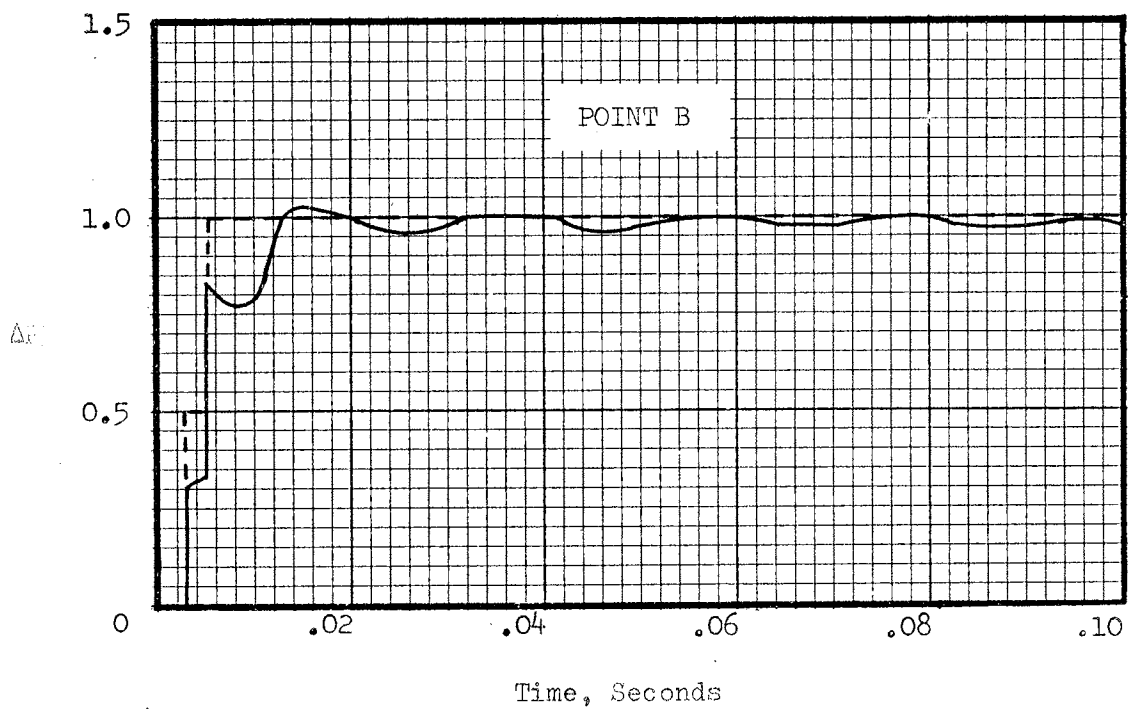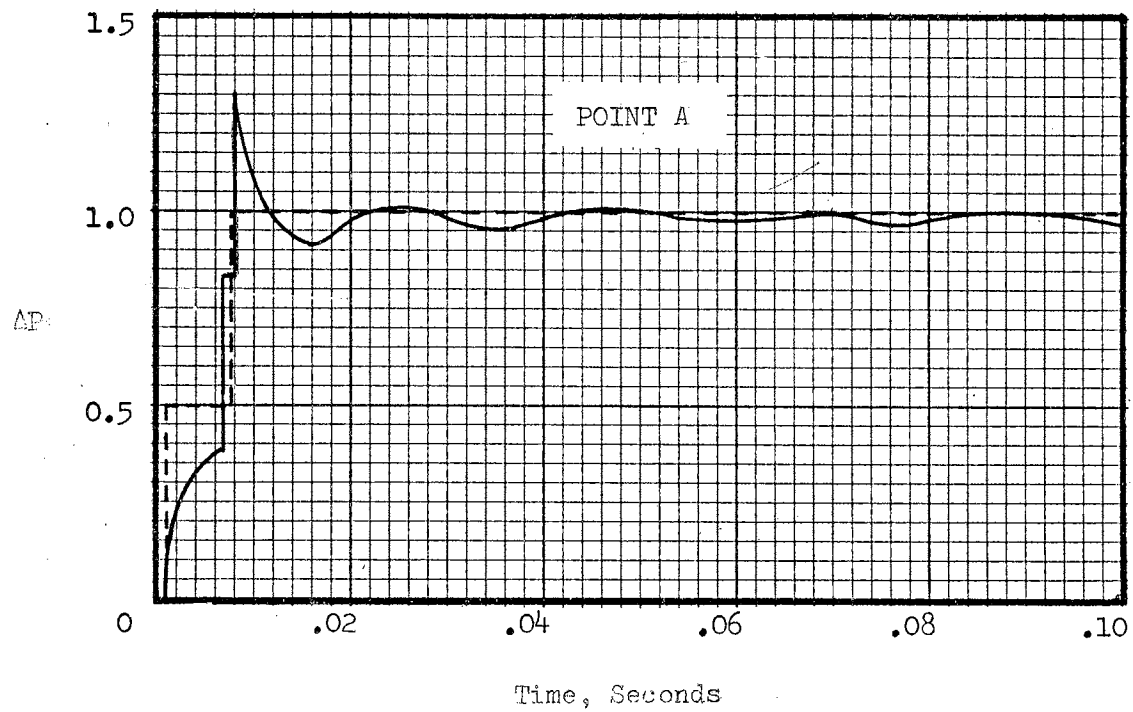
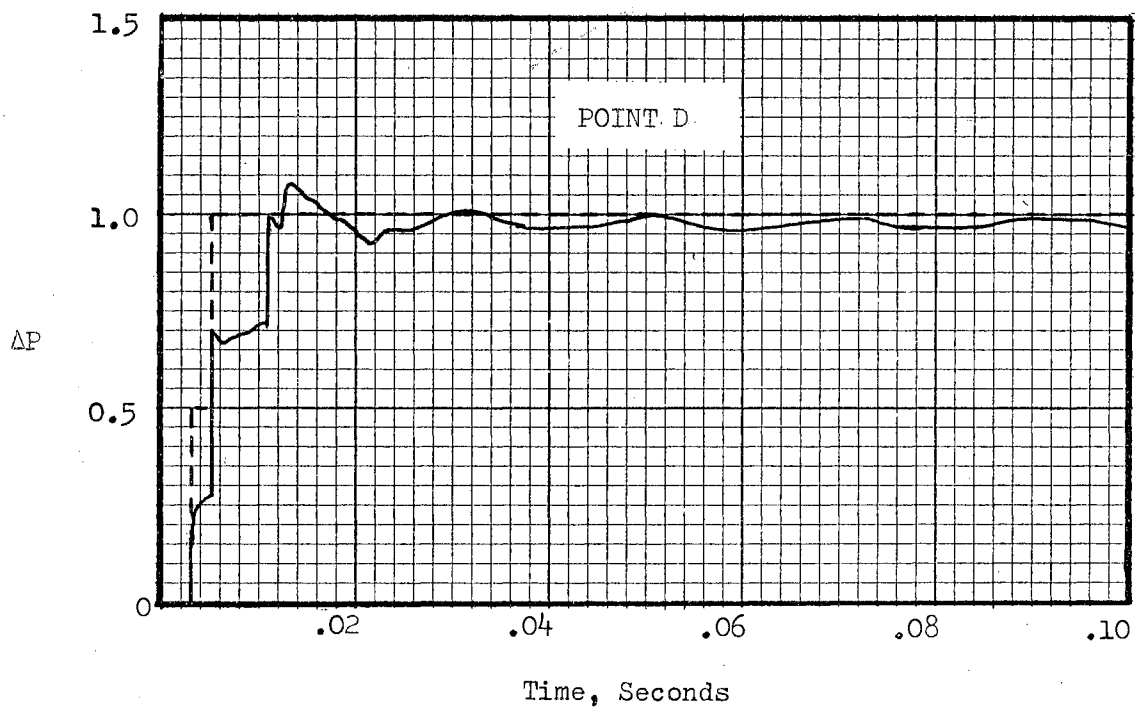Figure 26. Computed Pressure History by Analytical Method
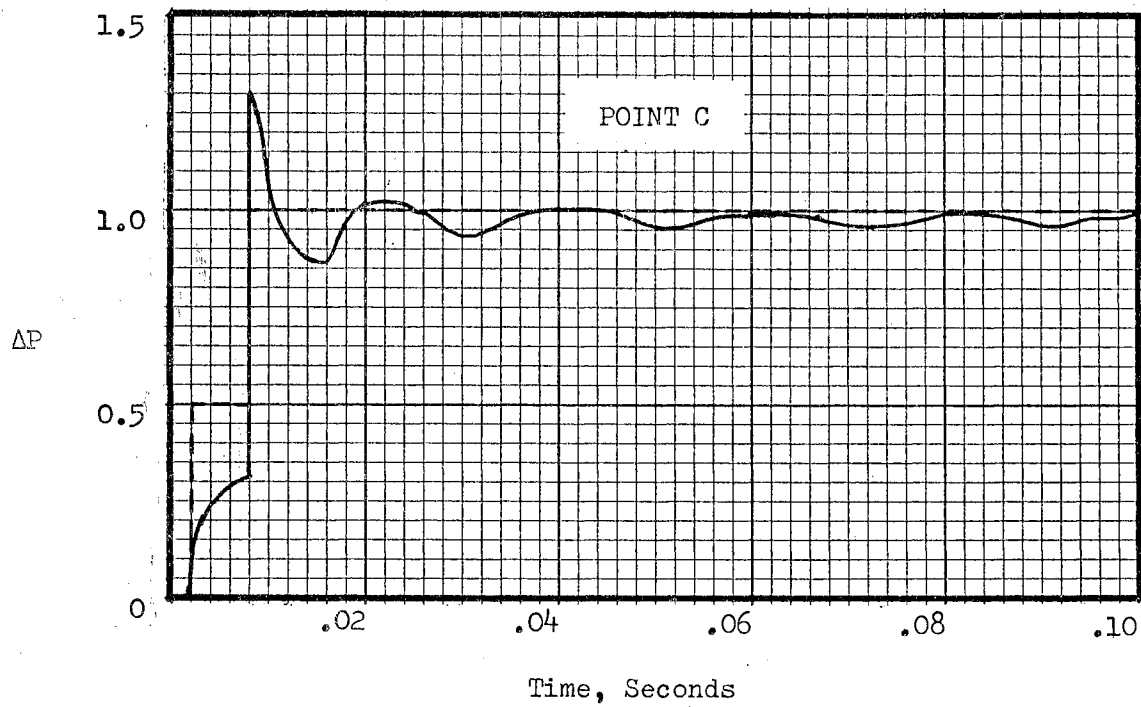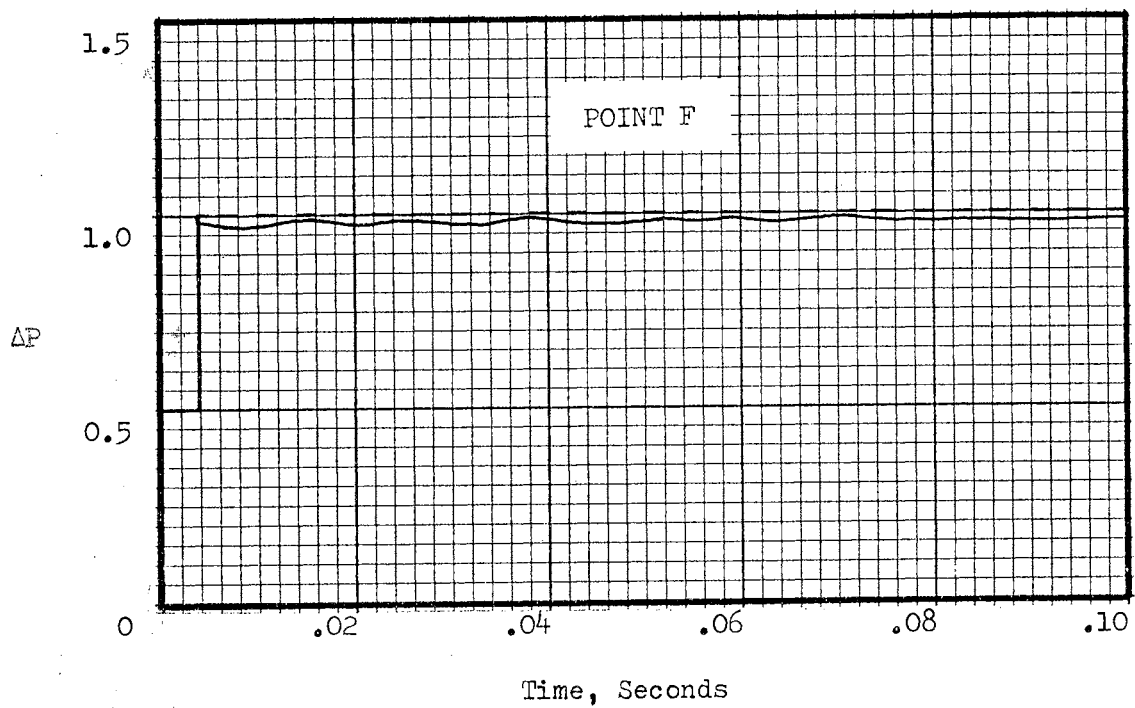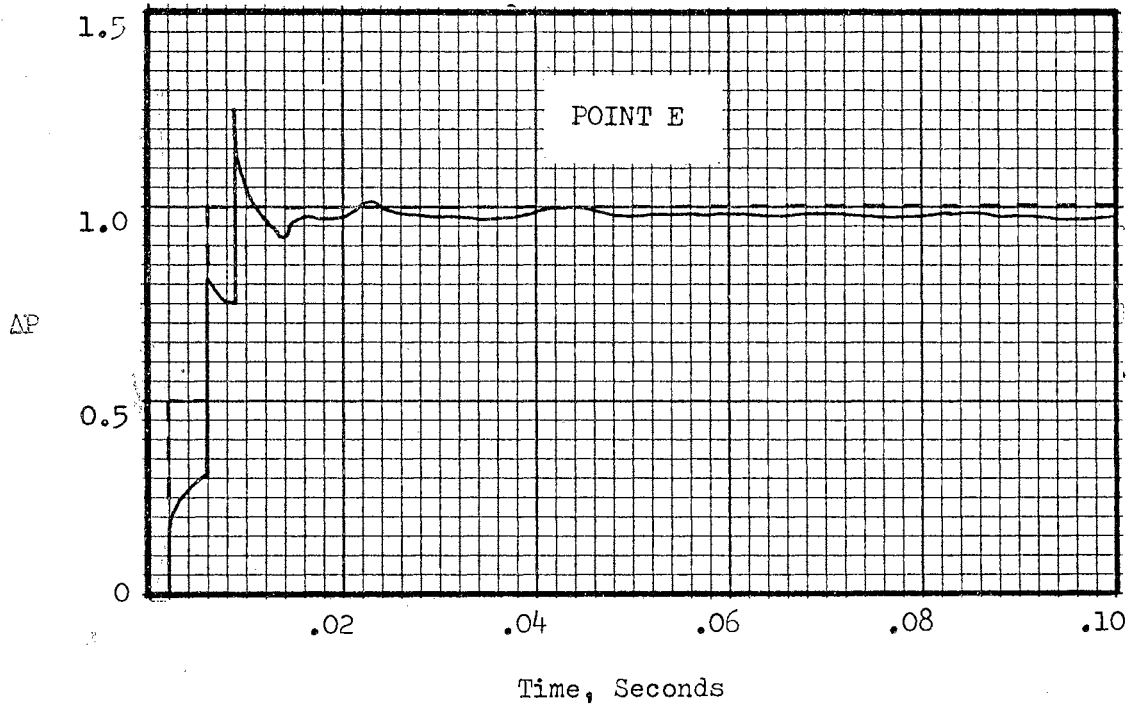for a Step-Wave of Unit Overpressure

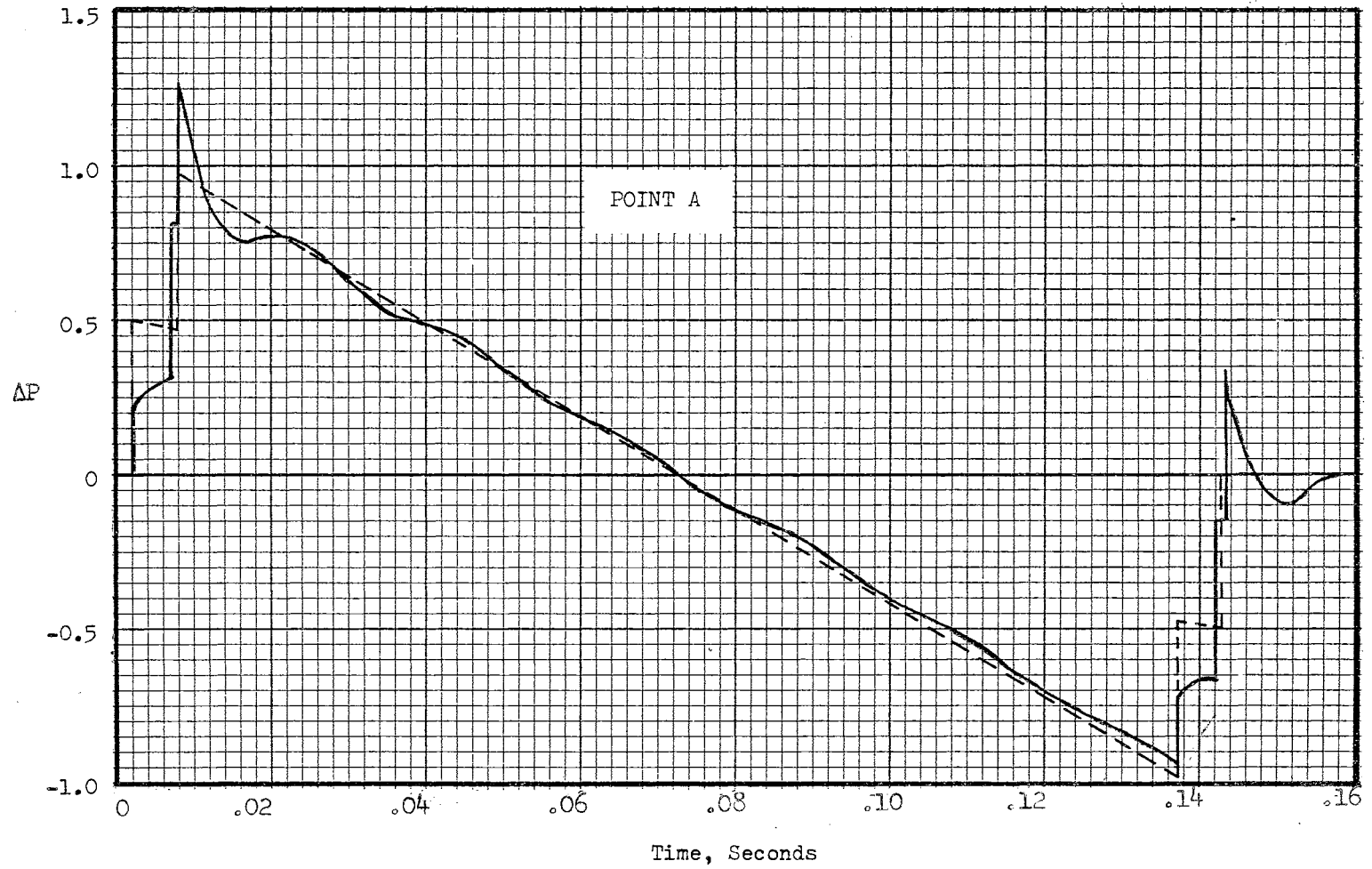Figure 26. (continued)

Figure 26. (continued)

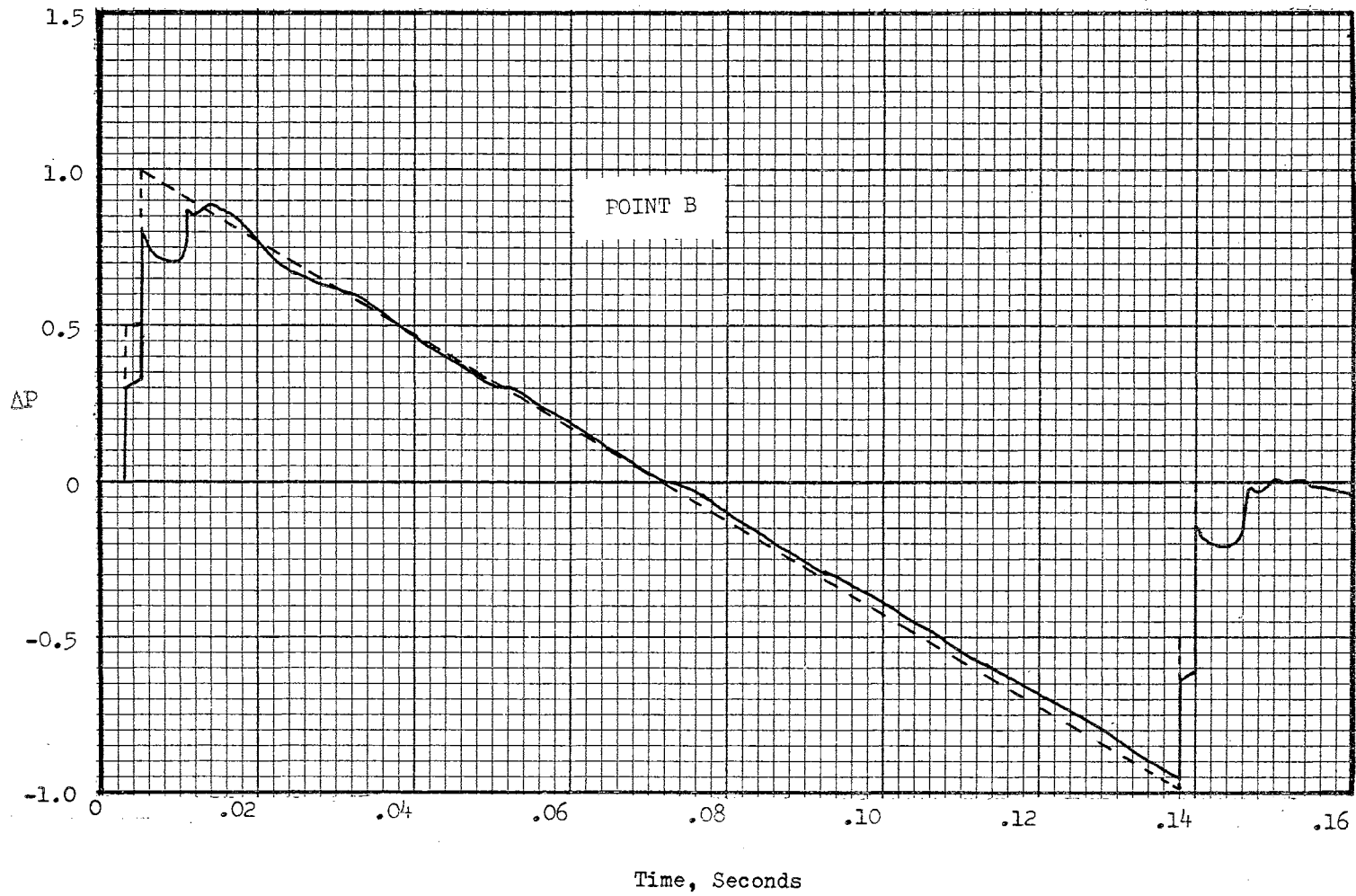Figure 27.  Computed Pressure History by Analytical Method for an N-Wave of Unit
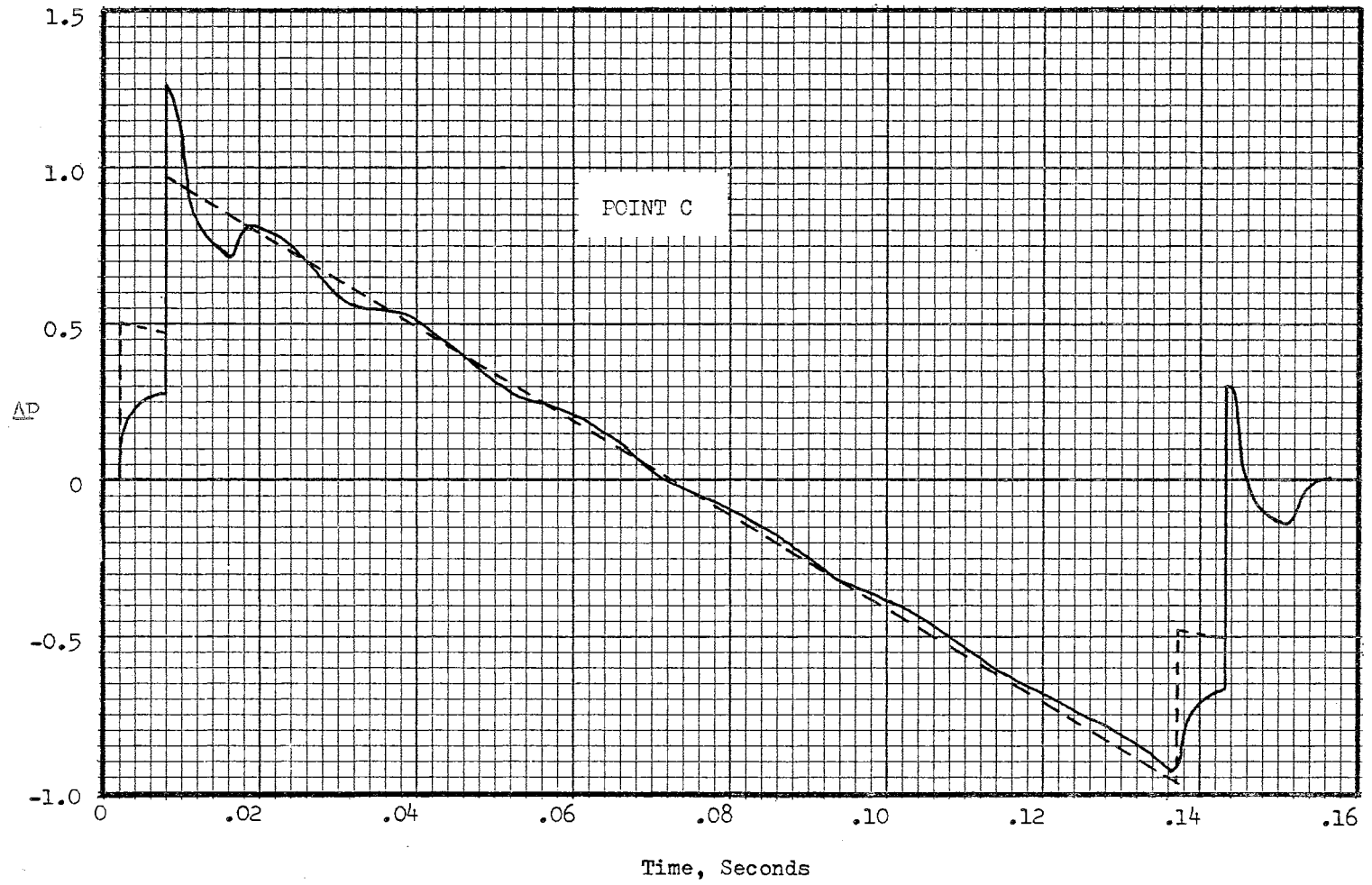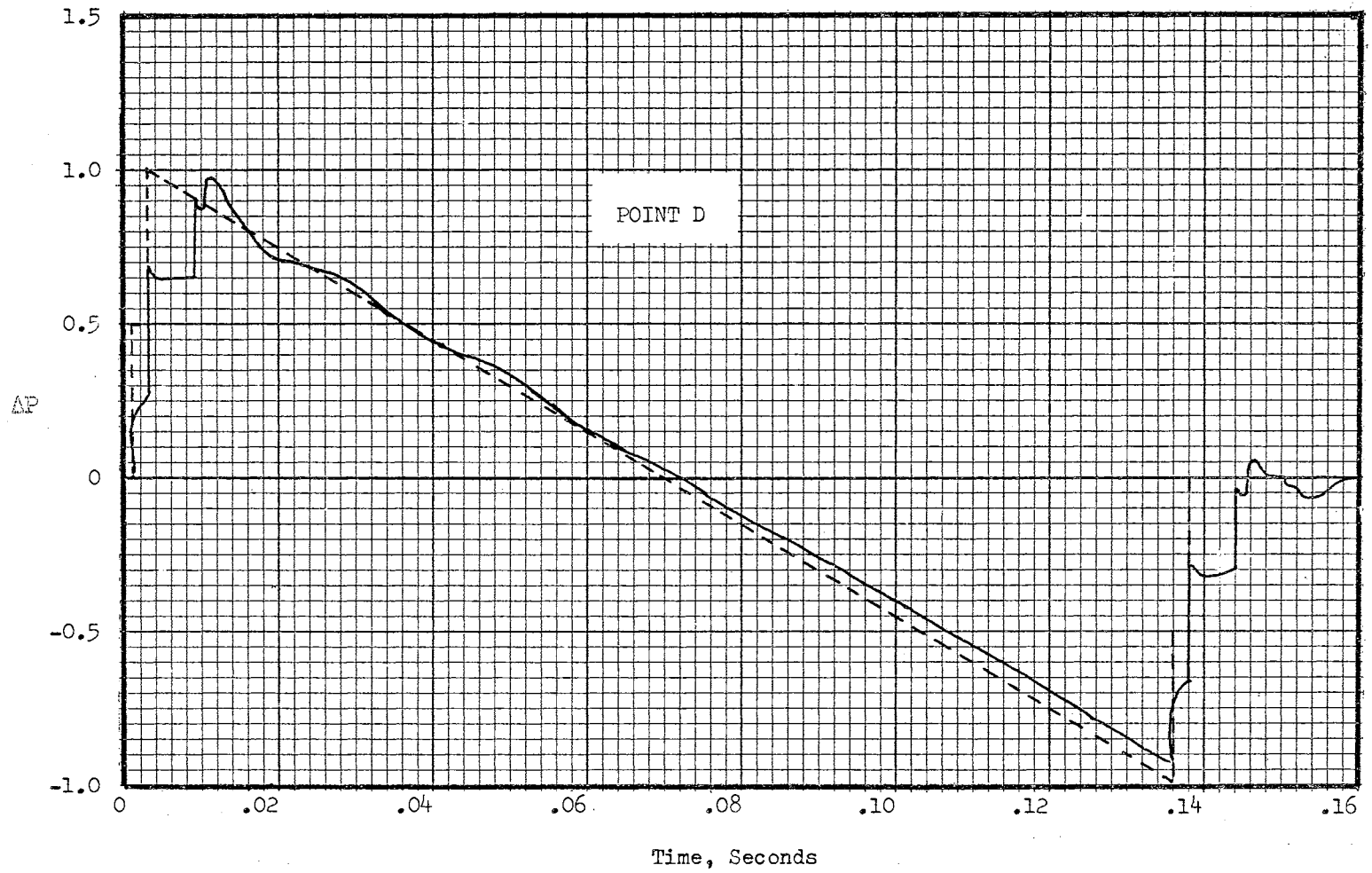Overpressure

Figure 27. (continued)
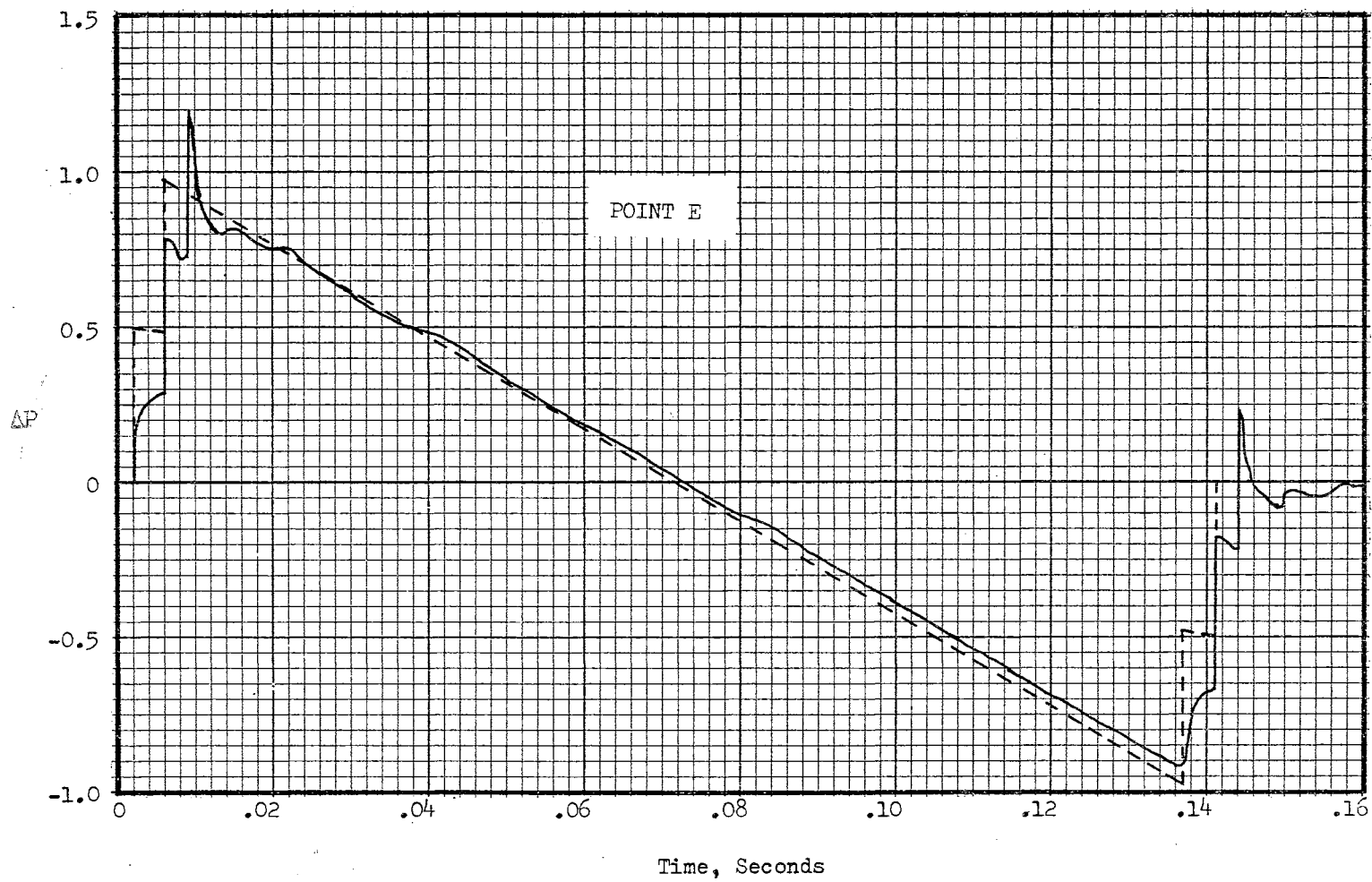
Figure 27. (continued)
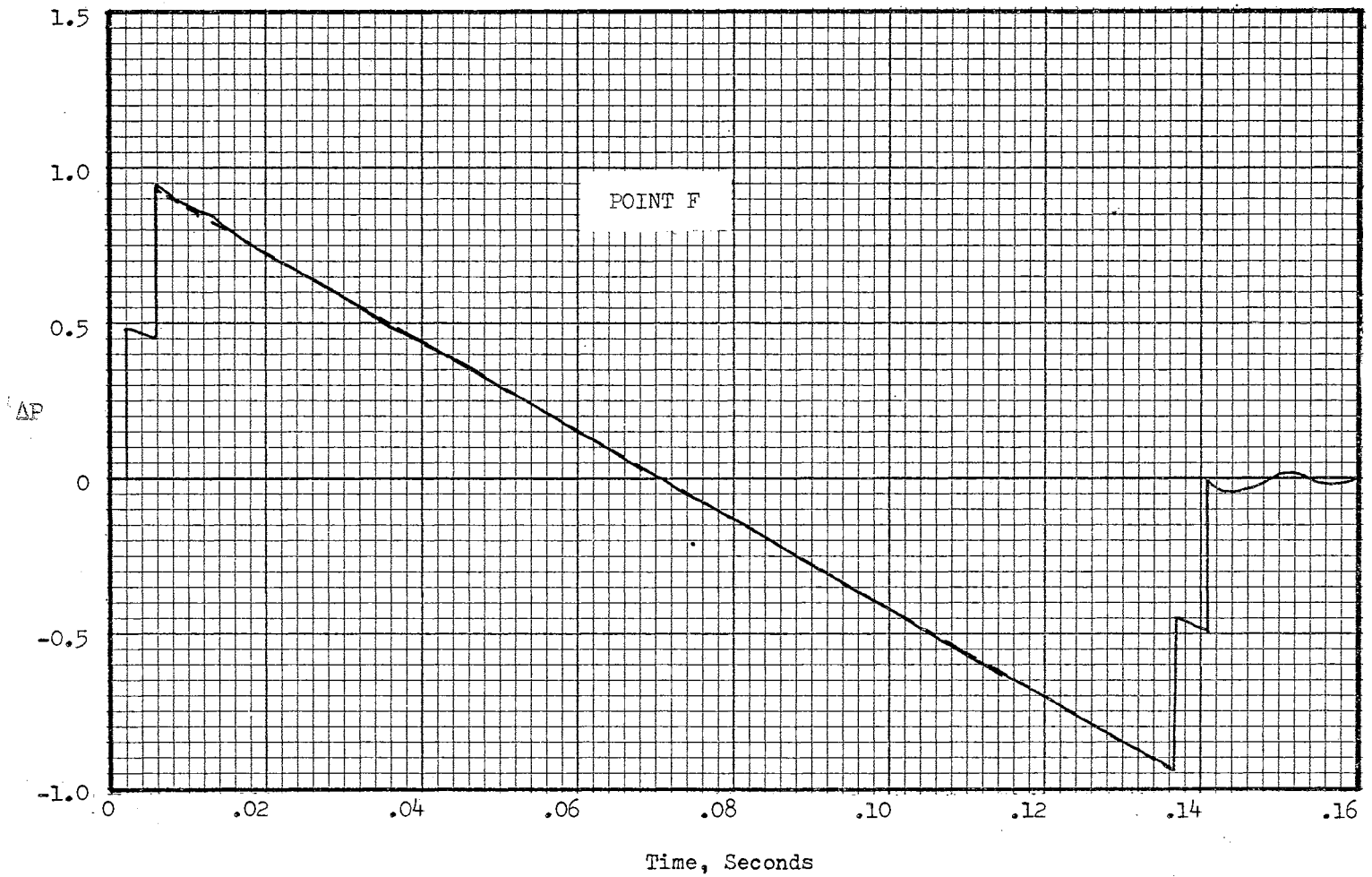
Figure 27. (continued)

Figure 27. (continued)

Figure 27. (continued)

from $k = 40$ and extending to $k_{max} = 140$. The objective was to estimate the pressure history at the same six points computed earlier by the analytical method, A through F, shown in Figure 28. A much larger field than necessary was chosen to reduce the errors that might be introduced at the flow plane boundaries, $k = k_{max}$, $\ell = 1$, and $\ell = \ell_{max}$, due to the inability of the boundary conditions to represent the physical boundaries. The shock wave angle, $\Phi_w$, was again taken as $70.1^\circ$, from the previous analysis. The mesh angle, $\chi$, was assumed to be the same as $\Phi_w$ so that the initial shock wave progressed the same number of net points in both x and y directions.

## Difference Equations for Field Points

Difference equations for field points were written for $u$, $v$, and $P$, with 's and 's treated as constants. Equations (5-22) and (5-23), were then

$$u_{k,\ell}^{n+1} = u_{k,\ell}^{n} - \frac{K_1}{2\rho_o}(P_{k+1,\ell} - P_{k-1,\ell})^n + \frac{\alpha}{2}(u_{k+1,\ell} + u_{k,\ell} - 2u_{k,\ell})^n$$

$$+ \frac{\beta}{2}(u_{k,\ell+1} + u_{k,\ell-1} - 2u_{k,\ell})^n ,$$

$$v_{k,\ell}^{n+1} = v_{k,\ell}^{n} - \frac{K_2}{2\rho_o}(P_{k,\ell+1} - P_{k,\ell-1})^n + \frac{\alpha}{2}(v_{k+1,\ell} + v_{k-1,\ell} - 2v_{k,\ell})^n$$

$$+ \frac{\beta}{2}(v_{k,\ell+1} + v_{k,\ell-1} - 2v_{k,\ell})^n , \qquad (6\text{-}15)$$

$$P_{k,\ell}^{n+1} = P_{k,\ell}^{n} - \frac{\gamma P_o}{2}\left[K_1(u_{k+1,\ell} - u_{k-1,\ell})^n + K_2(v_{k,\ell+1} - v_{k,\ell-1})^{\bar{n}}\right]$$

$$+ \frac{\alpha}{2}(P_{k+1,\ell} + P_{k-1,\ell} - 2P_{k,\ell})^n + \frac{\beta}{2}(P_{k,\ell+1} + P_{k,\ell-1} - 2P_{k,\ell})^n ,$$

where $P_o$ - atmospheric pressure, $\rho_o$ - atmospheric density.
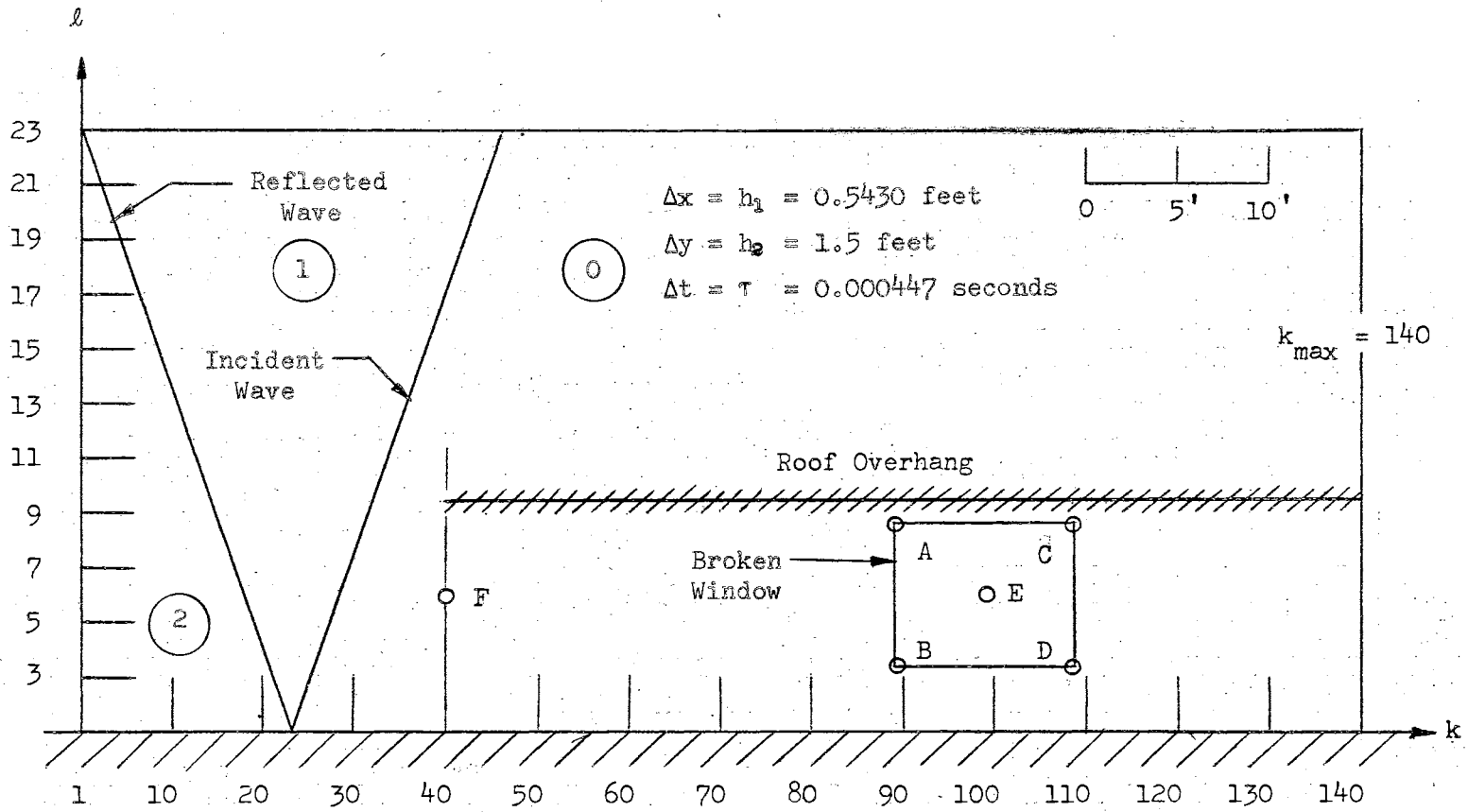
Figure 28. The Finite Difference Net

## Boundary Conditions

For the net points on the ground ($\ell = 1$), the difference Equations (6-15) were modified by using the boundary conditions,

$$P^n_{k,\ell-1} = P^n_{k,\ell+1} \; ,$$

$$u^n_{k,\ell-1} = u^n_{k,\ell+1} \; , \qquad\qquad (6\text{-}16)$$

$$v^n_{k,\ell-1} = - v^n_{k,\ell+1} \; .$$

For the net points adjacent to the roof overhang (see Figure 29), the difference equations were modified for the following boundary conditions:

For $\ell = 9$, $k = 40$ to 139:

$$P^n_{k,\ell+1} = P^n_{k,\ell} \; ,$$

$$u^n_{k,\ell+1} = P^n_{k,\ell} \; , \qquad\qquad (6\text{-}17)$$

$$v^n_{k,\ell+1} = - v^n_{k,\ell} \; .$$

For $\ell = 10$, $k = 40$ to 139:

$$P^n_{k,\ell-1} = P^n_{k,\ell} \; ,$$

$$u^n_{k,\ell-1} = u^n_{k,\ell} \; , \qquad\qquad (6\text{-}18)$$

$$v^n_{k,\ell-1} = - v^n_{k,\ell} \; .$$

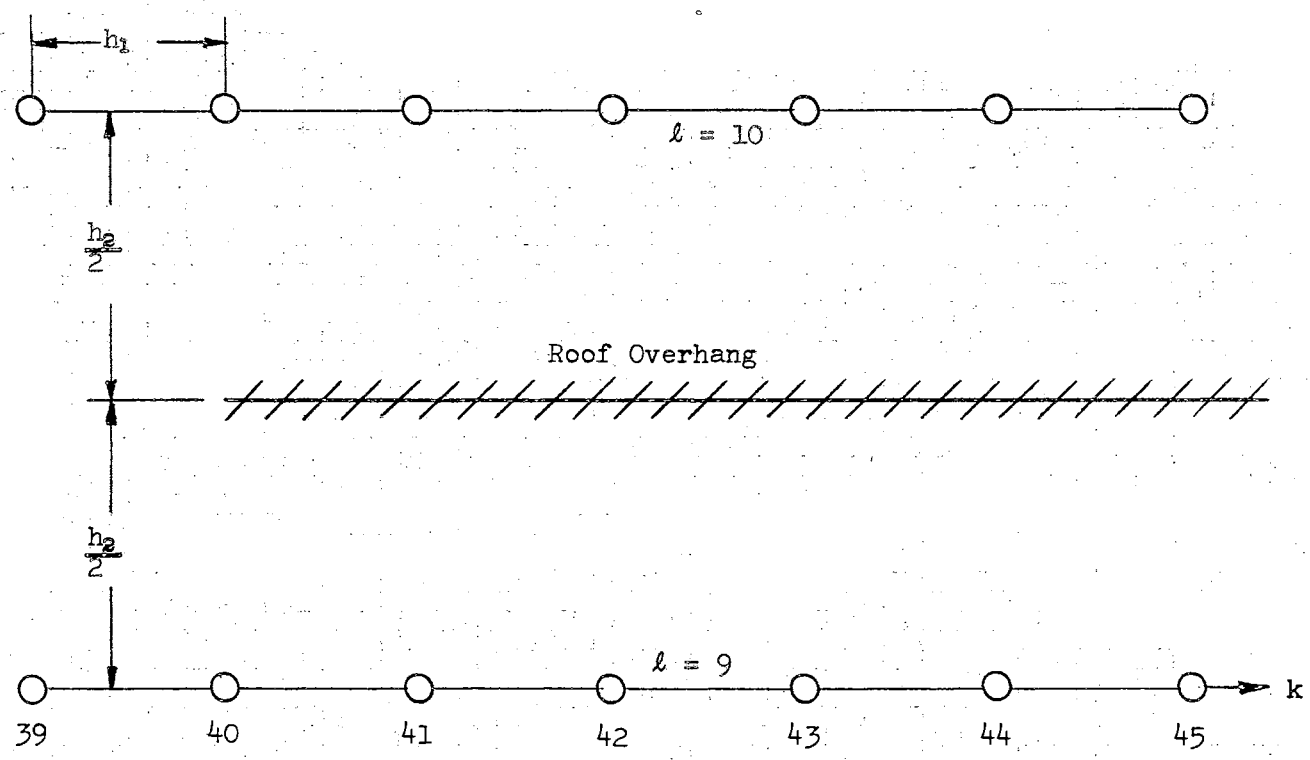Equations (6-16) to (6-18) were derived with the reflection technique described in Chapter V.

Figure 29. Net Points Adjacent to Roof Overhang

## Flow Plane Boundary Points

For the net points at $\ell = 1$: (left boundary)

$$P^{n+1}_{k,\ell} = f_1(t) ,$$

$$u^{n+1}_{k,\ell} = f_2(t) ,$$

$$(6\text{-}19)$$

$$v^{n+1}_{k,\ell} = f_3(t) ;$$

$f_1(t)$, $f_2(t)$, and $f_3(t)$ are functions of shock wave position at time $t$, assuming that the roof overhang's influence is negligible. To justify this assumption, a large field was chosen.

For the net points at $\ell = \ell_{max}$: (top boundary)

$$P^{n+1}_{k,\ell} = P^{n+1}_{k,\ell-1} ,$$

$$u^{n+1}_{k,\ell} = u^{n+1}_{k,\ell-1} ,$$

$$(6\text{-}20)$$

$$v^{n+1}_{k,\ell} = v^{n+1}_{k,\ell-1} .$$

These conditions force the incident and reflected shocks to become straight and parallel to the y-axis at the top boundary. In spite of its inability to represent the proper physical conditions, this proved to be better than any other possible method, such as extrapolation. The criteria for selection of upper and right boundary representations was that waves incident on the boundary should be reflected as little as possible.

For the net points at $k = k_{max}$: (right boundary)

$$P^{n+1}_{k,\ell} = P^{n}_{k-1,\ell} ,$$

$$(6\text{-}21)$$

$$u^{n+1}_{k,\ell} = u^{n}_{k-1,\ell} , \qquad v^{n+1}_{k,\ell} = v^{n}_{k-1,\ell} .$$

The following numerical values were used in the computations:

$$T_o = 83^\circ \text{ F .}$$

$$c = \text{constant} = c_o = 1142.8 \text{ ft/sec .}$$

$$P_o = 2000 \text{ psf .}$$

$$\rho = \text{constant} = \rho_o = 0.002145 \text{ slugs/ft}^3 \text{ .}$$

$$\Delta x = h_1 = h_2 \cot \Phi_w = 0.5430 \text{ feet .}$$

$$\Delta y = h_2 = 1.5 \text{ feet .}$$

$$K = 1/c = 0.000875 \text{ seconds.}$$

$$K_1 = h_1/\tau = K \sin \chi = 0.000824 \text{ seconds.}$$

$$K_2 = h_2/\tau = K \cos \chi = 0.000297 \text{ seconds.}$$

$$\Delta t = \tau = 0.000447 \text{ seconds.}$$

$$\omega = 1.$$

$$\alpha = K\omega c \sin^2 \chi = \sin^2 \chi = 0.884.$$

$$\beta = K\omega c \cos^2 \chi = \cos^2 \chi = 0.114.$$

### Computations and Results of the Numerical Method

Computer programs were written for both a step input with incident-plus-reflected wave strength of 1 psf, and for an N-wave having bow-to-tail wave time interval of 0.135 seconds and a strength of 1 psf. The initial conditions assumed for the step input in regions (0), (1), and (2) of Figure 28, were:

$$P_o = 2000 \text{ psf .}$$

$$u_o = 0 .$$

$$v_o = 0 .$$

$$P_1 = 2001 \text{ psf .}$$

$$u_1 = \frac{c(P_1 - P_o)}{P_o} \sin \chi .$$

$$v_1 = \frac{c(P_1 - P_0)}{P_0} \cos \chi.$$

$$P_2 = 2002 \text{ psf.}$$

$$u_2 = 2u_2.$$

$$v_2 = 0.$$

The N-wave was treated the same way as in the previous analysis except that here 302 expansions waves were taken so that they were spread by a distance of one field point width in the x-direction. Initial conditions in region (0) were the same as above, but in regions (1) and (2) algebraic sums of the incident and reflected compression and expansion waves were considered.

Pressure histories for the six points, A through F, were computed by interpolation of the adjacent field points for both a step input and an N-wave. On an IBM 7040 computer, about 60 minutes were required to compute the pressure history for the field of 3220 points from 0 to 0.18 seconds (415 time planes), printing the values for the six points at each 0.001 seconds interval. The programs were quite simple and it took only 2.7 milli-seconds for each point-time plane.

As a check on the validity and the applicability of the numerical method, the results were plotted and compared with the results obtained by the analytical method. In Figures 30 and 31, the pressure distribution at points A through F are shown for a step input and for an N-wave respectively. The dotted lines represent the results of the analytical method. As can be seen, the agreement is very good.
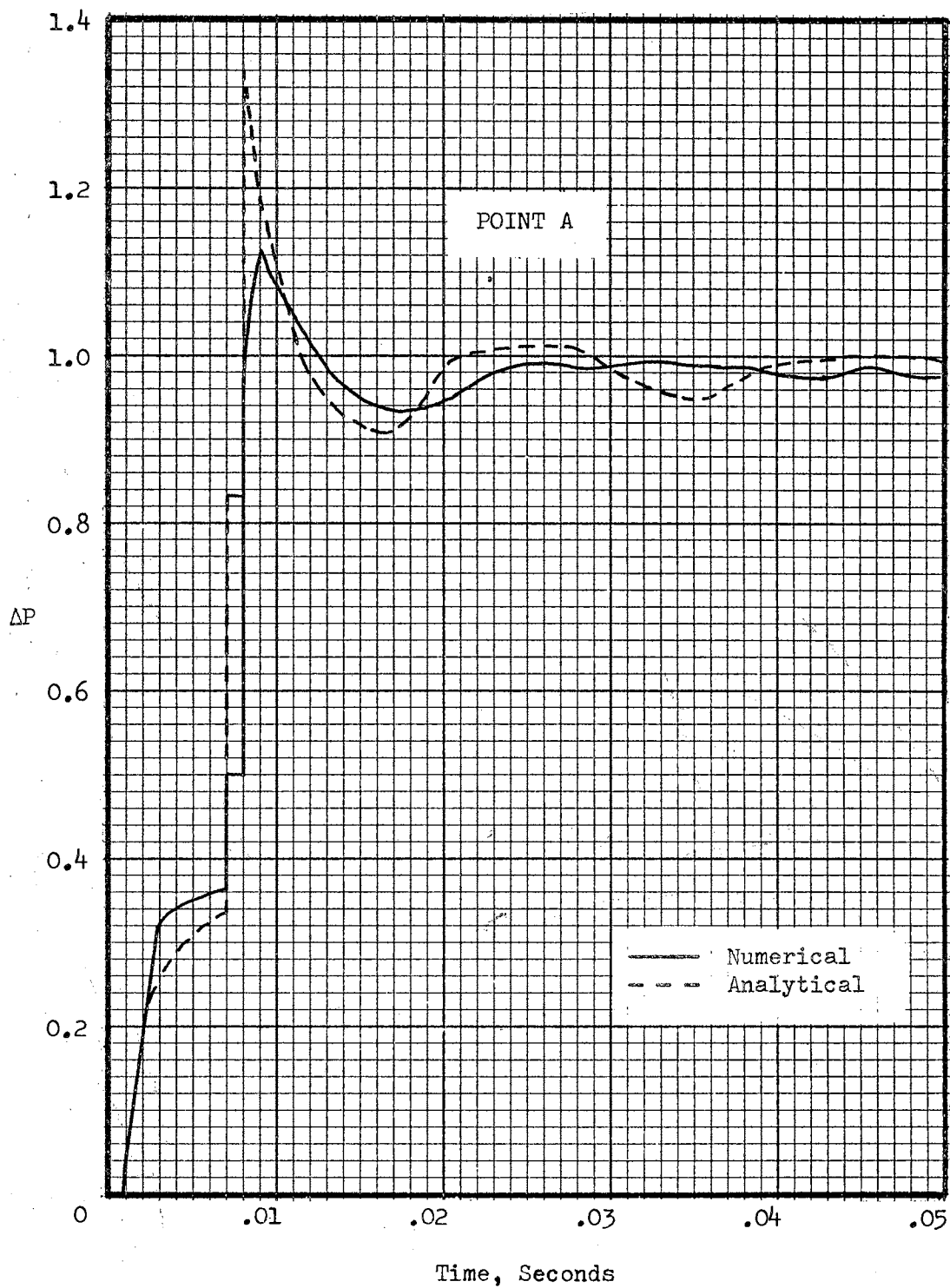
Figure 30. Comparison of Computed Pressure Histories by
Numerical and Analytical Methods for a Step-
Wave of Unit Overpressure
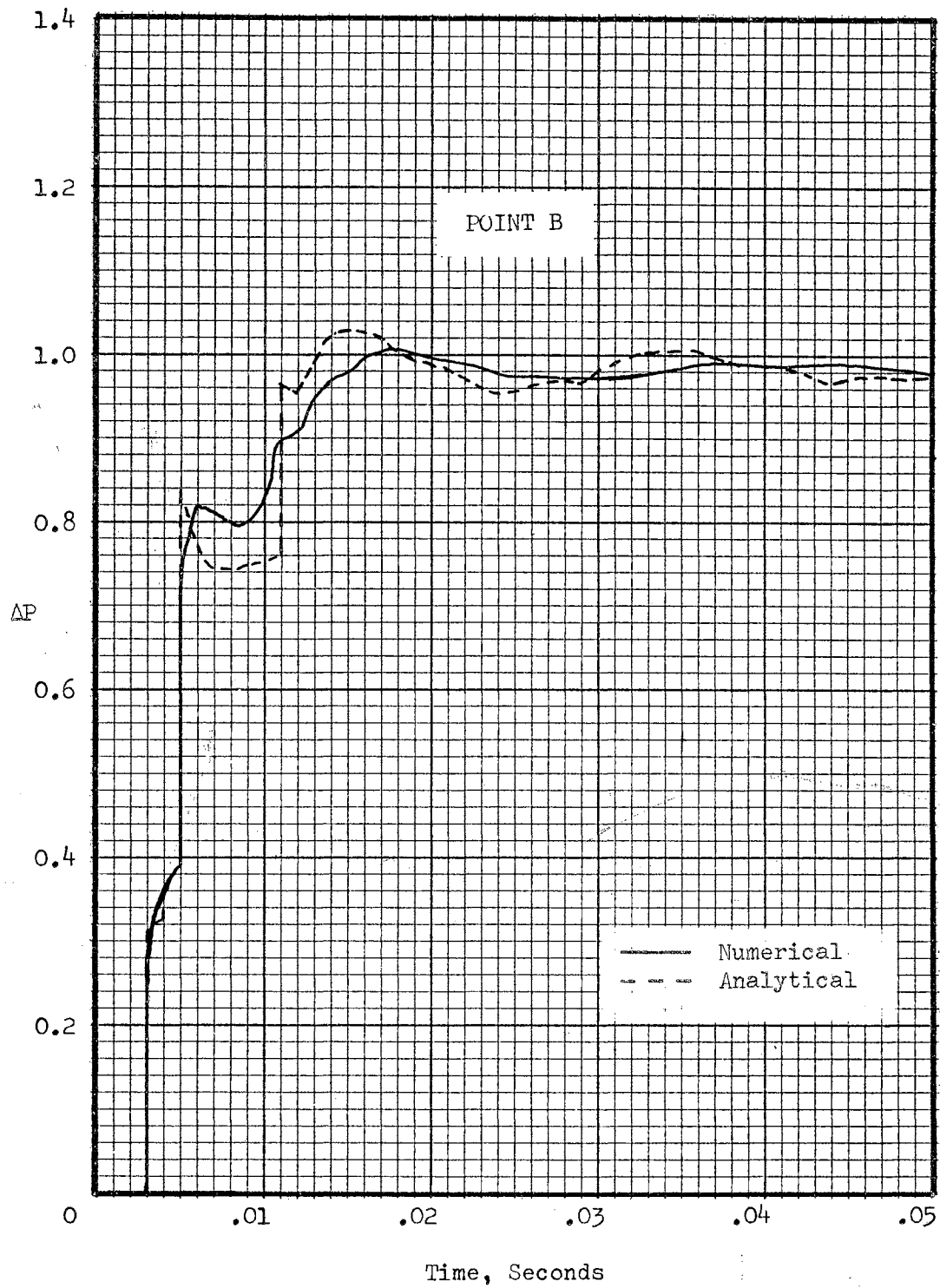
Figure 30. (continued)

Figure 30. (continued)

Figure 30.  (continued)

Figure 30. (continued)

Figure 30. (continued)

Figure 31.  Comparison of Computed Pressure Histories by Numerical and Analytical
Methods for an N-Wave of Unit Overpressure

Figure 31. (continued)
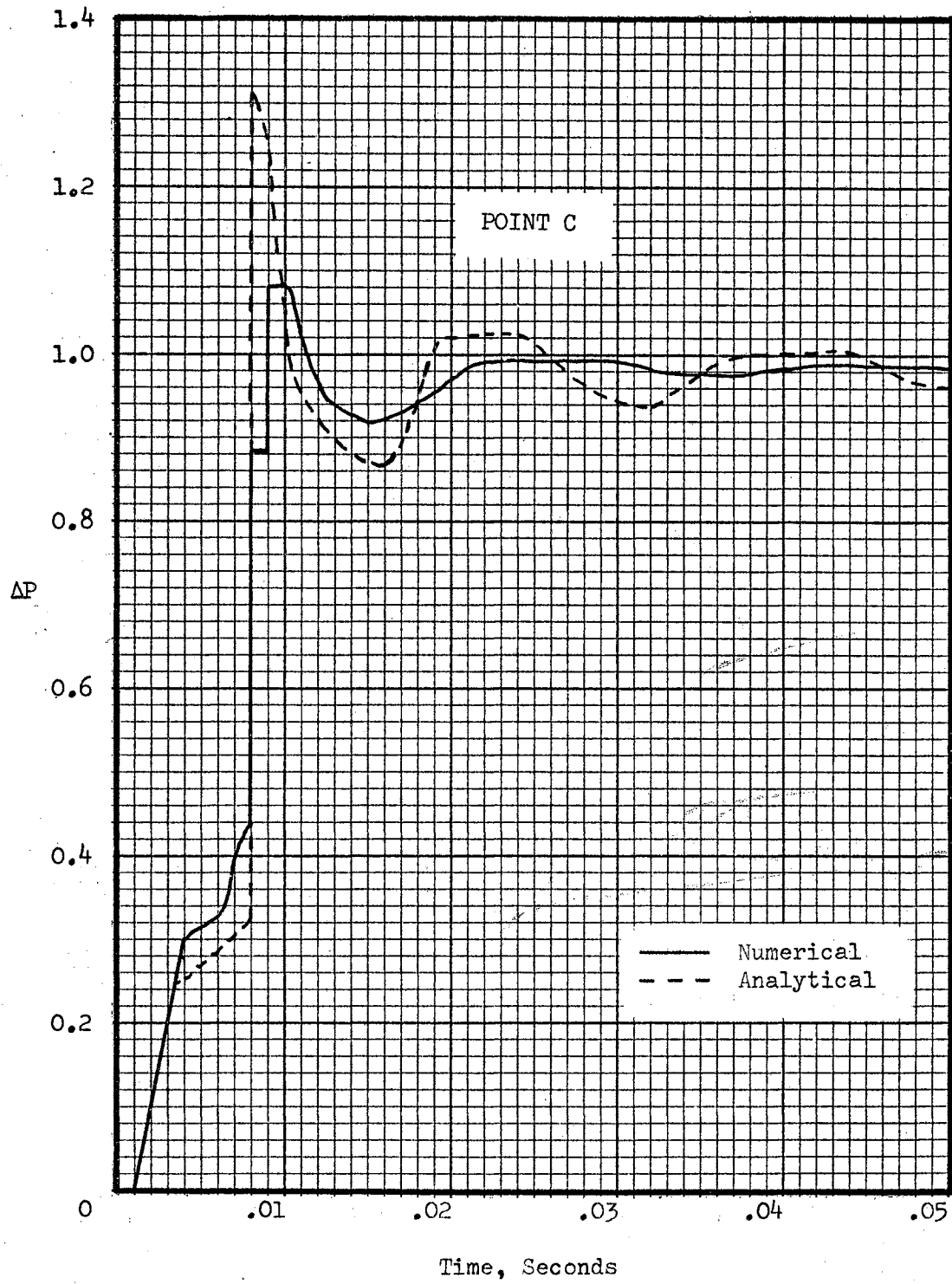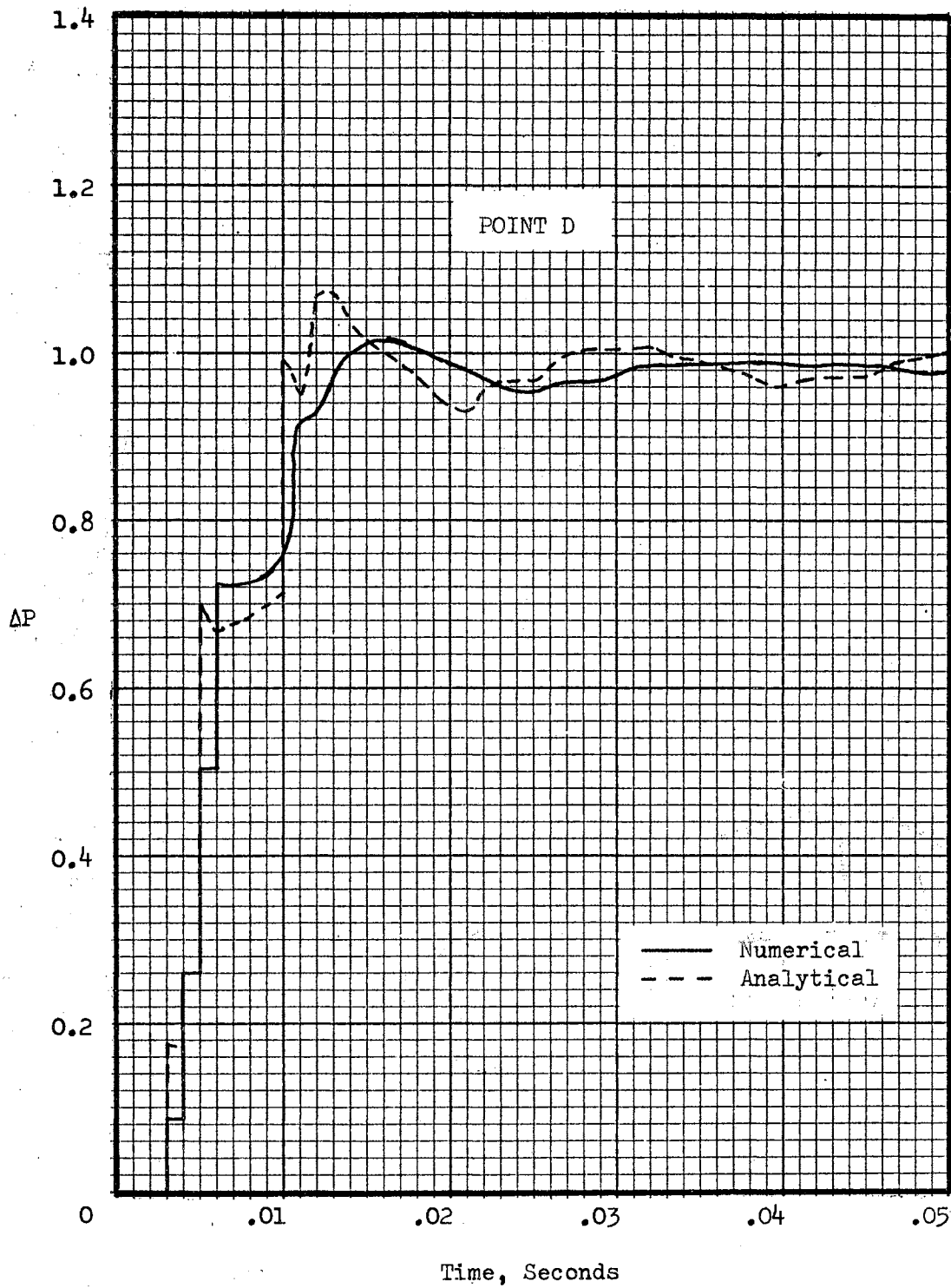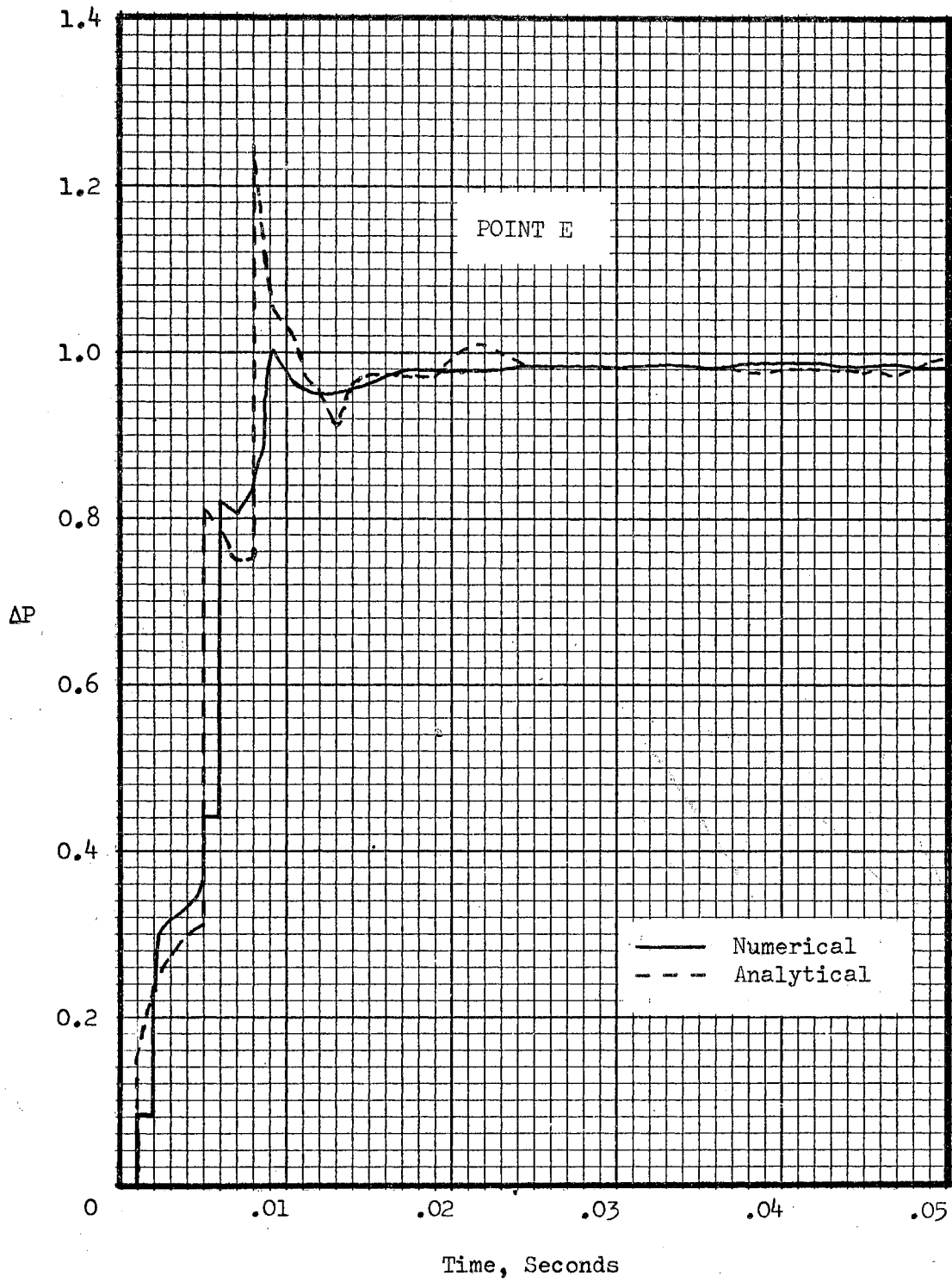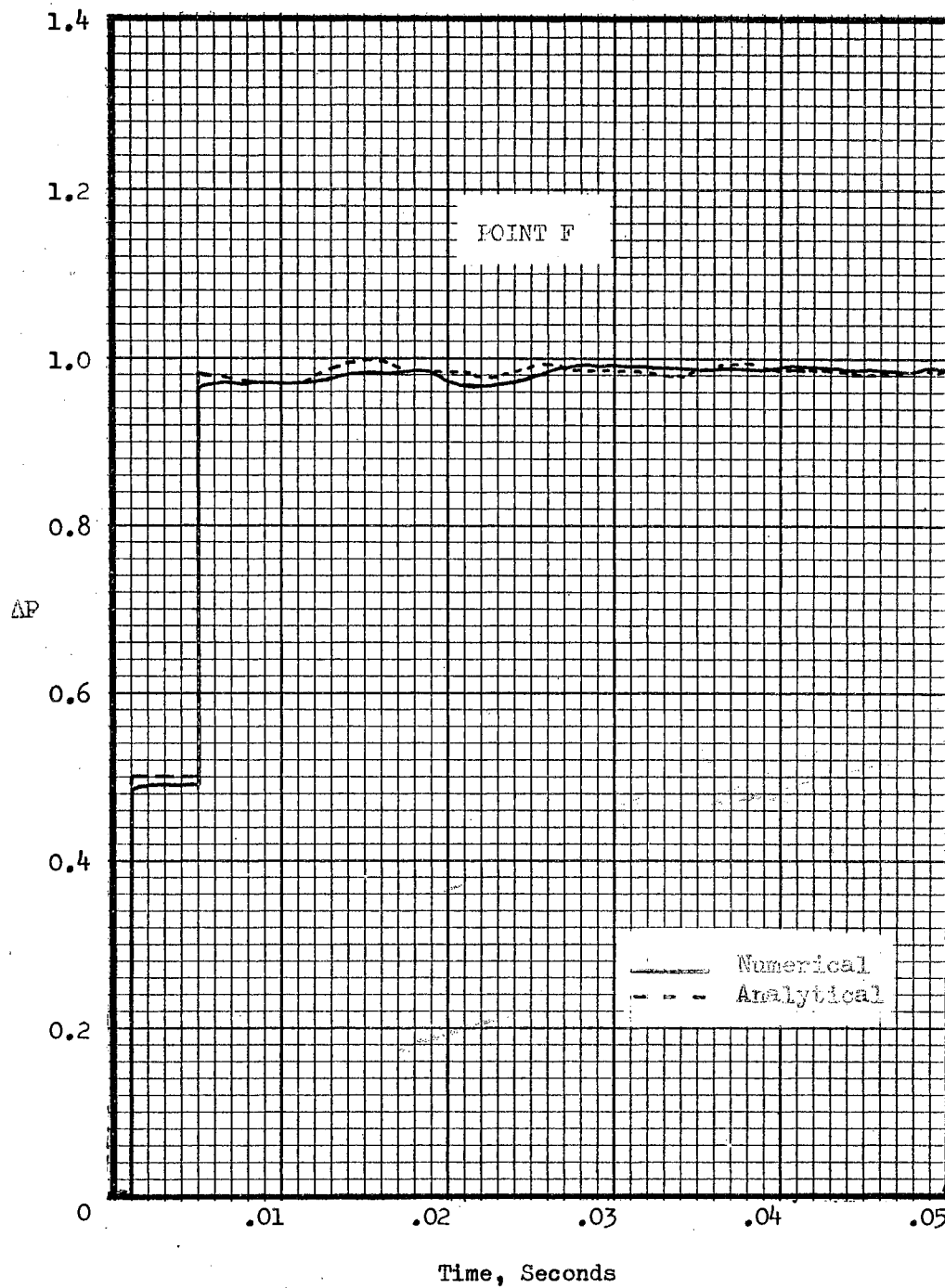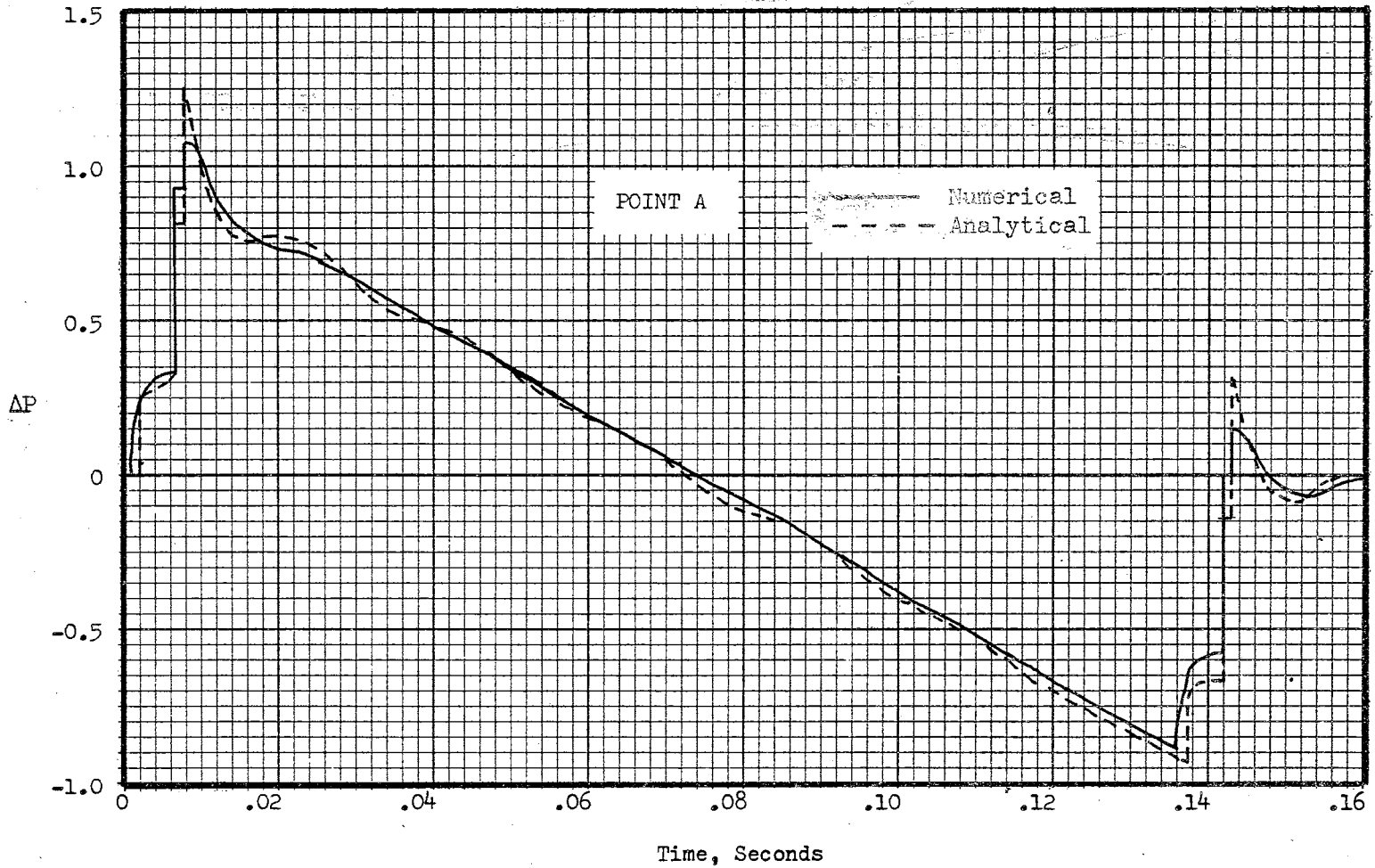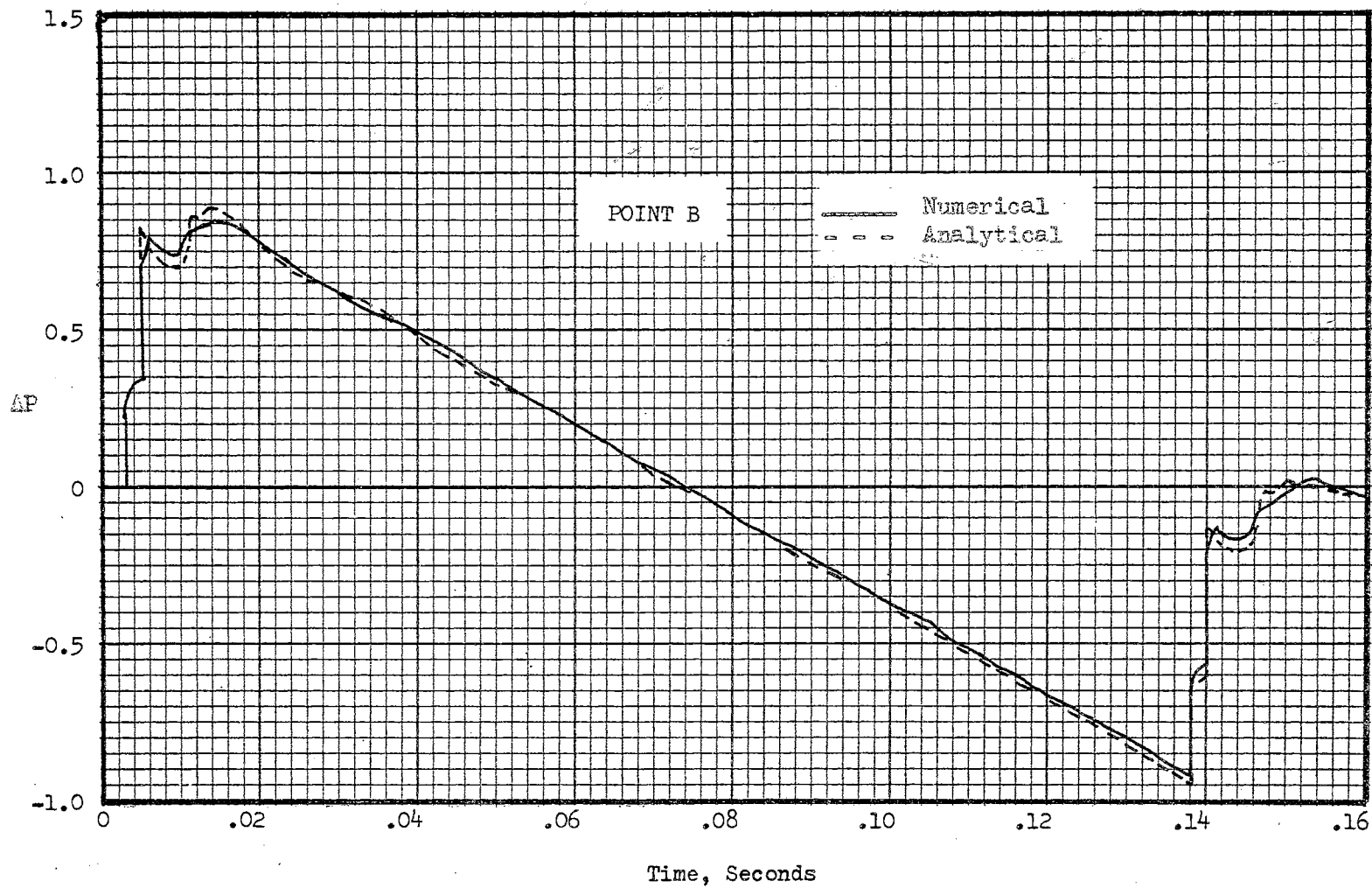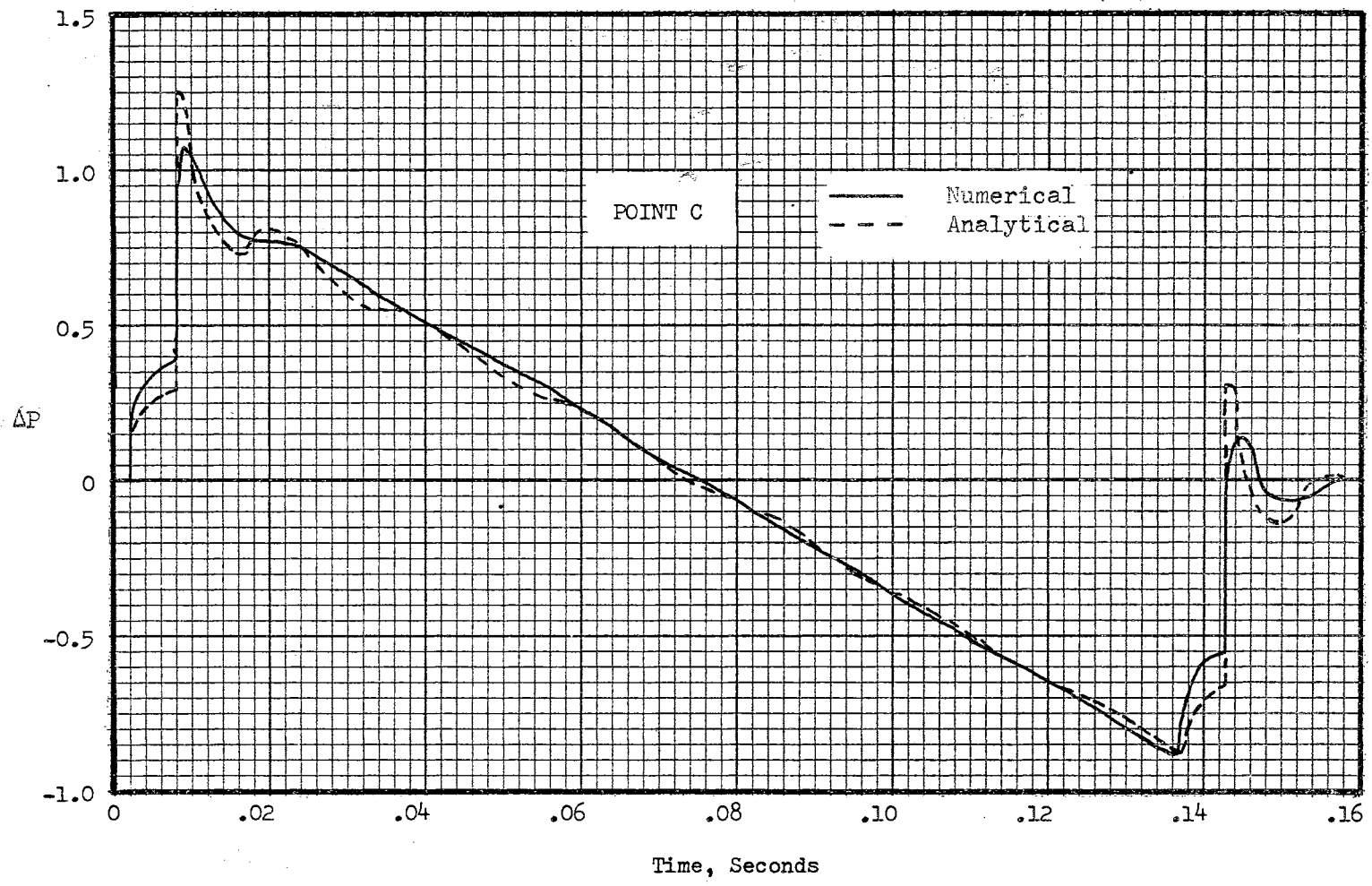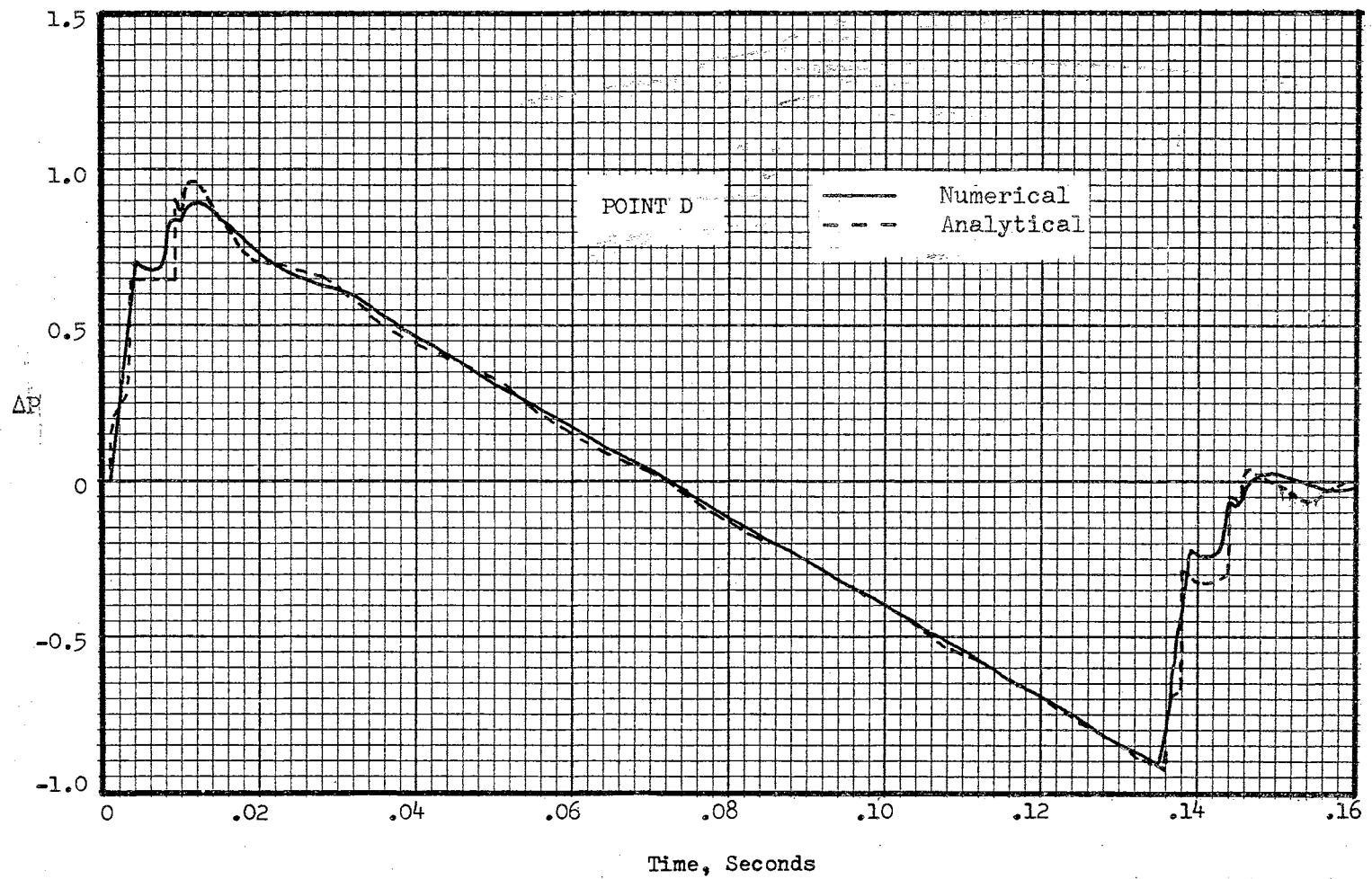
Figure 31. (continued)

Figure 31. (continued)
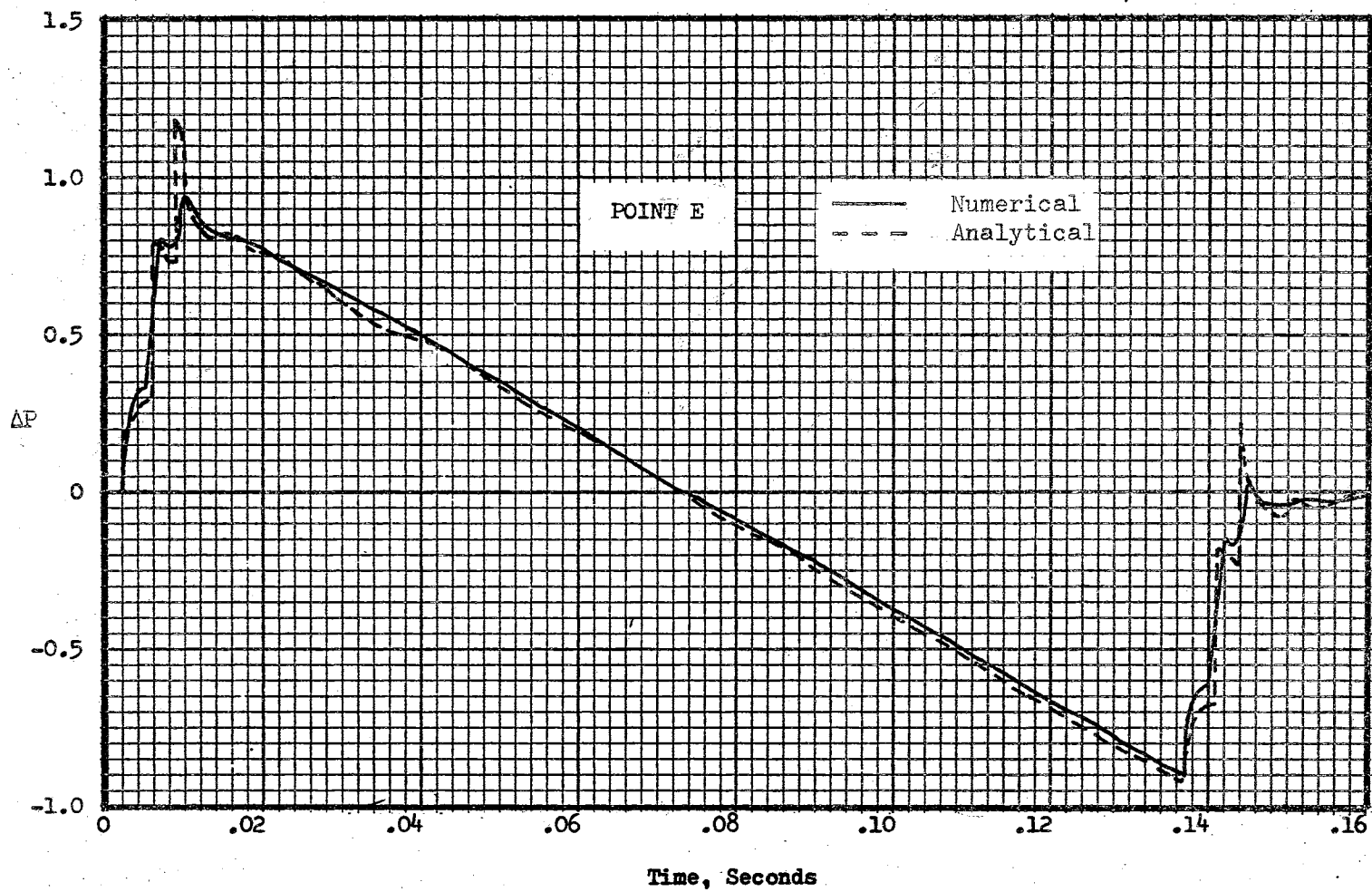
Figure 31. (continued)
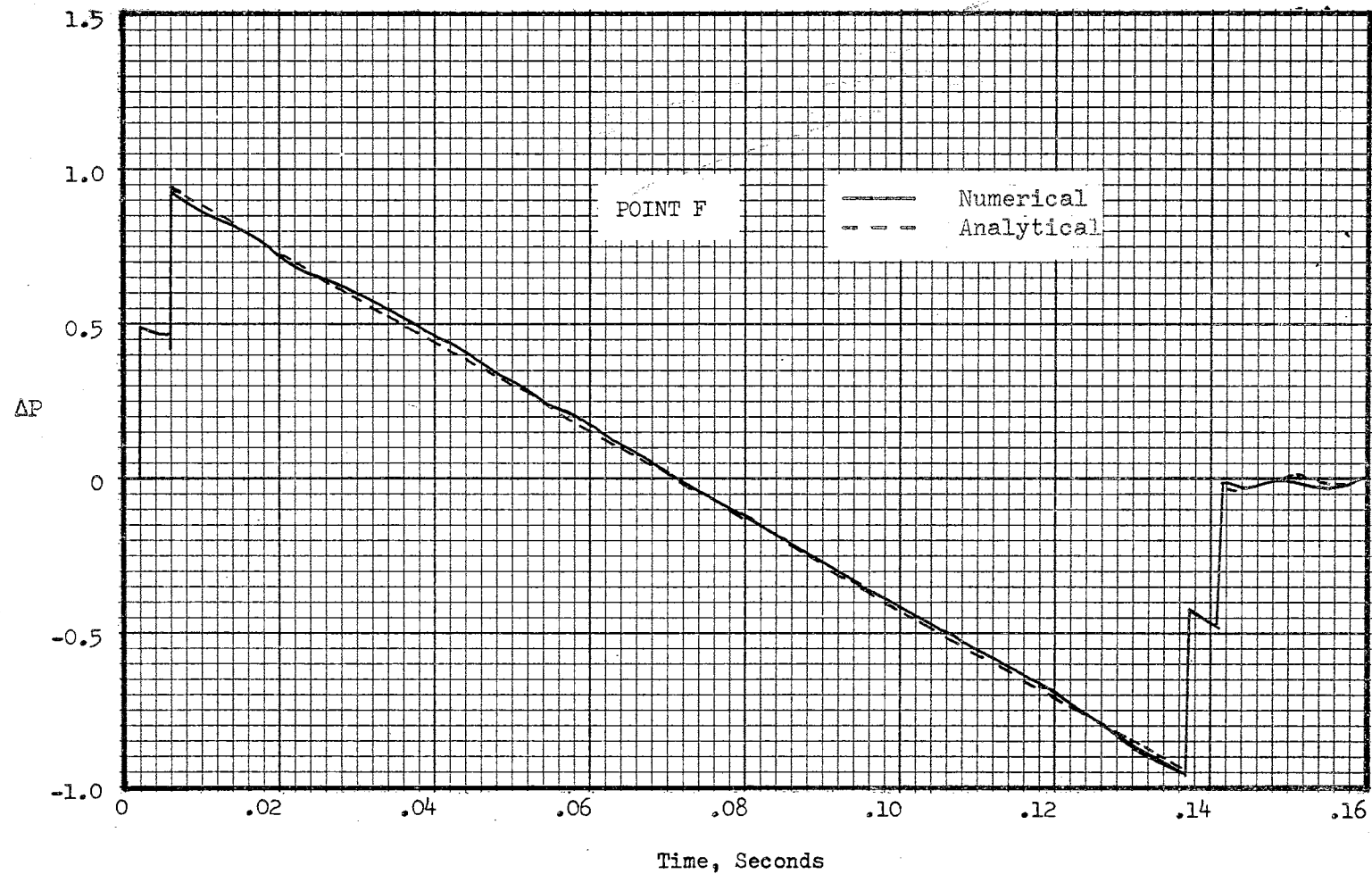
Figure 31. (continued)

## Discussion of the Results

For a two-dimensional analysis, both analytical and numerical methods produced essentially the same results. To test the validity of the results, point F was located in such a way that one can intutively reason that the roof overhang effects are negligible at this point. In Figures 26, 27, 30, and 31, pressure distribution for point F by both analytical and numerical methods was almost the same as the pressure distribution if the roof overhang were removed. These results indicate the validity of both the methods. The analytical method rests on solid physical and mathematical foundations. The primary objective in trying the numerical method was to investigate its applicability to a sonic boom wave problem. If one looks at the results for points A through F in Figures 30 and 31, the comparison of the numerical and analytical methods was excellent excepting that the numerical method smoothens out the peak overpressures. Of course, this is to be expected in this numerical technique due to the addition of the blurring terms. Solutions were sought for smaller values of the blurring terms but they were unstable in the shock regions. Thus, one must be prepared to sacrifice some accuracy to apply the numerical method. But unlike the analytical method, the numerical technique can be extended to a three-dimensional problem which will be of great use in sonic boom wave/structure interaction problems. Due to the simplicity of the weak wave equations involved the computation time would be much less than in the case of a strong shock wave problem such as those reported in References (8) and (10).

CHAPTER VII

CONCLUSIONS AND RECOMMENDATIONS

Conclusions

Three methods were presented in Chapter III for calculating the
time-of-arrival of an incident wave and the time interval between
incident and reflected waves for a wall facing the wave. These gave
almost identical results for small offset distances (10,000 feet or
less) from the flight track. The differences in results were greatest
at low Mach numbers and large offset distances(up to 70,000 feet).
The conical wave analysis (Method I) deviated most greatly from the
other two. Method II, which assumed an atmosphere with a realistic
linear variation of acoustic velocity with altitude up to the tropo-
pause, is recommended for problems where shock wave angles are to be
found accurately. Method III, which made the simplifying assumption
of constant ray angle projection in the vertical plane normal to the
flight path, and used the linear variation of acoustic velocity as in
Method II, is considered to be the most practical method. That is, it
achieves nearly the same result as the more exact method, but with
considerably less computation time. This method is proposed to provide
a means of computing incident wave time relationships when wind effects
are not significant.

For a two-dimensional analysis to predict the pressure-history

of a sonic boom wave diffracted and reflected by corners and walls,
both analytical and numerical methods were developed. The numerical
method compared well with the analytical method excepting that the
numerical method smoothened the peak overpressures. Boundaries do
present considerable difficulties in the numerical method and it is
very important to apply boundary conditions consistent with the
physical problem in consideration. The analytical method rests on
firm physical and mathematical foundations. The numerical method is
therefore concluded to be a flexible, practical technique for computing
the multiple reflection and diffraction problems generally associated
with sonic boom interactions with structures.

<div align="center">Recommendations for Future Work</div>

Since most sonic boom interactions are three-dimensional in nature,
the numerical method should be extended to three dimensions. No
special difficulty is anticipated in this except for increased com-
plexity and the need for a large capacity computer. On the IBM 7040
computer with a storage capacity of 32,000 storage positions, flow
fields of about 3600 points, such as (20 x 15 x 12), (20 x 20 x 9),
and (15 x 15 x 16), can be handled.

Several interesting problems should be attempted by the two and
three dimensional numerical methods, including those corresponding to
any test data which may become available. At present Dr. G. W. Zumwalt,
Prof. L. J. Fila, and the author are working at Oklahoma State Uni-
versity in a "Sonic Boom" research project sponsored by National
Aeronautics and Space Administration. Studies of the propagation of
disturbances, such as gusts, in a sonic boom wave and the wave shape

changes in the vicinity of the aircraft, are being undertaken. The author believes that the numerical method developed in this study and be effectively used in these studies.

In this work sonic boom waves were assumed to be produced by aircraft in level flight. The equations of the method (Method II) which assumes an atmosphere with a linear variation of acoustic velocity can be modified to apply to sonic boom waves produced by aircraft in maneuvering flights to predict the time-of-arrival of an incident wave and the time interval between incident and reflected waves for a wall facing the wave.

Another numerical approach may be possible. For a weak wave, the conservation laws can be combined into a single equation, a Laplace equation for pressure with second order derivatives in time and as well as space derivatives. Proper stability study should be undertaken to attempt to solve this equation numerically in the presence of weak shocks. If it is possible to handle sonic boom wave problems with this single equation, much larger fields can be handled since only three variables ($P^{n-1}$, $P^n$, $P^{n+1}$) have to be stored in computer programs instead of the six variables ($P^n$, $P^{n+1}$, $u^n$, $u^{n+1}$, $v^n$, $v^{n+1}$) that are to be stored in the method developed here. However, solid-wall boundaries appear to present difficulties which may be insurmountable.

# A SELECTED BIBLIOGRAPHY

1. Andrews Associates, Inc., and Hudgins, Thompson, Ball and Associates, Inc. "Final Report on Studies of Structural Response to Sonic Booms," for the Federal Aviation Agency, Vol. 1, February, 1965.

2. Simpson, J. D. "The Transient Response of a Helmholtz Resonator with Application to Sonic Boom Response Studies." Ph.D.Thesis, Oklahoma State University, May, 1966.

3. Whitehouse, G. D. "Coupled and Uncoupled Panel Response to Sonic Boom Type Inputs." Ph.D. Thesis, Oklahoma State University, May, 1967.

4. Reddy, N. N. "Response Spectra of Coupled Acoustical Resonators to Transient Excitation." Ph.D. Thesis, Oklahoma State University, May, 1967.

5. Rusanov, V. V. "The Calculation of the Interaction of Non-Stationary Shock Waves and Obstacles." National Research Council of Canada Library, Ottawa, Canada, Technical Translation 1027 by D. A. Sinclair, 1962. Translated from: Zhurnal Vychislitelnoi Fiziki, Akademiya Nauk, SSSR 1, Vol. 1, No. 2, 1961, p. 267.

6. Randall, D. G. "Methods for Estimating Distributions and Intensities of Sonic Bangs." British Aeronautical Research Council, Report and Memoranda No. 3113, August, 1967.

7. Lansing, D. L. "Application of Acoustic Theory to Prediction of Sonic-Boom Ground Patterns from Maneuvering Aircraft." National Aeronautics and Space Administration, TN-D-1860, October, 1964.

8. Tyler, L. D. "Numerical Solutions of the Flow Field Produced by a Plane Shock Wave Emerging into a Crossflow." Ph.D. Thesis, Oklahoma State University, May, 1965; Published as Engineering Research Report SBW-10 by Tyler, L. D. and G. W. Zumwalt.

9. Walker, W. F., and L. D. Tyler. "Literature Survey on Shock Wave Interactions with Shocks and Bodies." Oklahoma State University Research Report SBW-7, 1965.

10. Walker, W. F. "A Numerical Solution for the Interaction of a Moving Shock Wave with a Turbulent Mixing Region." Ph.D. Thesis, Oklahoma State University, May, 1966.

11. Busemann, A. "Infinitesimale Kegelige Uberschallstromung." Schriften der Deutschen Akademie fur Luftfahrshung, Vol. 7B, No. 3, p. 105, 1943. (Translation NACA TM 1100).

12. Luneberg, R. K. "Mathematical Theory of Optics." Brown University Lectures, 1944.

13. Keller, J. B. "Mechanics of Continuous Media." New York University Lectures, 1949-1950.

14. Keller, J. B., and A. Blank. "Diffraction and Reflection of Pulses by Wedges and Corners." Comm. Pure and Appl. Math., Vol. IV, No. 1, June, 1951.

15. Von Neumann, J. "Oblique Reflection of Shocks." John Von Neumann Collected Works, Vol. VI, New York: Macmillan, 1963, p. 238.

16. Ting, L. "Diffraction and Reflection of Weak Shocks by Structures." Journal of Mathematics and Physics, XXXII, 2-3, p. 102, July-October, 1953.

17. Whitham, G. B. "On the Propagation of Weak Shocks." J. Fluid Mechanics, Vol. 1, 1956, p. 290.

18. Ting, L. "Diffraction of Disturbance Around a Convex Right Corner with Applications in Acoustics and Wing-Body Interference." J. Aero. Sci., Vol. 24, 1957, p. 281.

19. Filippov, I. G. "On the Theory of Diffraction of Weak Shock Waves Round Contours of Arbitrary Shape." PMM, Vol. 27, Pt. 1, 1963, p. 73.

20. Reines, F., and J. Von Neumann. "The Mach Effect and Height of Burst." John Von Neumann Collected Works, Vol. VI, New York: Macmillan, 1963, p. 309.

21. Lax, P. "On Discontinuous Initial Value Problems for Nonlinear Equations and Finite Difference Schemes." LAMS - 1332, 1953.

22. Lax, P., and B. Wendroff. "Systems of Conservation Laws." Comm. Pure and Appl. Math., Vol. XIII, 1960, p. 217.

23. Lax, P. "Hyperbolic Systems of Conservation Laws II." Comm. Pure and Appl. Math., Vol. X, 1957, p. 537.

24. Von Neumann, J., and R. D. Richtmeyer. "A Method for the Numerical Calculation of Hydrodynamic Shocks." J. Appl. Physics, Vol. 21, 1950, p. 232.

25. Holf, E. "The Partial Differential Equation $U_t + UU_x = \mu U_{xx}$." Comm. Pure and Appl. Math., Vol. III, 1950, p. 201.

26. Oleninik, O. A. "Construction of a Generalized Solution of the Cauchy Problem for a Quasi-Linear Equation of First Order by the Introduction of Vanishing Viscosity." American Mathematical Society Translations, Vol. 33, Series 2m, 1963, p. 277.

27. Burstein, S. Z. "Numerical Methods in Multidimensional Shocked Flows." AIAA, Vol. 2, No. 12, 1964, p. 2111.

28. Richtmeyer, R. D. "Difference Methods for Initial-Value Problems." Interscience, New York, 1957.

29. Fox, L. "Numerical Solution of Ordinary and Partial Difference Equations." Addison Wesley, Reading, Massachusetts, 1962.

APPENDIX

STABILITY ANALYSIS OF THE DIFFERENCE EQUATIONS

No general method has been developed to determine stability re-
quirements for the non-linear difference equations derived in Chapter V.
For any difference method, it is necessary to determine the conditions
that are to be met to assure that a perturbation will not increase with-
out bound with increasing time. Richtmeyer (28) has concluded that
even for a first order non-linear system, there exists no rigorous
analysis whereby stability criteria can be determined. The common
approach is to linearize the equations and apply the general methods
for stability of linear equations (29, p. 223). Here, a stability
study for the plane geometry flow case for a sonic boom wave is made
by applying the Fourier technique developed by Rusanov (5) and applied
by Tyler (8) and Walker (10).

The stability analysis is performed by first allowing the dependent
variables u, v, and p to change slightly and assuming $\rho$ and $\gamma$ to be
constants in the general difference Equation (5-28). The effect of the
variation on the equation is investigated by introducing a general per-
turbation variable $\varphi$. A change in $\varphi_{k,\ell}^{n+1}$ will cause a variation in $f_{k,\ell}^{n+1}$
and the resulting change,

$$df_{k,\ell}^{n+1} = \frac{df}{d\varphi}\, \delta\varphi_{k,\ell}^{n+1} = \frac{df}{d\varphi}\, \delta\varphi_{k,\ell}^{n} - \frac{K_1}{2}\frac{dF^x}{d\varphi}\, (\delta\varphi_{k+1,\ell} - \delta\varphi_{k-1,\ell})^n - \frac{K_2}{2}\frac{dF^y}{d\varphi}$$

$$(\delta\varphi_{k,\ell+1} - \delta\varphi_{k,\ell-1})^n + \frac{\delta}{2}\frac{df}{d\varphi}\, (\delta\varphi_{k+1,\ell} - 2\delta\varphi_{k,\ell} + \delta\varphi_{k-1,\ell})^n$$

$$+ \frac{\beta}{2} \frac{df}{d\varphi} (\delta\varphi_{k,\ell+1} - 2\delta\varphi_{k,\ell} + \delta\varphi_{k,\ell-1})^n ,  \tag{1}$$

is obtained assuming that the functional values of some terms are independent of position; for example:

$$\frac{dF^x_{k+1,\ell}}{d\varphi_{k+1,\ell}} = \frac{dF^x_{k,\ell}}{d\varphi_{k,\ell}} = \frac{dF^x_{k-1,\ell}}{d\varphi_{k-1,\ell}} = \frac{dF^x}{d\varphi} .  \tag{2}$$

The next step is to express the perturbation term $\delta\varphi$ as a product of its initial value and its wave components. In equation form, this is written as

$$\delta\varphi^n_{k,\ell} = \xi^n e^{i[k\psi_1 + \ell\psi_2]} \delta\Phi^o_{1,1} ,  \tag{3}$$

where $\delta\varphi^o_{1,1}$ is the initial perturbation value, and $\psi_1$ and $\psi_2$ are any real numbers. The value of $\xi$ dictates the condition for stability. In order to satisfy the stability condition for Equation (1), the propagated error $\delta\varphi^n_{k,\ell}$ must be bounded. Hence, $\xi^n$ in Equation (3) must be convergent, and thus should satisfy the condition

$$|\xi| \leq 1 .  \tag{4}$$

If Equation (3) is substituted into Equation (1), the resulting expression is

$$(\xi-1)\frac{df}{d\varphi} + iK_1 \frac{dF^x}{d\varphi} \sin \psi_1 + iK_2 \sin \psi_2 \frac{dF^y}{d\varphi}$$

$$+ 2 \left[\alpha \sin^2 \frac{\psi_1}{2} + \beta \sin^2 \frac{\psi_2}{2} \frac{df}{d\varphi}\right] = 0 .  \tag{5}$$

After substitution of the values for the expressions f, $F^x$, and $F^y$ from Equation (5-23), the derivatives in Equation (5) are expressed as

$$\frac{df}{d\varphi} = \begin{Bmatrix} \frac{du}{d\varphi} \\ \frac{dv}{d\varphi} \\ \frac{dP}{d\varphi} \end{Bmatrix} ; \quad \frac{dF^x}{d\varphi} = \begin{Bmatrix} \frac{dP}{\rho d\varphi} \\ 0 \\ \gamma P\frac{du}{d\varphi} + u\frac{dP}{d\varphi} \end{Bmatrix} ; \quad \frac{dF^y}{d\varphi} = \begin{Bmatrix} 0 \\ \frac{dP}{\rho d\varphi} \\ \gamma P\frac{dv}{d\varphi} + v\frac{dP}{d\varphi} \end{Bmatrix} .  \tag{6}$$

Equation (5) represents a system of three simultaneous equations and the expressions for the derivatives are obtained from Equation (6). The three simultaneous equations are written as

$$(\xi-1)\frac{du}{d\varphi} + iK_1 \sin \psi_1 \frac{1}{\rho}\frac{dP}{d\varphi} + \left[2\alpha \sin^2 \frac{\psi_1}{2} + 2\beta \sin^2 \frac{\psi_2}{2}\right]\frac{du}{d\varphi} = 0$$

$$(\xi-1)\frac{dv}{d\varphi} + iK_2 \sin \psi_2 \frac{1}{\rho}\frac{dP}{d\varphi} + \left[2\alpha \sin^2 \frac{\psi_1}{2} + 2\beta \sin^2 \frac{\psi_2}{2}\right]\frac{dv}{d\varphi} = 0 \tag{7}$$

$$(\xi-1)\frac{dP}{d\varphi} + iK_1 \sin \psi_1 \left[\gamma P\frac{du}{d\varphi} + \gamma u\frac{dP}{d\varphi}\right] + iK_2 \sin \psi_2 \left[\gamma P\frac{dv}{d\varphi} + \gamma v\frac{dP}{d\varphi}\right]$$

$$+ \left[2\alpha \sin^2 \frac{\psi_1}{2} + 2\beta \sin^2 \frac{\psi_2}{2}\right]\frac{dP}{d\varphi} = 0 \ .$$

For a sonic boom case, the velocities u, and v are negligible. Hence by the comparison of the orders of magnitudes of various terms in expression (7), the terms containing u, and v can be neglected and the derivatives are eliminated by solving the three equations simultaneously. The resulting expression is

$$\left[\xi-1 + 2\alpha \sin^2 \frac{\psi_1}{2} + 2\beta \sin^2 \frac{\psi_2}{2}\right]^2 + c^2 \left[K_1^2 \sin^2 \psi_1 + K_2^2 \sin^2 \psi_2\right] = 0 \ , \tag{8}$$

where

$$c = \text{speed of sound} = \sqrt{\frac{\gamma P}{\rho}} \ .$$

Equation (8) in combination with Equation (4) is used to establish the stability criteria and, unfortunately, no simple solution is available due to its complexity. Therefore $\xi$ is evaluated as the angles $\psi_1$ and $\psi_2$ assume large and small values. For large values of $\psi_1$ and $\psi_2$,

$$\psi_1 = \psi_2 = \pi \ , \tag{9}$$

Equation (8) is reduced to

$$\xi_\ell = 1 - 2(\alpha + \beta) \ . \tag{10}$$

If Equation (4) is imposed on Equation (10), the result is

$$0 \leq \alpha + \beta \leq 1 . \tag{11}$$

For small angles of $\psi_1$ and $\psi_2$, they become

$$\psi_1 = \sin \psi_1 , \qquad \psi_2 = \sin \psi_2 , \tag{12}$$

and Equation (8) is approximated by

$$\left(\xi_S - 1 + \frac{\alpha \psi_1^2}{2} + \frac{\beta \psi_2^2}{2}\right)^2 + c^2 \ (K_1^2 \ \psi_1^2 + K_2^2 \ \psi_2^2) . \tag{13}$$

The roots of Equation (13) are

$$\xi_S = 1 - \frac{1}{2} \ (\alpha \psi_1^2 + \beta \psi_2^2) \pm \sqrt{-c^2 \ (K_1^2 \ \psi_1^2 + K_2^2 \ \psi_2^2)} . \tag{14}$$

From Equation (14), the real and imaginary parts are found to be

$$R(\xi_S) = 1 - \frac{1}{2} \ (\alpha \psi_1^2 + \beta \psi_2^2) \tag{15}$$

and

$$I(\xi_S) = \pm \sqrt{c^2 \ (K_1^2 \ \psi_1^2 + K_2^2 \ \psi_2^2)} . \tag{16}$$

From Equations (15) and (16):

$$\begin{aligned}
\xi_S{}^2 &= [R(\xi_S)^2 + I(\xi_S)^2] \\
&= 1 - \alpha \psi_1^2 - \beta \psi_2^2 + \frac{\alpha^2 \ \psi_1^4}{4} + \frac{\beta^2 \ \psi_2^4}{4} \\
&\quad + c^2 \ (K_1^2 \ \psi_1^2 + K_2^2 \ \psi_2^2) .
\end{aligned} \tag{17}$$

By expressing inequality (4) as

$$1 - \left| \xi_S \right|^2 \geq 0 \tag{18}$$

Equation (17) reduces to

$$\alpha \psi_1^2 + \beta \psi_2^2 \geq c^2 \ (K_1^2 \ \psi_1^2 + K_2^2 \ \psi_2^2) , \tag{19}$$

Where $\psi_1^4$ and $\psi_2^4$ terms are neglected in view of the small angles assumption. Letting

$$\cos \theta = \frac{K_1 \psi_1}{[K_1^2 \psi_1^2 + K_2^2 \psi_2^2]^{\frac{1}{2}}} \quad, \text{ and } \sin \theta = \frac{K_2 \psi_2}{[K_1^2 \psi_1^2 + K_2^2 \psi_2^2]^{\frac{1}{2}}} \qquad (20)$$

reduces Equation (19) to

$$\frac{\alpha \cos^2 \theta}{K_1^2} + \frac{\beta \sin^2 \theta}{K_2^2} \geq c^2 \ . \qquad (21)$$

If Equation (5-31) is substituted into inequality (21), the resulting expression is

$$\frac{\alpha \cos^2 \theta}{\sin^2 \chi} + \frac{\beta \sin^2 \theta}{\cos^2 \chi} \geq K^2 c^2 \ . \qquad (22)$$

Inequality (11) can be written as

$$\alpha + \beta = K\omega c \qquad (23)$$

so long as

$$0 \leq K\omega c \leq 1 \ . \qquad (24)$$

Any expression for $\alpha$ and $\beta$ can be chosen in Equation (24) as long as inequality (24) is satisfied. Therefore with

$$\alpha = K\omega c \sin^2 \chi$$

$$\beta = K\omega c \cos^2 \chi \ , \qquad (25)$$

Equation (22) is expressed as

$$K\omega c (\cos^2 \theta + \sin^2 \theta) \geq K^2 c^2$$

$$K\omega c \geq K^2 c^2 \qquad (26)$$

Inequalities (24) and (26) are combined to yield

$$K^2 c^2 \leq K\omega c \leq 1 \ . \qquad (27)$$

The time step K can be evaluated from Equation (27) and the maximum

time step that can be used in the computations is

$$K = \frac{1}{c_{max}} .$$

(28)

For a sonic boom wave, assuming c as a constant, Equation (28) reduces
to

$$K = \frac{1}{c} .$$

(29)

This is the value used in the computations described in Chapter VI.

VITA


Balusu M. Rao

Candidate for the Degree of

Doctor of Philosophy


Thesis: ANALYSIS OF SONIC BOOM WAVES INCIDENT ON STRUCTURES

Major Field: Mechanical Engineering

Biographical:

  Personal Data: Born in Penjendra, Andhra Pradesh, India,
     July 21, 1938, the son of Satyanarayana and Annapurnamma.

  Education: Graduated from Sri Raja Rangappa Rao's Board High
     School, Nuzvid, Andhra Pradesh, 1953; earned the Bachelor
     of Engineering degree in Electrical Engineering from the
     Andhra University, Waltair, 1959; earned the Master of
     Engineering degree in Aeronautical Engineering from the
     Indian Institute of Science, Bangalore, India, 1961;
     completed the requirements for the Doctor of Philosophy
     degree in Mechanical Engineering in December, 1966.

  Professional Experience: Aeronautical Engineer, Hindustan
     Aircraft Ltd., Bangalore, India, June, 1961, to August,
     1963; Graduate Assistant, Oklahoma State University,
     January, 1964, to December, 1966.

  Organizations: Member of American Institute of Aeronautics and
     Astronautics, American Society of Mechanical Engineers.